國 立 中 央 大 學

大 氣 科 學 學 系

碩 士 論 文

Investigating hygroscopic cloud-seeding effects in liquid-water clouds in northern Taiwan: in-situ measurements and model simulation

研 究 生：林凱翊

指導教授：鍾高陞 博士、王聖翔 博士

中 華 民 國 一一一 年 六 月

國立中央大學圖書館學位論文授權書

填單日期：111 / 07 / 13　　2019.9 版

授權人姓名	林凱翊	學 號	109621017
系所名稱	大氣科學學系	學位類別	☑碩士 □博士
論文名稱	Investigating hygroscopic cloud-seeding effects in liquid-water clouds in northern Taiwan: in-situ measurements and model simulation	指導教授	鍾高陞 博士 王聖翔 博士

學位論文網路公開授權

授權本人撰寫之學位論文全文電子檔：

・在「國立中央大學圖書館博碩士論文系統」.

(　)同意立即網路公開

(√)同意 於西元 2023 年 02 月 01 日網路公開

(　)不同意網路公開，原因是：_____

・在國家圖書館「臺灣博碩士論文知識加值系統」

(　)同意立即網路公開

(√)同意 於西元 2023 年 02 月 01 日網路公開

(　)不同意網路公開，原因是：_____

依著作權法規定，非專屬、無償授權國立中央大學、台灣聯合大學系統與國家圖書館，不限地域、時間與次數，以文件、錄影帶、錄音帶、光碟、微縮、數位化或其他方式將上列授權標的基於非營利目的進行重製。

學位論文紙本延後公開申請 (紙本學位論文立即公開者此欄免填)

本人撰寫之學位論文紙本因以下原因將延後公開

・延後原因

(　)已申請專利並檢附證明，專利申請案號：

(√)準備以上列論文投稿期刊

(　)涉國家機密

(　)依法不得提供，請說明：_____

・公開日期：西元 2023 年 02 月 01 日

※繳交教務處註冊組之紙本論文(送繳國家圖書館)若不立即公開，請加填「國家圖書館學位論文延後公開申請書」

研究生簽名：林凱翊　　指導教授簽名：鍾高陞 王聖翔

*本授權書請完整填寫並親筆簽名後，裝訂於論文封面之次頁。

國家圖書館學位論文延後公開申請書

Application for Embargo of Thesis/Dissertation

申請日期：民國 111 年 07 月 13 日

Application Date: 2022 / 07 / 13 (YYYY/MM/DD)

申請人姓名 Applicant Name	林凱翊	**學位類別** Graduate Degree	☑碩士 Master ☐博士 Doctor	**畢業年月** Graduation Date (YYYY/MM)	民國 111 年 06 月
學校名稱 University	國立中央大學		**系所名稱** School/Department	大氣科學學系	
論文名稱 Thesis / Dissertation Title	Investigating hygroscopic cloud-seeding effects in liquid-water clouds in northern Taiwan: in-situ measurements and model simulation				
延後公開原因 Reason for embargo	☐涉及機密 Contains information pertaining to the secret. ☐專利事項，申請案號： Filing for patent registration. Registration number: ☑依法不得提供，請說明：準備以上列論文投稿期刊 Withheld according to the law. Please specify.				
申請項目 Options	☑紙本論文延後公開 Delay public access to the printed copies of my thesis, but leave the online bibliographic record open to the public.			☑書目資料延後公開 Delay public access to online bibliographic record of my thesis.	
公開日期 Delayed Until	民國 112 年 02 月 01 日 2023 / 02 / 01 (YYYY/MM/DD)			☐不公開 Prohibited from public access.	

申請人簽名：
Applicant Signature: 林凱翊

指導教授簽名：
Advisor Signature: 鍾高陞 王聖翔

學校認定/審議單位章戳：
Seal of the Authorization Institute:

【說明】

1. 依教育部107年12月5日臺教高(二)字第1070210758號函及109年3月13日臺教高通字第1090027810號函，請據實填寫本申請書並檢附由學校認定或審議單位認定之證明文件，經由學校向本館提出申請，無認定或審議單位章戳者退回學校處理。
2. 論文尚未送交國家圖書館，請於提送論文時，夾附親筆簽名申請書1份。
3. 論文已送達國家圖書館，請將親筆簽名申請書一式2份掛號郵寄10001臺北市中山南路20號國家圖書館館藏發展及書目管理組，並於信封註明「學位論文延後公開申請書」。
4. 本館保存之學位論文依學位授予法應提供公眾於館內閱覽紙本，或透過獨立設備讀取電子資料檔，二者依表單填寫日期公開。

【Notes】

1. Please fill in all blanks and attach the certification documents approved by the university and apply through the university. The application form will not be accepted for processing until all information, signatures, and stamps are included.
2. If the thesis or dissertation is not yet submitted to the NCL, please attach the signed application form to the thesis or dissertation.
3. If the thesis or dissertation has been submitted to the NCL, please send a registered letter with 2 copies of the signed application form attached. The letter should be addressed to "Collection Development Division", National Central Library with a note in the envelope indicating "Application for delay of public release" to the following address. No.20, Zhongshan S. Rd., Zhongzheng District, Taipei City 10001, Taiwan (R.O.C.)
4. The delayed date of printed copies and the independent viewing equipment will synchronize.

(**申請者免填**，以下由國家圖書館填寫 For Internal Use)

承辦單位_館藏組：_____ 日期/處理狀況：

典藏地：_____ 登錄號：_____ 索書號：

會辦單位_知服組：_____ 日期：_____ ☐移送並註記，原上架日期：

論文系統：_____ 日期：

國立中央大學碩士班研究生
論 文 指 導 教 授 推 薦 書

大氣科學學系大氣物理碩士班 學系/研究所 林凱翊 研究生

所提之論文 Investigating hygroscopic cloud-seeding effects in liquid-water clouds in northern Taiwan: in-situ measurements and model simulation

係由本人指導撰述，同意提付審查。

指導教授 鍾高陞 王聖翔 (簽章)

111 年 6 月 16 日

1110616

國立中央大學碩士班研究生
論文口試委員審定書

大氣科學學系大氣物理碩士班 學系/研究所 林凱翊 研究生
所提之論文 Investigating hygroscopic cloud-seeding effects in liquid-water clouds in northern Taiwan: in-situ measurements and model simulation
經由委員會審議，認定符合碩士資格標準。

學位考試委員會召集人 陳瑜華

委　　員 林沛暐

王聖翔

鍾高陞

中　華　民　國　111　年　06　月　30　日

摘要

全球暖化導致乾旱之強度與頻率增加；於 2021 年，台灣亦面臨近百年來最為嚴重之乾旱，也因此促使政府嘗試發掘解決辦法，而吸濕性粒子種雲似乎為一種兼具可行性與可能性之方法，用以解決水資源匱乏之問題。本研究嘗試結合現地觀測與數值模擬，探究吸濕性氣膠種雲在種雲過程中所需要的環境條件及雲微物理變化特徵，針對北台灣集水區建立人工種雲與降雨的個案研究，並提出一個有效且具科學基礎的人工種雲策略。

在 2019-2021 年期間，吾人針對台灣乾季共實施了 4 次東眼山種雲觀測實驗，建立高時間解析度之氣象與氣膠觀測，觀測結果發現：種雲焰劑之施放導致水氣競爭效應以及凝結過程的產生，並且於施放地域生成更多的雨滴。在數值模擬方面，吾人利用 WRF 模擬 2020 年 10 月 21-22 日之種雲實驗個案，以自行開發之雲微物理參數化方案(WDM6-NCU)進行雲微物理模擬，WDM6-NCU 雲微物理參數化方案可利用 43 個細格描述雲凝結核之粒徑分布，可給定觀測所得之種雲焰劑粒徑分布，更真實及完整地計算雲凝結核之活化過程，模式模擬結果顯示：就人工種雲效率來說，雲內種雲相較於在雲底種雲可以增加更多降水，且增加種雲播撒面積與種雲粒子濃度可以增加數倍的降水生成；對於雲微物理過程，雨滴之碰併過程的增強為造就降水增加之主要原因，且吸濕性粒子大於 0.4 μm 有助於引發後續一連串成雲降雨過程。整體而言，本研究開發出一套本土化的人工種雲氣象模式，成功地解釋暖雲種雲至降雨之過程，搭配觀測資料之分析與驗證，可做為未來人工種雲實務作業之重要依據。

Abstract

Global warming causes droughts to increase in intensity and frequency. In 2021, Taiwan faced the most serious drought in the past hundred years, prompting Taiwan government to seek ways to deal with the problems of water scarcity. Hygroscopic cloud seeding seems to be a possible solution to create more water resources. The goals of this study attempt to investigate the suitable environmental conditions for hygroscopic cloud seeding and its impacts on cloud microphysics by both observation and model simulation. Furthermore, based on a case study of hygroscopic cloud seeding in northern Taiwan catchment, an effective and scientific strategy of hygroscopic cloud seeding seeks to be proposed.

During 2019-2021, four Dongyan mountain cloud-seeding experiments were executed with meteorological and aerosol observation, and the results indicate that: the seeding agents can strengthen the competition effect and the condensation process. Moreover, the concentration of raindrops increases after doing cloud seeding. For model simulation, the WRF model with a hybrid cloud-seeding microphysics scheme, WDM6-NCU, which is able to describe seeded CCNs size distribution by 43 bins and precisely evaluate the activation of seeded CCNs, is used to simulate the case on 21-22 October 2020 with a series of sensitivity tests on cloud seeding. Results of model simulation show that: more precipitation is developed in the scenarios seeding at the in-cloud region, and seeding in a bigger domain and higher hygroscopic particles concentration are able to increase several folds of rainfall. Regarding the microphysics processes, the main reason causes the enhancement of precipitation is the strengthening of the accretion process of raindrops, and those hygroscopic particles bigger than 0.4 μm are the main factor contributing to cloud-seeding effects. In conclusion, this study

develops a hybrid cloud-seeding microphysics scheme, which successfully explains the process from launching cloud seeding to developing rainfall and matches the features of observation data. In addition, the results of this study can be used as a guidance for the future operation of cloud seeding in Taiwan.

Acknowledgment

時間總是毫不留情地走著，在中央大學，我走過了大學與碩士共六年的時光，其中碩士班的每件事情總讓我刻骨銘心，冒著雨上山架儀器、徹夜調整模式設定、熱血的在凌晨三點進行種雲實驗，這些種種我想我一輩子都不會忘記，也因為這些寶貴的經歷才能促使這篇論文的誕生。

而這篇論文的完成我最要感謝的是我的兩位指導老師：鍾高陞博士以及王聖翔博士。鍾老師一步一步的帶領我深入探索雲微物理的世界，並且給予我很大的自由空間，讓我無限的暢遊在研究世界中；王老師則總是不辭辛勞地陪著我上山下海的奔波，並總能一語中的的指點我觀測的設計與資料分析的方向。在兩位老師的指導下我獲益匪淺，對老師們的感謝也並非三言兩語能夠盡述，僅在此獻上最深的致意!同時也感謝林能暉老師與陳淑華老師兩位口試委員的建議，使本篇論文能夠更加完善。

謝謝廖宇慶老師、陳台琦老師、鍾高陞老師以及張偉裕老師帶領著雷達實驗室不斷前進,在研究上也提供我許多幫助與鼓勵;感謝立昕在我對雲物理參數化還一無所知時,手把手的教導我，並時常給予關心；感謝大柯總是不厭其煩地為我解惑，並且時常與我們聊天談心；感謝翔昱在讀書會總能給我許多非常受用的建議；謝謝晨豪與秉學當初願意陪我一起探究 WDM6 的奧秘；謝謝顯榮時常與我討論並教導我操作許多工具；謝謝同屆的好夥伴沛蓉，這兩年謝謝你在我遇到瓶頸總是耐心的開導；謝謝雷達實驗室的大家，陷入低潮的我總能在實驗室的歡笑聲中再次點燃希望之火，在雷達實驗室的生活非常的快樂!

謝謝鵬翔、育慎、崑旭、筱臻、張倢、洪琳、智寬、承泰、景岳，你們讓我的碩士生活更加充實愉快;謝謝高中好朋友珍竹,在我碩一最迷茫的階段總是願意傾聽;最後,謝謝我的家人,雖然每次開心的與你們分享研究你們都沒反應,但謝謝你們的一路支持,未來我將會更加努力!

Outline

Table list

Figure list

Chapter 1. Introduction

Drought happens more frequently due to global warming (Bo-Tao, 2021). In 2021, Taiwan faced the most serious drought in the past hundred years, prompting Taiwan government to seek ways to deal with the problems of water scarcity. Cloud seeding, the common method of weather modification, seems to be a possible solution to create more water resources. According to Lelieveld (1993), 80 % of cloud droplets are not able to reach the ground, which means that the transformation of cloud droplets to raindrops is inefficient. Thus, since the 20th century, several countries have been committed to cloud-seeding research. However, because of the different environmental conditions in different countries, it is not suitable to use the same cloud-seeding strategies all over the world. There are 2 main strategies of cloud seeding that are always adopted, including ice cloud seeding, which is aimed at ice clouds, and warm cloud seeding, which is aimed at liquid water clouds.

For the dry season (i.e., October to April) in Taiwan, the clouds are mainly warm clouds, which base is about 500 m above mean sea level and the thickness is relatively thin. (Chen, 1995). In addition, due to the prevailing northeasterly wind, the weather systems are usually maintained for a long period and supply plenty of water vapor. Therefore, warm cloud seeding is the more appropriate way to be applied in Taiwan. Hygroscopic cloud seeding is a type of warm cloud seeding, and it is also the method that has been used in Taiwan. In hygroscopic cloud seeding, the seeding agents, which serve as efficient cloud condensation nuclei (CCN) or giant CCN (GCCN: diameter larger than 1μm), play an important role to strengthen the condensation and collision-coalescence process to widen the droplet size distribution (DSD)

and increase precipitation efficiency (Jensen and Lee, 2008; Jung et al., 2015; Tessendorf et al., 2021). The process from spreading seeding agents to developing rainfall spent about 10-20 minutes (Silverman, 2000; Tonttila, 2021). Figure 1.1 displays the theory of hygroscopic cloud seeding. However, though there are clear theory concepts of cloud seeding, it is still challenging to observe the convincing scientific evidence.

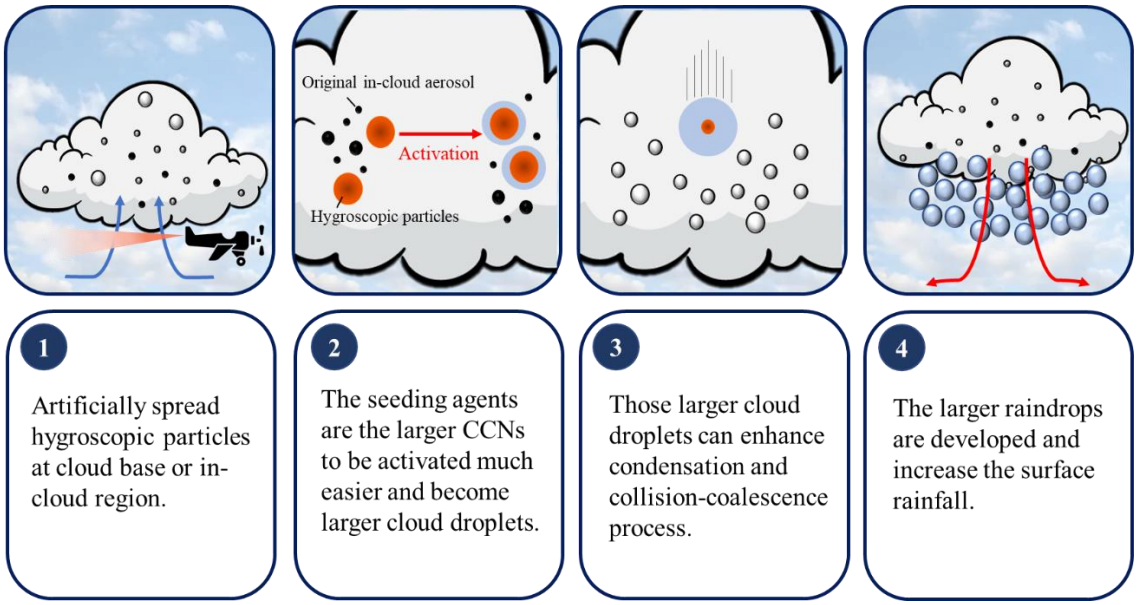

Figure 1.1 The schematic depicts the theory of hygroscopic cloud seeding. The concept of schematic design comes from: https://biostudizz.weebly.com/haze--cloud-seeding.html.

In the past, the effects of cloud seeding was usually verified by the statistical approach, which is based on the comparison of multiple observational samples with the scenarios of seeding and non-seeding, e.g. Silverman (2000) and Tessendorf et al. (2021), etc. However, this method is sometimes full of high uncertainties (Guo et al., 2015). Recently, due to the improvement of observation, more instruments, e.g. cloud radar and cloud droplet probe, are applied to investigate the cloud-seeding effects to find out the direct observational evidence. However, fewer studies have achieved this goal because it is hard to distinguish whether the

signal of precipitation is the response of cloud seeding or the meteorological variations (Kerr, 1982; Mather et al., 1997; Silverman, 2003; Flossmann et al., 2019).

On the other hand, model simulation has the ability to generate several realizations of each scenario and provides the advantage of separating the cloud-seeding signal from the natural phenomenon. Caro et al. (2002) concluded that the hygroscopic particles with a radius between 0.5 and 6 μm are optimal for enhancing precipitation in warm clouds. Moreover, according to Segal et al. (2004), the increment of precipitation by hygroscopic cloud seeding is mainly due to the particles with diameters of 1.5-2.5 μm. The reason for enhancing precipitation by doing cloud seeding with giant CCN is due to the strengthening of the auto-conversion and the accretion process (Tonttila et al., 2021). However, most of the studies of warm-cloud-seeding simulation are simulated by one-dimensional cloud parcel model or based on the ideal case, which may be not always represent the environmental condition in reality.

Recently, there is a remarkable improvement of the technique of both observation and model simulation in Taiwan. Regarding the observation, two new instruments, including LWC-300 and Aerosol spectrometer, can be set up. Thus, it makes us able to gain more complete in-situ observational data set. For model simulation, the new microphysics scheme WDM6-NCU, which is modified from WDM6 by NCU (see section 3.3.3 for more details), can be used to precisely simulate warm cloud seeding as the realistic cases. With the hybrid scheme the simulation results should reflect to more realistic outcome. Encouraged by these improvements, the promising prospect of the results of cloud-seeding experiments are expected.

Taiwan Cloud Seeding Research Project (TCSRP) targets to examine the hygroscopic cloud seeding effects and funded by Water Resources Agency. There are two experiments in

TCSRP, including the Dongyan Mountain cloud-seeding experiment and the Miaopu validation experiment. The Dongyan Mountain cloud-seeding experiment is formed to explore the direct observational evidence of the hygroscopic cloud seeding effects because of several advantages in the observational site, including the semi-enclosed condition, in-cloud environment, and well-set instruments (some details will be discussed in section 3.1.1). In the operation, Miaopu is selected as the region that conducts cloud seeding by drone known as Miaopu validation experiment, because the location is closer to the reservoir. Moreover, seeding with drones makes the seeding height more flexible.

This study attempts to investigate the direct observational evidence by the Dongyan Mountain cloud-seeding experiment and conduct a series of cloud-seeding sensitivity test in Miaopu by model simulation to evaluate the cloud-seeding impacts in the Shihmen region. Table 1 shows the advantage and purpose of the experiments in TCSRP. Furthermore, based on a case study of hygroscopic cloud seeding in northern Taiwan catchment, an effective and scientific strategy of hygroscopic cloud seeding would be proposed.

Table 1 The advantage and purpose of the field campaigns in Taiwan Cloud Seeding Research Project (TCSRP).

TCSRP	**Advantage**	**Purpose**
Dongyan Mountain cloud-seeding experiment	Carefully selected environment and comprehensive observation	Investigate the direct observational evidence of cloud seeding effects.
Miaopu validation experiment	More practical and closer to the reservoir	Investigate the impacts of cloud seeding by the model simulation.

Chapter 2. Cases overview

On 21-22 October 2020, the typhoon Saudel, was located in southwestern Taiwan, and accompanied the co-movement of the northeast monsoon, which caused the stronger northeastern wind and brought plenty of water vapor to northern Taiwan. Figure 2.1 shows the weather map at 00 UTC on 22 October 2020. The skew T diagrams at 12:00 UTC on 21 October 2020, 00:00 UTC on 22 October 2020, and 12:00 UTC on 22 October 2020 (Figure 2.2) also display that the environment was saturated below the mean sea level height of about 3000 m.

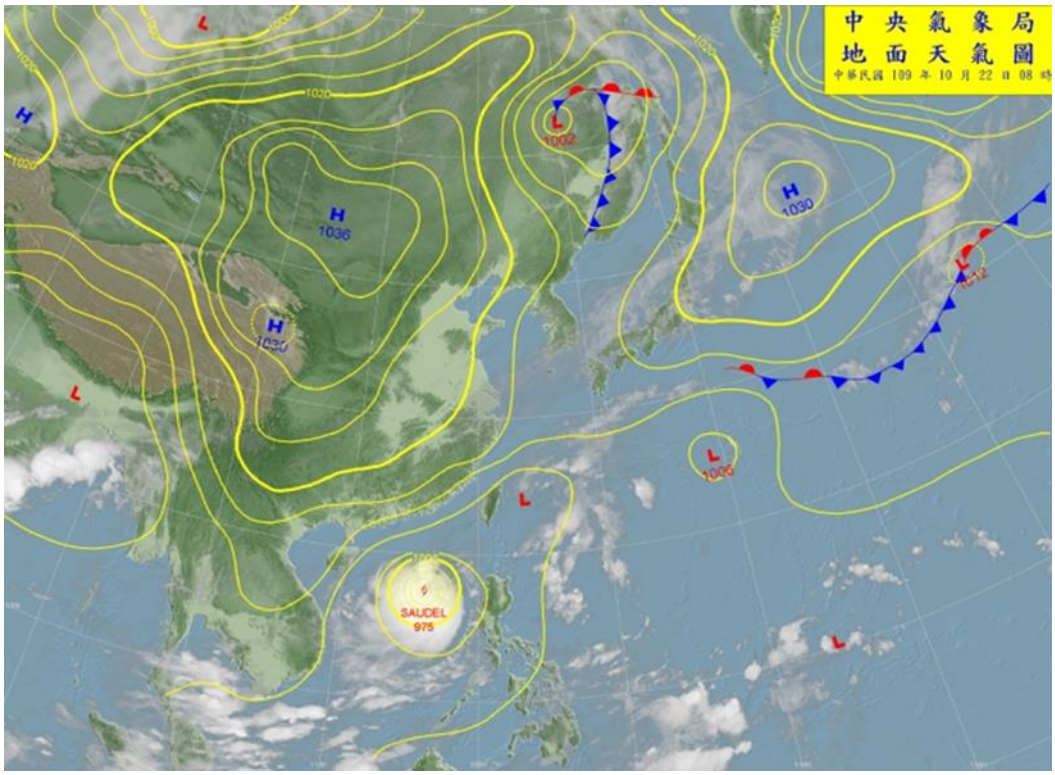

Figure 2.1 The weather map at 00 UTC on 22 October 2020. Source: CWB.

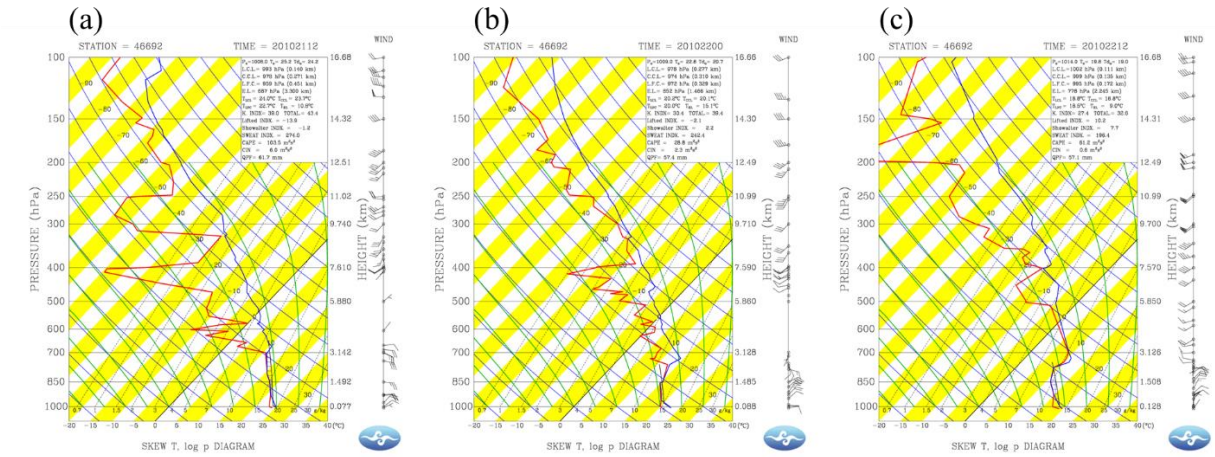

Figure 2.2 The skew T diagrams at (a) 12:00 UTC on 21 October 2020, (b) 00:00 UTC on 22 October 2020, and (c) 12:00 UTC on 22 October 2020.

At 20:00 UTC on 21 October 2020, the stratiform precipitation in northern Taiwan was observed by the radars (Figure 2.3), and the infrared image of Himawari8 (Figure 2.4) shows that northern Taiwan was mainly affected by lower clouds. In addition, the site in Dongyan Mountain is wrapped by clouds, and the relative humidity is above 90 %. Therefore, the cloud-seeding experiment had been carried out at the Dogyan Mountain during 20:00-22:00 UTC on 21 October 2020.

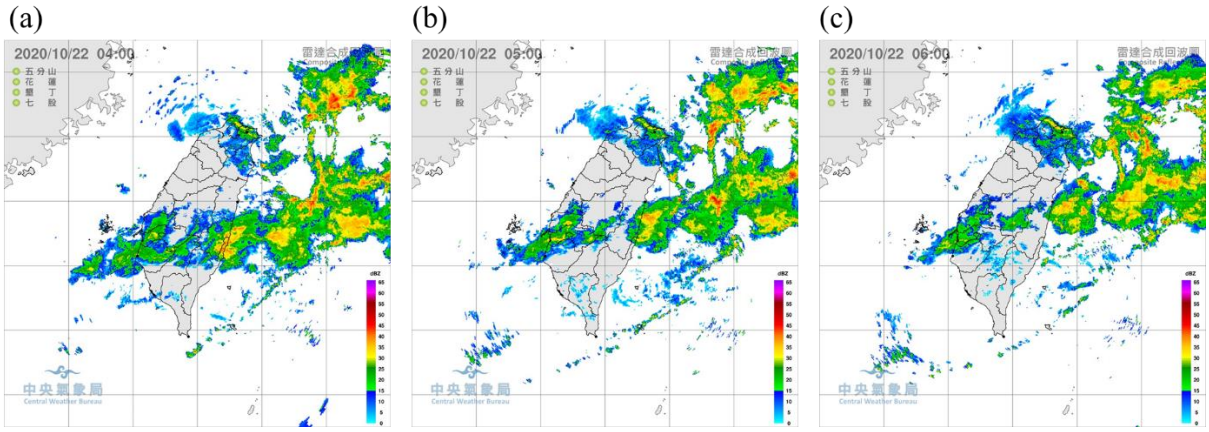

Figure 2.3 Composite maximum radar reflectivity at (a) 20:00 UTC, (b) 21:00 UTC, and (c) 22:00 UTC on 21 October 2020. Source: CWB.

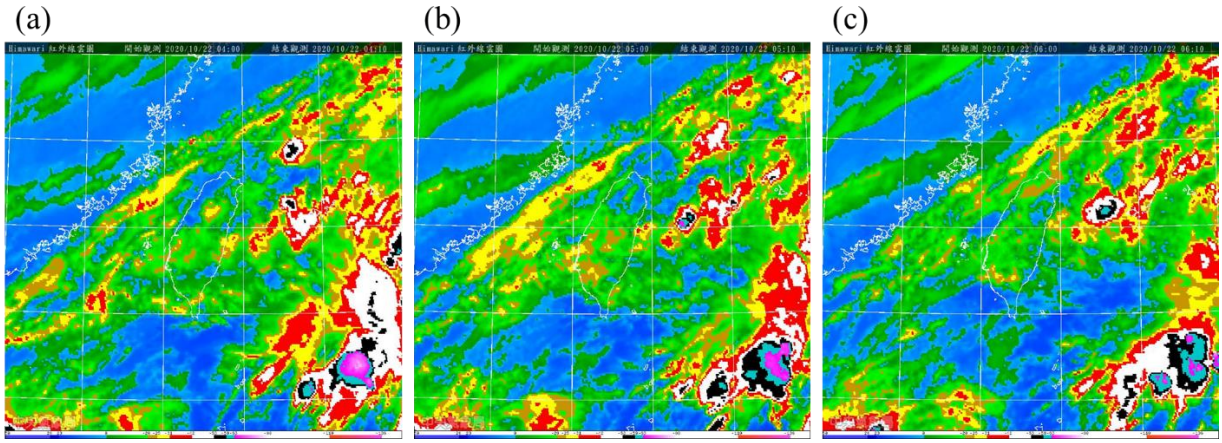

Figure 2.4 The infrared image of Himawari8 at (a) 20:00 UTC, (b) 21:00 UTC, and (c) 22:00 UTC on 21 October 2020. Source: CWB.

Also, at 06:00 UTC on 22 October 2020, the stratiform precipitation in northern Taiwan is still sustained and observed by the radars and Himawari8 (Figure 2.5 and Figure 2.6). Therefore, the cloud-seeding validation experiment had been executed in Miaopu during 14:30-16:30 UTC on 22 October 2020. Furthermore, this case is selected to do a series of sensitivity test on cloud

seeding in the model simulation.

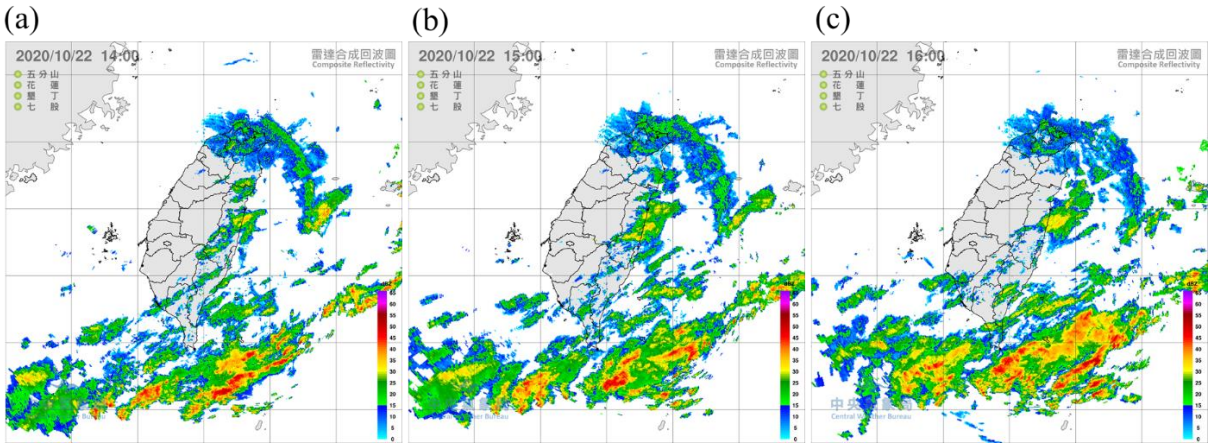

Figure 2.5 Composite maximum radar reflectivity at (a) 06:00 UTC, (b) 07:00 UTC, and (d) 08:00 UTC on 22 October 2020. Source: CWB.

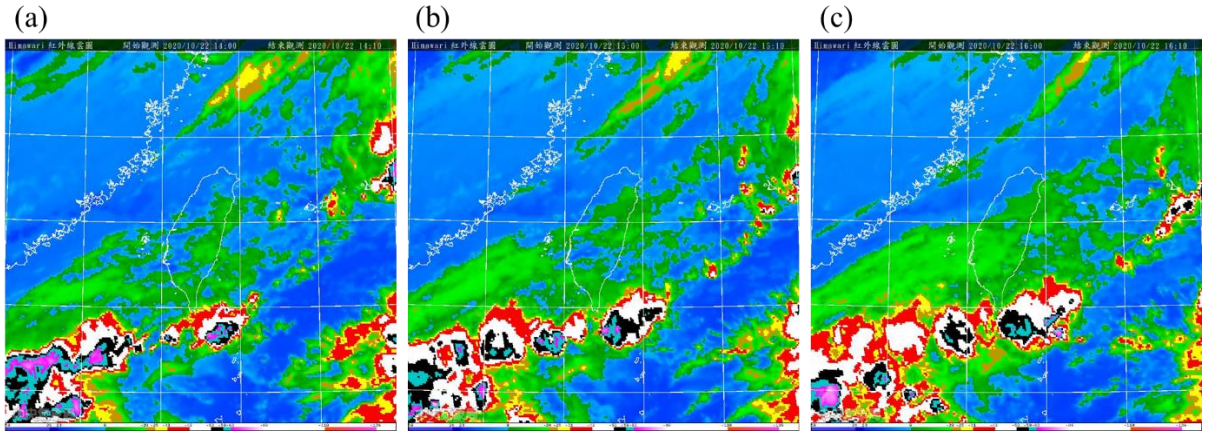

Figure 2.6 The infrared image of Himawari8 at (a) 06:00 UTC, (b) 07:00 UTC, and (c) 08:00 UTC on 22 October 2020. Source: CWB.

Another event is on 28 April 2021. In this event, there was a cold front near northern Taiwan, and plenty of water vapor was brought by southwestern wind. Figure 2.7 displays the weather map at 12 UTC on 28 April 2021. The skew T diagrams at 00:00 UTC on 28 April 2021

and 12:00 UTC on 28 April 2021 (Figure 2.8) also show that the environment was saturated below the mean sea level height of about 7000 m. At 11:00 UTC on 28 April 2021, the precipitation in northern Taiwan was observed by the radars (Figure 2.9), and the infrared image of Himawari8 (Figure 2.10) depicts that northern Taiwan was mainly affected by lower clouds. In addition, the site in Dongyan Mountain is wrapped by clouds, and the relative humidity is above 90 %. Therefore, the cloud-seeding experiment had been conducted in Dongyan Mountain during 11:00-13:00 UTC on 28 April 2021.

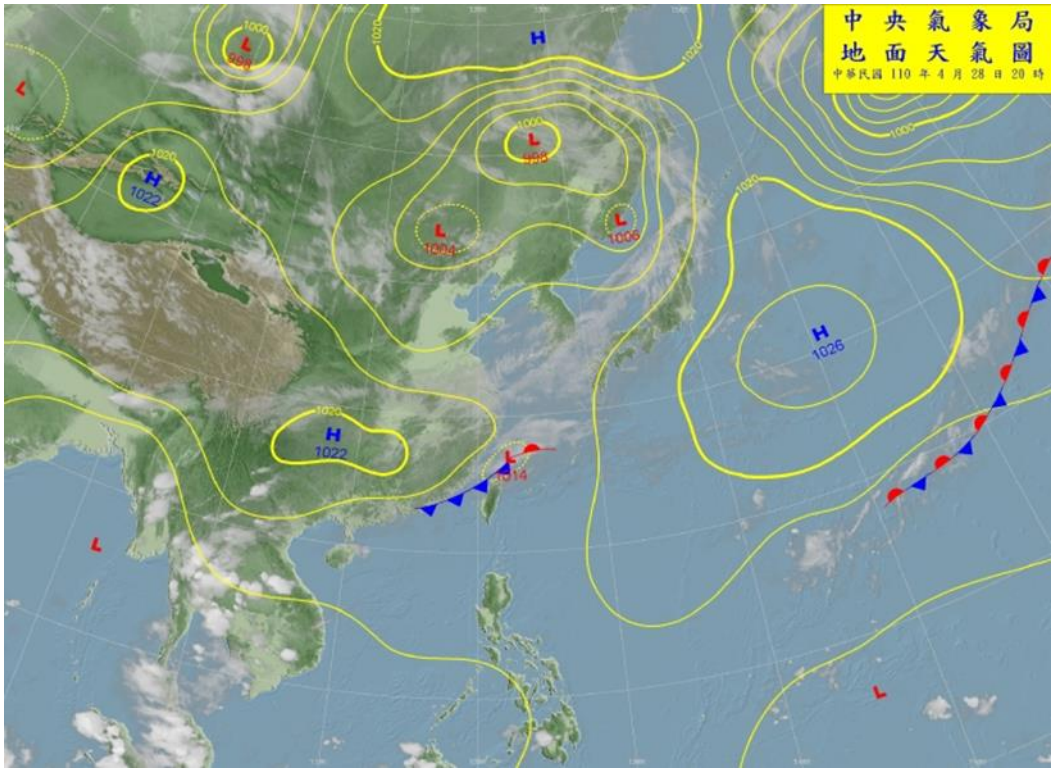

Figure 2.7 The weather map at 12 UTC on 28 April 2021. Source: CWB.

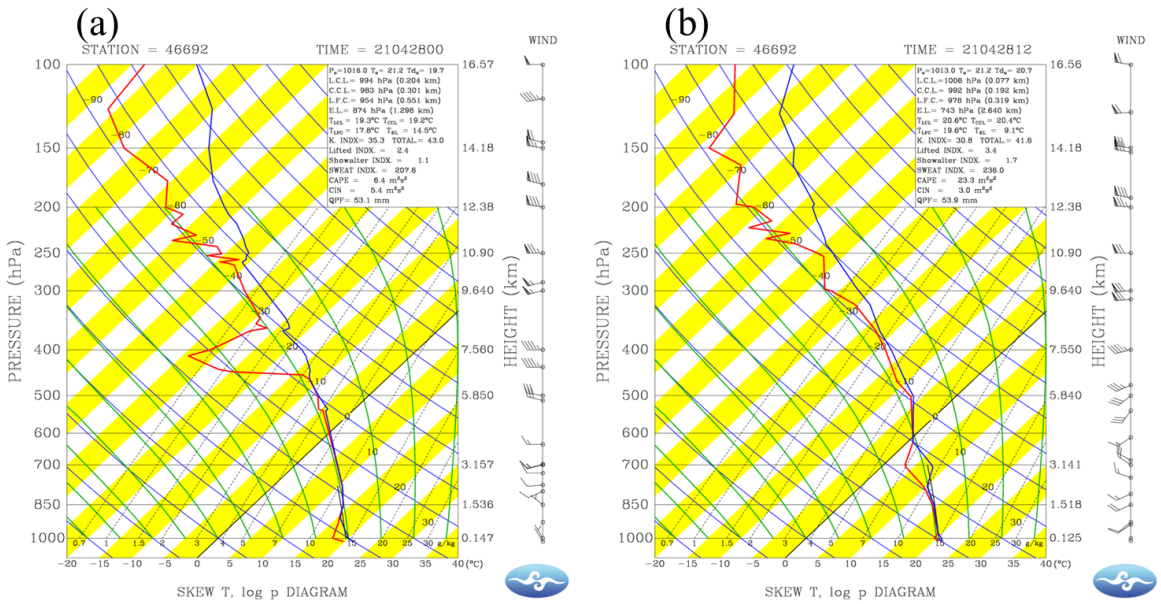

Figure 2.8 The skew T diagrams at (a) 00 and (b) 12 UTC on 28 April 2021. Source: CWB.

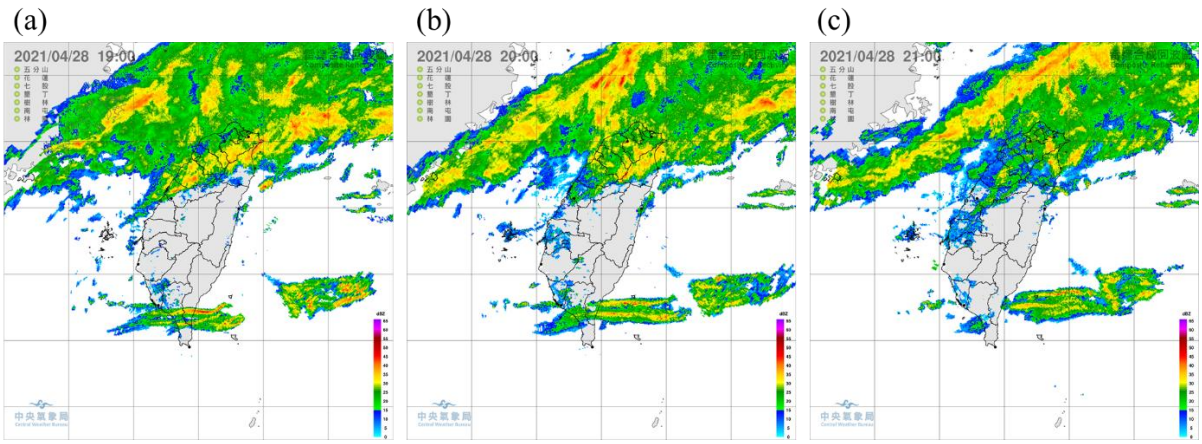

Figure 2.9 Composite maximum radar reflectivity at (a) 11:00 UTC, (b) 12:00 UTC, and (c) 13:00 UTC on 28 April 2021. Source: CWB.

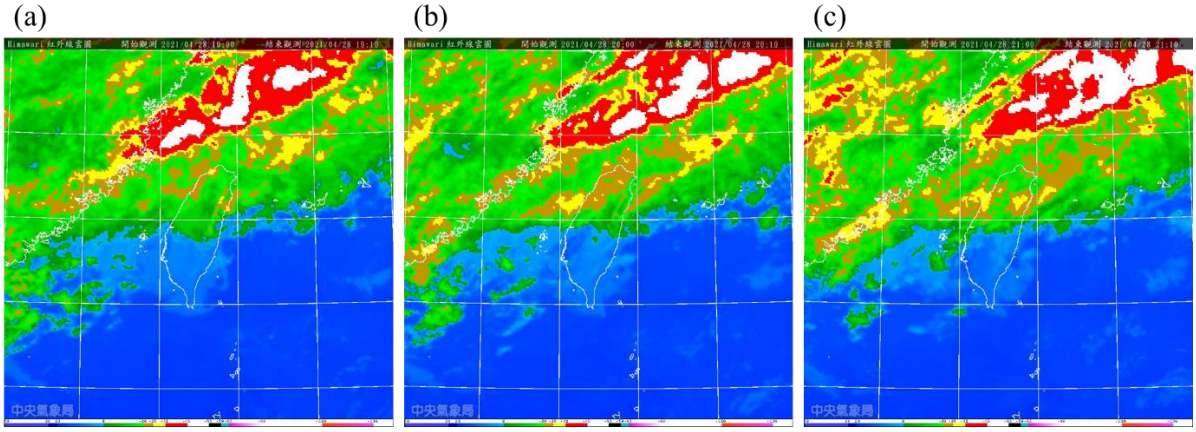

Figure 2.10 The infrared image of Himawari8 at (a) 11:00 UTC, (b) 12:00 UTC, and (c) 13:00 UTC on 28 April 2021. Source: CWB.

Chapter 3. Data and method

3.1 Dongyan Mountain cloud-seeding experiment

3.1.1 Experiment design and data description

Dongyan mountain is located at the region near Shihmen reservoir, which is extremely important to supply water resources in northern Taiwan. In addition, the site we choose to conduct the cloud-seeding experiment has the advantages of being located at a semi-enclosed area and nearing clouds base. Thus, this site is appropriate to investigate the impacts of the hygroscopic particles in clouds and to study the cloud-seeding effects near the Shihmen region. Figure 3.1 shows the location of the Dongyan mountain site.

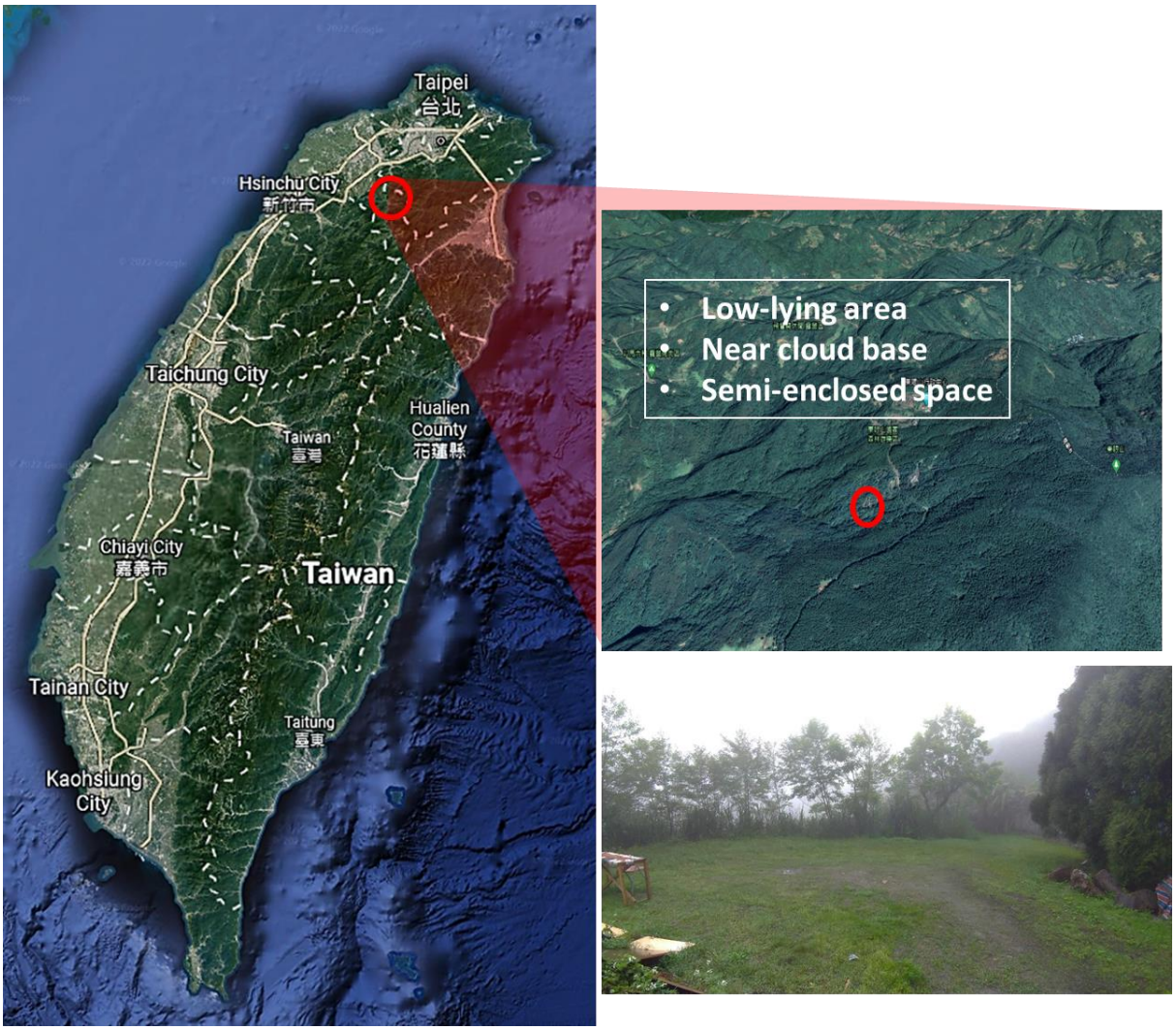

Figure 3.1 The location of Dongyan mountain site (Red circle).

In the Dongyan mountain cloud-seeding experiment, several instruments were deployed, including LWC-300, Aerosol Spectrometer (MODEL 11-D), Automatic weather stations, and Joss-Waldvogel Disdrometer (JWD). LWC-300, an instrument implemented by Droplet Measurement Technologies (DMT), is the hot-wire liquid water sensor that calculates liquid water content from the heat losses which is caused by the vaporization of water droplets that collide on the coiled wire maintained at 150 ° C. Aerosol Spectrometer (MODEL 11-D), developed by GRIMM, is based on the light scattering at single particles with diode laser to

resolve the particles with diameter ranging from 0.25 - 35.1 μm. Automatic weather stations, developed by Vaisala, is able to measure the basic parameters, e.g. temperature, pressure, relative humidity, etc. JWD takes the vertical momentum of raindrops impact on the surface of rubber membrane and evaluates the concentration of raindrops size from 0.359 – 5.373 mm. Table 2 gives the list and details of the instruments in this research. Figure 3.2 shows the pictures of the instruments.

Table 2 List and details of the instruments used in this research.

Instrument	**Measurement**	**Range**
LWC-300	Liquid water content	0-3 g m^{-3}
Aerosol Spectrometer (11-D)	Aerosol size distribution	0.25 – 35.1 μm
JWD	Droplets size distribution	0.359 – 5.373 mm
Automatic weather station	Basic parameters	

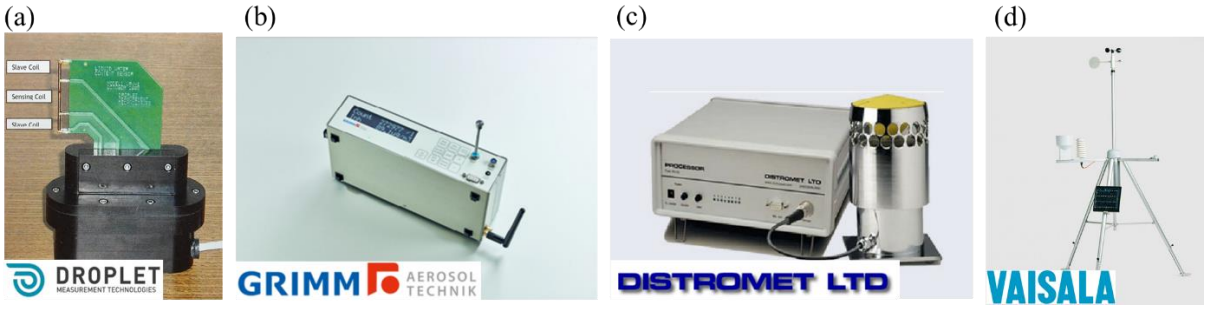

Figure 3.2 The pictures of the instruments, (a) LWC-300, (b) Aerosol Spectrometer (MODEL 11-D), (c) JWD, and (d) Automatic weather station.

Regarding the seeding agents, the hygroscopic cloud seeding agent named Chemical Systems Research Division (CSRD) flare, which developed by National Chung-Shan Institute of Science & Technology, is used in the experiment. The material in CSRD flare is mainly the component of NaCl. The combusted seeding agents of CSRD flare have been certified no

harmful to the environment.

In this research, two cases, including the case on 21 October 2020 and 28 April 2021, are selected to execute the Dogyan Mountain field campaign. In these 2 events of cloud-seeding experiments, 2 CSRD flares were burned in each experiment in the Dongyan Mountain site, which is about 800 m above mean sea level, and the instruments measured the data for each event during 20:00-22:00 UTC on 21 October 2020 (04:00-06:00 LST on 22 October 2020) and 11:00-13:00 UTC on 28 April 2021 (19:00-21:00 LST on 28 April 2021).

3.2 Chamber sampling experiment of seeding agent

3.2.1 Experimental description and design

The size distribution of CCN plays an influential role to affect cloud microphysics processes. Several studies mention that the different sizes of CCNs will cause the entirely different features of clouds and precipitation, e.g. Yin (2000), Bruintjes (2003), Segal et al. (2004), Rosenfeld and M. (2008), Rosenfeld et al. (2014), Guo et al. (2016), and Lee et al. (2016). According to the research above, the larger CCNs (larger than 2 μm) are optimal for increasing precipitation, but the high concentration of small CCNs can suppress rainfall or postpone the onset of precipitation. Therefore, the chamber sampling experiment was conducted to better characterize the size distribution of CCN, which is extremely important in the cloud-seeding experiment for both observation and model simulation.

In this experiment, ten combustions of small fraction CSRD seeding agents (about 0.3

gram of each piece) are conducted in the smoke chamber, which volume is about 62 liters, and the particles were sampled per 6 seconds by Aerosol Spectrometer (Model 11-D). To make the hygroscopic particles be evenly distributed in the chamber, five small fans are designed and set in the chamber (Figure 3.3 and Figure 3.4 (a)). In addition, there are totally 200 samples of CSRD seeding agents and 10 minutes between each burn, to ensure the consistency of the size distribution and reduce the bias of the sampling. Based on the design of chamber sampling experiment, the aerosol size distribution and concentration are able to be evaluated more accurately (the results show in section 4.2).

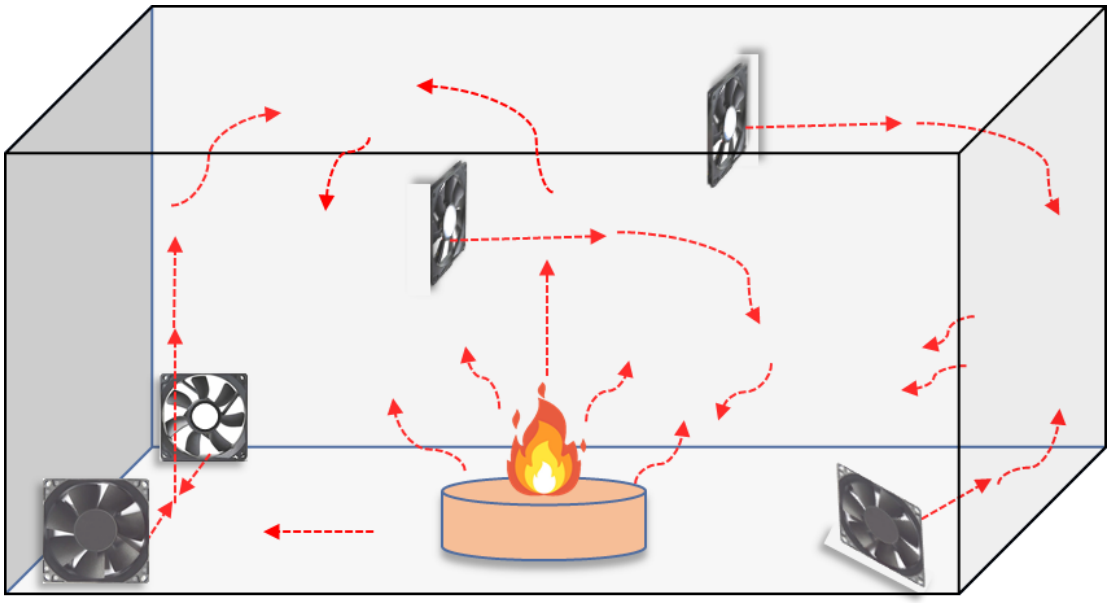

Figure 3.3 The schematic of designed chamber.

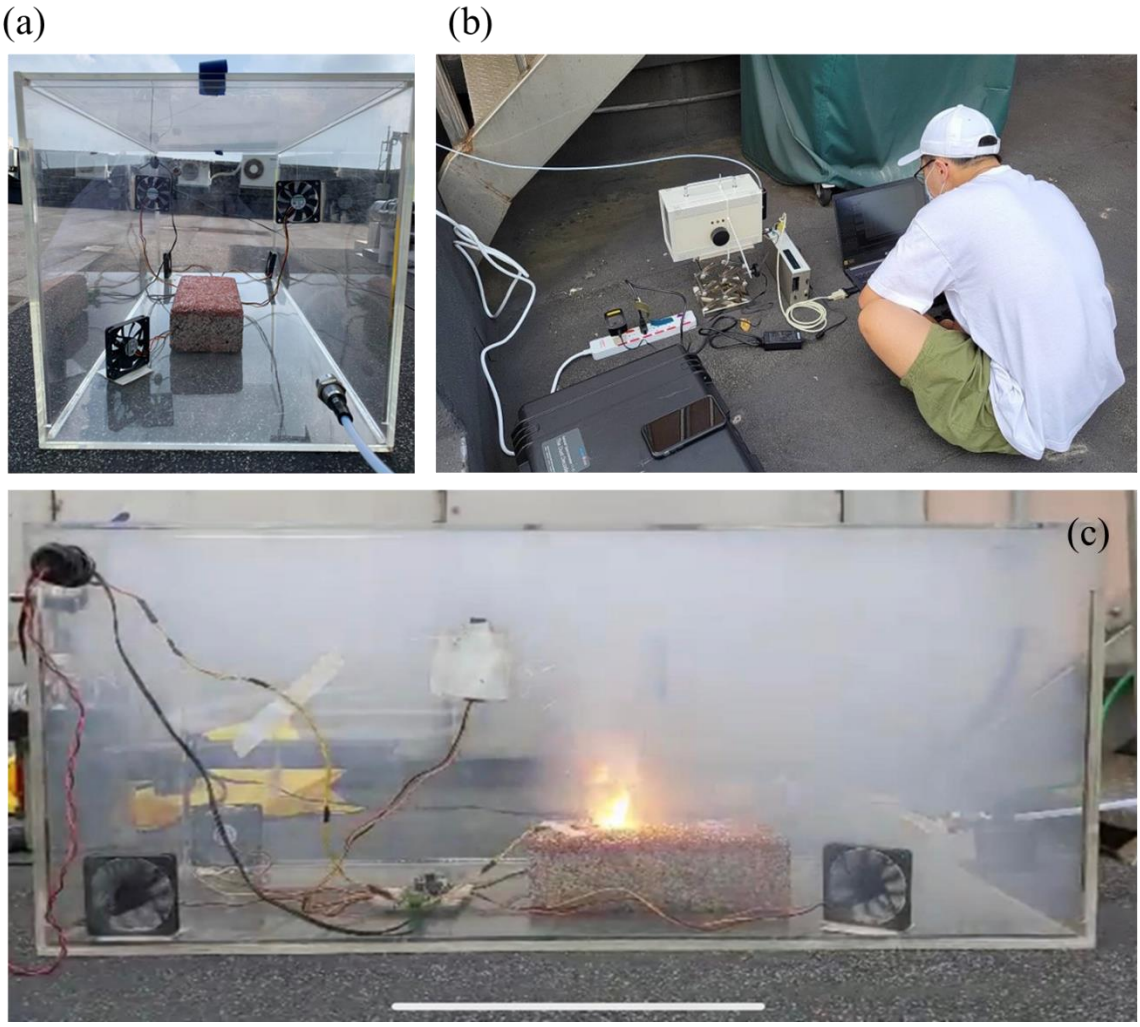

Figure 3.4 (a) The picture of our designed chamber and (b), (c) the experiment situation.

3.3 Model simulation of Miaopu validation experiment

3.3.1 Model configuration

This study uses the fully compressible and non-hydrostatic Weather Research and Forecasting (WRF) model version 3.9.1 to simulate 3-dimensional meteorologic parameters,

e.g. wind, perturbation potential temperature, water vapor, hydrometeor variables, etc. In the WRF model, it uses eta coordinate which allows the grids to follow the complex terrain and applies the third-order Runge Kutta numerical method for solving the time split integration of governing equation. In addition, the grids of simulation are engaged with Arakawa C grid, which makes the thermal parameters be arranged at the center grids but makes wind speed variables be arranged at the staggered grids.

In this research, five nested domains are built (Figure 3.5) with 52 vertical levels that are below 10 hPa and the horizontal resolutions are 27, 9, 3, 1, and 0.333 km corresponding to 190×151, 301×250, 301×301, 271×406, and 202×202. Besides, the initial and boundary conditions are generated from NCEP FNL operational model global tropospheric analysis with 0.25° resolution. Regarding the first to the fourth domain (D01-D04), the simulation is integrated from 12:00 UTC 21 October 2020 to 12:00 UTC 22 October 2020 with the time step of 90, 30, 10, and 10/3 s respectively. However, for the fifth domain (D05), it is simulated from 06:00 UTC 22 October 2020 to 09: 00 UTC 22 October 2020 with the timestep of 1 s. Figure 3.6 displays the timeline of the simulation.

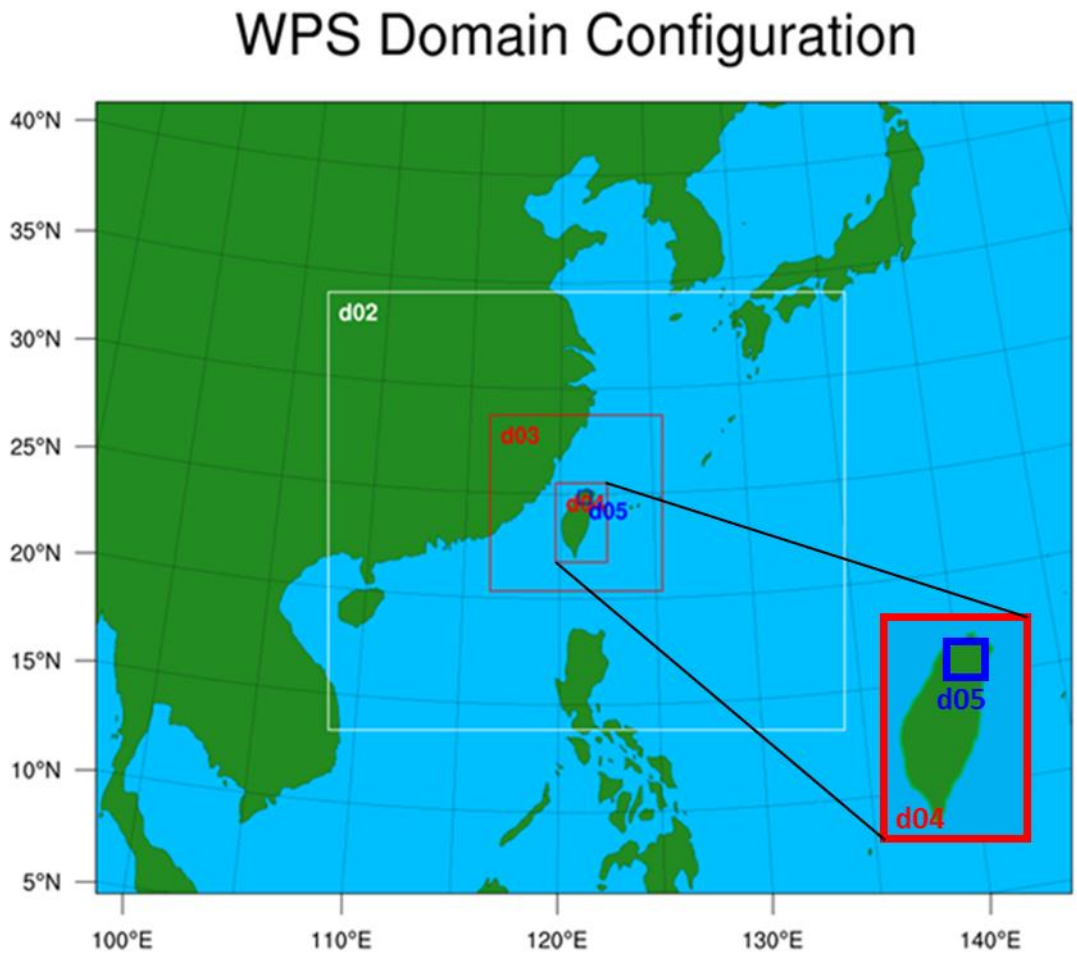

Figure 3.5 Setting of the nested domain. Five nested domains are built.

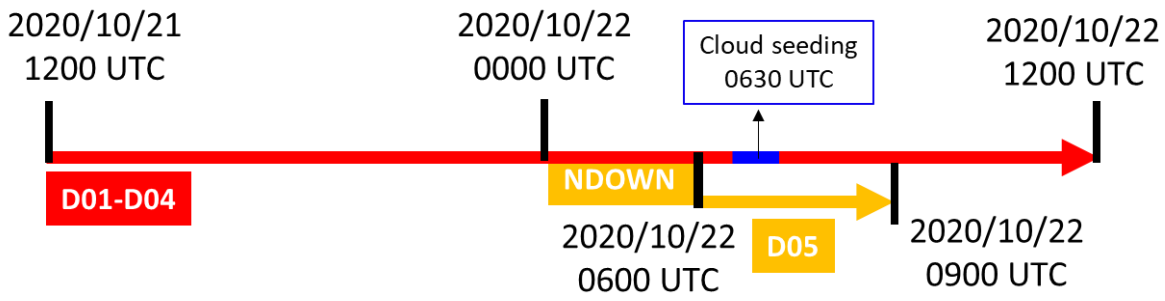

Figure 3.6 The schematic of the timeline in the simulation

The physics parameterizations used in this study include Rapid Radiative Transfer Model (RRTM) longwave scheme (Mlawer et al., 1997), Dudhia shortwave scheme (Dudhia, 1989), Yonsei University (YSU) planet boundary scheme (Hong et al., 2006), Grell Devenyi ensemble cumulus scheme (Grell and Dévényi, 2002), Monin-Obukhov land surface scheme (Monin and Obukhov, 1954), and WRF Double Moment 6-category scheme (Lim and Hong, 2010) modified by NCU (WDM6-NCU) microphysics scheme, which will be discussed in more details in Chapter 3.3. Regarding the cumulus scheme, it is only used in D01 and D02. For the planet boundary scheme, Yonsei University (YSU) is used in D01-D04 and Large Eddy Simulation (LES) is used in D05. Table 3 is the summary of the model configuration. According to Weigel et al. (2007) and Xue et al. (2014), the simulation with high-resolution (the resolution is smaller than 800 m) LES has the good ability to reproduce flow characteristics over complex terrain. Thus, the model configuration could have better simulation toward reality.

Table 3 The summary of the model configuration.

WRF 3.9.1	**D01**	**D02**	**D03**	**D04**	**D05**
Horizontal resolution	27 km	9 km	3 km	1 km	333 m
Timestep	90 s	30 s	10 s	10/3 s	1 s
Vertical level	52 eta levels				
Microphysics scheme	WDM6_NCU				
PBL scheme	YSU				LES
Initial and boundary condition	NCEP FNL (0.25˚× 0.25˚)				

3.3.2 The WDM6 scheme (Lim and Hong, 2010)

The WDM6 scheme is a semi-double-moment bulk microphysics scheme, that cloud

droplets and raindrops are able to be prognosed not only mixing ratio but also number concentration, and the cloud-raindrop size distribution are assumed to follow the function as

$$n_x = N_x \frac{\alpha_x}{\Gamma(\mu_x)} \lambda_x^{\alpha_x \mu_x} D_x^{\alpha_x \mu_x - 1} e^{-(\lambda_x D_x)^{\alpha_x}}, \quad (1)$$

in which the x represents the type of hydrometeor, including clouds and rain. In Eq. (1), λ_x, μ_x, and α_x are slope parameter and two dispersion parameters respectively, and N_x and D_x represent the predicted value of total number concentration and diameter of the certain hydrometeor category. Moreover, the dispersion parameters of rain, μ_R, and α_R, are set as 2 and 1 which provide the advantage of simulating the more reasonable shape of raindrop size distribution.

Moreover, for CCNs effects, the relationship of the number of activated CCN (n_a) and the supersaturation (S_w) is used in WDM6 as the following equation (Twomey's relationship):

$$n_a = (n + N_c)\left(\frac{S_w}{S_{max}}\right)^k, \quad (2)$$

where n, Nc, and S_{max} are the total CCN number concentration, the cloud droplets number concentration, and the supersaturation needed to activate the total particle count respectively. In Eq. (2), k is typically set as the range from 0.3 to 1.0. In addition, in order to predict the production rate of the cloud water mixing ratio by the CCN activation (P_{cact}), it can be expressed as

$$P_{cact} = \frac{4\pi\rho_w}{3\rho_a} r_{act}^3 \times n_a \quad , \quad (3)$$

where ρ_w and ρ_a are the density of water and air. Besides, in Eq. (3), r_{act} is the radius for activated droplets, which is set as the fixed value, 1.5 μm, in WDM6. In fact, seldom of microphysics

schemes have the ability to describe CCNs effects. Therefore, the WDM6 scheme gives us the opportunity to improve the method of evaluating CCNs effects and investigate the hygroscopic cloud-seeding effects.

3.3.3 The WDM6-NCU scheme

Because the cloud-seeding impacts is extremely sensitive on the CCNs size distribution and the value r_{act}, therefore, in WDM6-NCU microphysics scheme, more precisely method, that the seeded CCNs are described by 43 size bins (Bin-resolving method), is used to evaluate CCNs effects. Figure 3.7 displays the schematic of the two different methods to describe aerosol size distribution. In addition, the size distribution of the seeded CCNs is based on the sampling measurement in a chamber as mentioned in section 3.2 and section 4.2, which is fitted into a trimodal lognormal function as

$$\frac{dN}{d\ lnr_n} = \sum_{i=1}^{3} \frac{n_i}{\sqrt{2\pi}\ log\sigma_i\ ln10} \exp\left[-\left(\frac{lnr_n - lnR_i}{\sqrt{2}\ ln\sigma_i}\right)^2\right], \quad (4)$$

where r_n, n_i, R_i, and σ_i are the radius of the particle, the total number concentration, geometric mean radius, and geometric standard deviation for each mode (indicated by subscript i). The complete CCNs size distribution can provide the advantage to precisely calculate the critical radius based on Köhler theory, and the bins of CCNs extending the critical radius will be able to be activated to the corresponding liquid bins. The function of critical radius (r_{cr}) can be expressed as

$$r_{cr} = \frac{A}{3}\left(\frac{4}{BS_w{}^2}\right)^{1/3}, \quad (5)$$

where A is the parameter that relates to temperature, B is the parameter standing for different chemical matters, and S_w represents the supersaturation ratio. After calculating the number concentration and mixing ratio of the liquid bins, they will be contributed to the mixing ratio and number concentration of cloud and rain, and the microphysics processes will continue as the original WDM6. Thus, in WDM6-NCU, it has the advantages of not only reasonably taking CCNs effects into consideration but also helpfully investigating the cloud-seeding impacts.

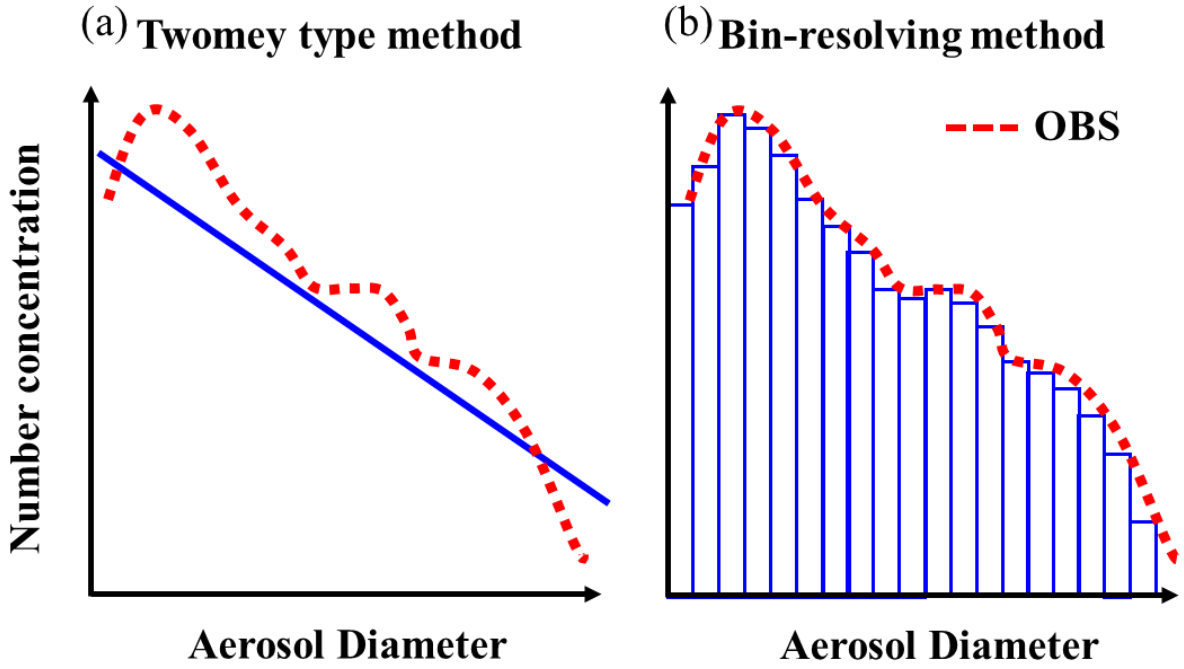

Figure 3.7 the schematic of the two different methods to describe aerosol size distribution. (a) Twomey type method is used in the WDM6, and (b) bin-resolving method is used in WDM6-NCU.

3.3.4 Experiment design

Regarding the model experiment, two parallel sets of realizations, including a control

simulation without seeding (Control run) and a set of experiments with the emission of seeding agents (Seed run) with CSRD size distribution (Section 4.2: Figure 4.14), are created to analyze the effects which caused by the aerosol perturbation. In addition, this study attempts to examine the impacts of executing cloud seeding in different heights and areas. Thus, in domain four (D04; 1 km horizontal resolution), five simulations are developed, including one Control run (Ctrl) and four Seed runs (Seed1 to Seed4), to study the cloud seeding effects that introducing hygroscopic particles into one horizontal grid (1 km × 1 km) at different seeding levels. In Seed 1, it seeds at about 500 m above mean sea level (cloud base), which is the most similar run to the field experiment. Seed 2 and Seed 3 are the simulation seeding between 1000 to 2000 m, and Seed 4 seeds at about 2200 m. The model experiments in D04 are summarized in Table 4.

Table 4 The summary of the experimental design in domain four (D04).

Experiment	**Description**	**Seeding area (km^2)**	**Seeding height (η/m)**
Ctrl	Normal aerosol concentration	none	None
Seed 1	Introduce CCN (with CSRD size distribution) into a certain region.	1 km^2	0.9865/500 m
Seed 2			0.9365/1000 m
Seed 3			0.905/1300 m
Seed 4			0.824/2200 m

However, the resolution of 1 km sometimes is not precise enough to interpret the microphysical products, and several studies attempt to investigate cloud-seeding effects by the simulation with finer grid resolution, e.g. Yin (2000), Tonttila et al. (2021), and Xue et al. (2014). Thus, this study develops domain five (D05) with a horizontal resolution of 333 m aims to explore much more detail of microphysics properties. The seeding heights in D05 are based on the results of D04, and two levels, which increase the least and the most rainfall in D04, are chosen (500 m and 1300 m are selected). Six runs are developed to introduce hygroscopic

particles in different areas, including 1, 10, 100 km^2, at these two seeding levels we chose. In addition, more two runs seeding in 1 km^2 but 100 times concentration of seeding agents are created. The model experiments in D05 are summarized in Table 5. The flow chart of the experimental procedure is given in Figure 3.8.

Table 5 The summary of the experimental design in domain five (D05).

Experiment	**Description**	**MUL factor of Concentration**	**Seeding area (km^2)**	**Seeding height (η/m)**
Ctrl	Normal aerosol concentration	none	none	None
Seed_500(1km^2)	Introduce CCN (with CSRD size distribution) into a certain region.	×1	1 km^2	0.9865/500 m
Seed_500(10km^2)			10 km^2	
Seed_500(100km^2)			100 km^2	
Seed_500(1km^2)_HC		×100	1 km^2	
Seed_1300(1km^2)		×1	1 km^2	0.905/1300 m
Seed_1300(10km^2)			10 km^2	
Seed_1300(100km^2)			100 km^2	
Seed_1300(1km^2)_HC		×100	1 km^2	

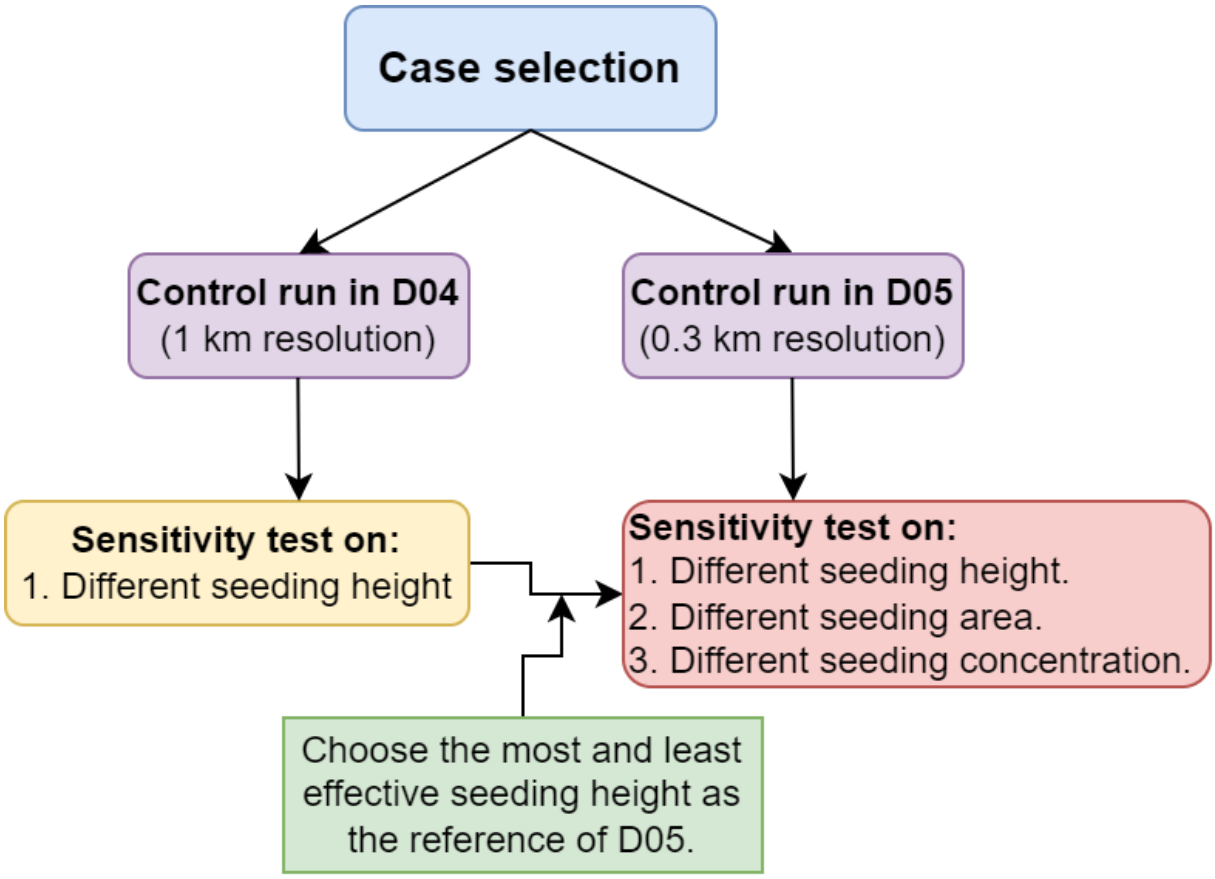

Figure 3.8 The schematic of the experiment design in the model simulation.

Chapter 4. Results and discussion

This study investigates the direct observational evidence after doing cloud seeding by Dongyan Mountain cloud-seeding experiment (the results show in section 4.1). In addition, to better characterize the CCN size distribution of the flare agents, the chamber sampling experiment was conducted (the results show in section 4.2). After achieving the CCN size distribution, it was applied to the model simulation with the hybrid cloud-seeding microphysics scheme, WDM6-NCU, and conducted a series of sensitivity tests on cloud seeding (the results show in section 4.3 and section 4.4). Finally, the suggestions for the criteria of cloud seeding are made (the results show in section 4.5).

4.1 Dongyan mountain cloud-seeding experiment

In this research, two cases, including the case on 21 October 2020 and 28 April 2021 (more details are discussed in Chapter 2: Case overview), are selected to execute the Dogyan Mountain cloud-seeding experiment. Table 6 displays the list of instruments in each event.

Table 6 The list of instruments in each event.

Case	Instrument
2020/10/21 20:00-22:00 UTC	LWC-300, 11-D, AMS
2021/04/28 11:00-13:00 UTC	LWC-300, 11-D, AMS, JWD

4.1.1 Case1 on 2020/10/22

In this event, two CSRD flares were combusted at 04:45 LST and 05:00 LST on 22 October 2020, and two seeded periods are defined as the intervals of 15 minutes after doing cloud seeding. In addition, the pre-seeding period and post-seeding period are the times of 20 minutes before the first seeded period and after the second seeded period respectively. During the experimental period, the environment was relatively calm, and the relative humidity was higher than 90 %.

Figure 4.1 shows the time series of aerosol size distribution and the four defined intervals that correspond to the different colors. It is obvious that the aerosol concentration becomes much higher after doing cloud seeding (Figure 4.1 and Figure 4.2). According to Figure 4.1 and Figure 4.2, the aerosol concentration in the first seeded period is much higher than the second seeded period, which means more hygroscopic particles were trapped in the Dongyan mountain site in the first seeded time. Therefore, the first seeded period is probably the better time to study the impacts of in-cloud hygroscopic aerosols, and this research also focuses on this interval in this event.

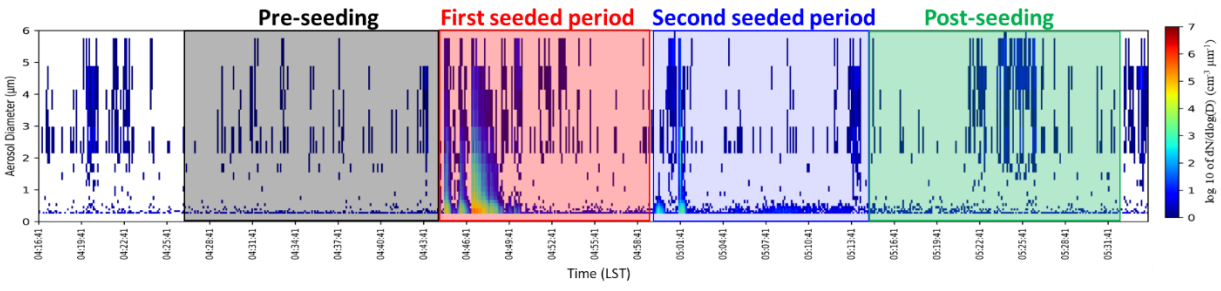

Figure 4.1 The time series (LST) of aerosol size distribution and the four defined periods that

correspond to the four different colors (Pre-seeding: black; First seeded: red; Second seeded: blue; Post-seeding: green).

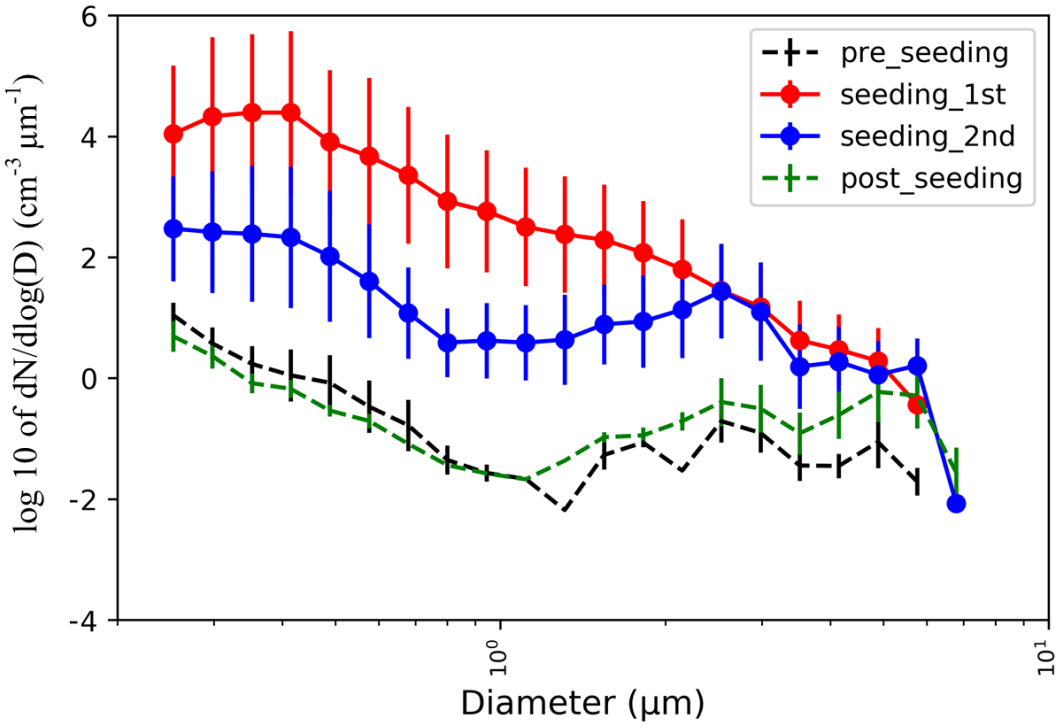

Figure 4.2 The average aerosol size distribution in four different periods that correspond to the four different colors (Pre-seeding: black; First seeded: red; Second seeded: blue; Post-seeding: green). The error bars represent the value of one standard deviation.

Figure 4.3 illustrates the increasing of liquid water content (LWC) (Figure 4.3: red arrow) that corresponds to the decrease of mixing ratio of water vapor (Figure 4.3: black arrow) during the first seeded period. This phenomenon is able to be interpreted by the competition effect, which is the process that the hygroscopic particles compete for water vapor to be activated to cloud droplets. In addition, there is a signal of temperature increment (Figure 4.3: pink arrow) in the first seeded period that seems to imply the latent heat release caused by the condensation process.

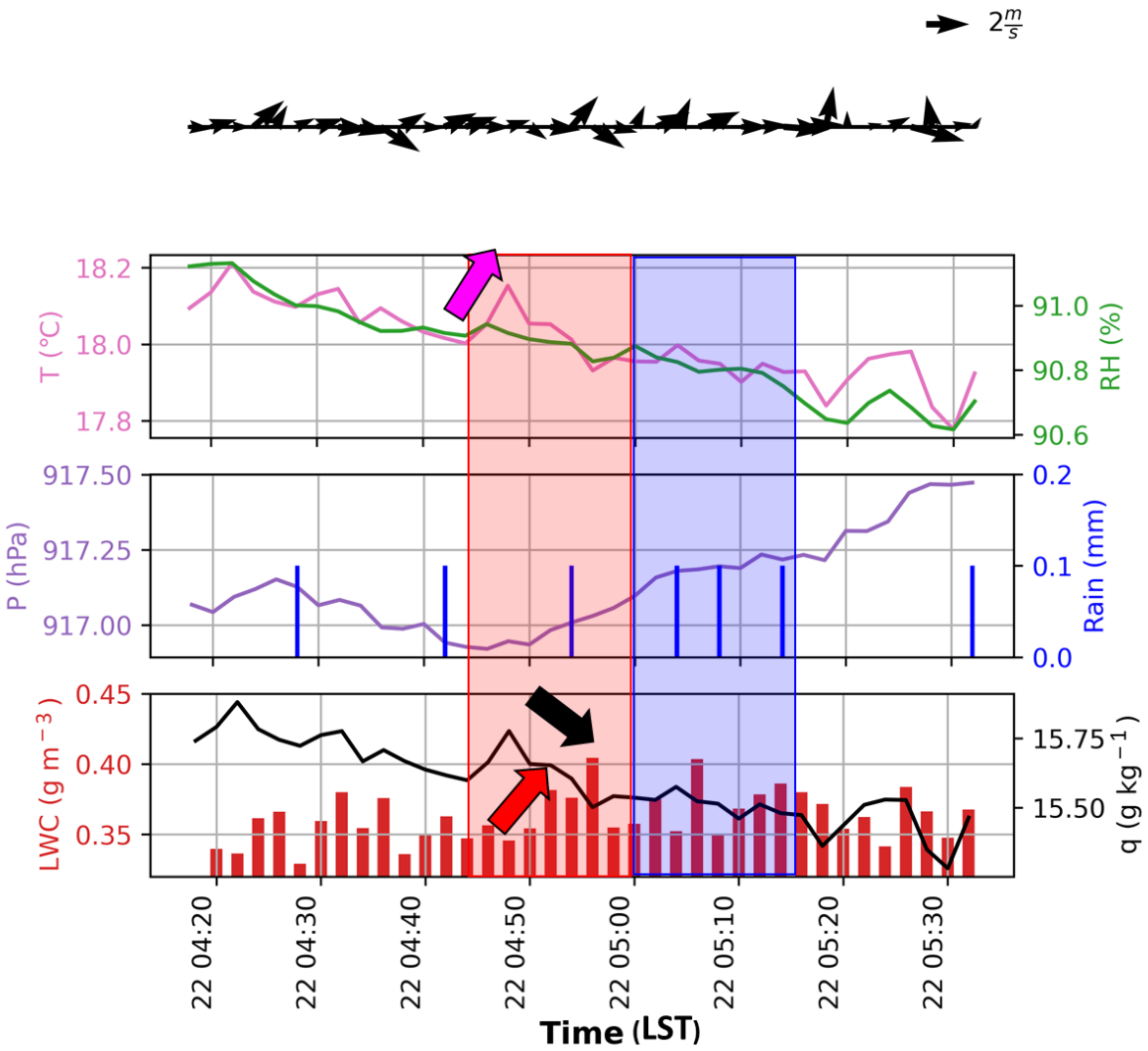

Figure 4.3 The time series (LST) of several parameters provided by AMS (Vaisala) and LWC-300. The shaded of red and blue means the periods of first and second seeded time.

In order to prove the existence of the condensation process, the equation of the pseudo adiabatic process relating to temperature variation (dT) is used to examine whether the increment of temperature in the first seeded period is reasonable. The equation of the pseudo adiabatic process is described as

$$\frac{dT}{T} = \frac{1}{\rho}\left(K \times \frac{dP}{P} - \frac{L}{T \times Cp} \times dw\right), \quad (6)$$

where T, ρ, P, dP, and dw are environment temperature, air density, pressure, the variation of pressure, and the variation of water content respectively. In Eq.6, K and C_p are the constant, and L is 2453 (J g^{-1}) in this event. According to Eq.6, the variation of temperature is about 0.11 K, if the assumption of dw that equals 0.05 g m^{-3}, which represents the increment of LWC in the first seeded period, is made. Thus, having this additional evidence gives us more confidence that the condensation process is strengthened after doing cloud seeding.

4.1.2 Case2 on 2021/04/28

Also, in this event, two CSRD flares are combusted at 19:48 LST and 20:22 LST on 28 April 2021, and two seeded periods are defined as the intervals of 20 minutes after doing cloud seeding. In addition, the pre-seeding period and post-seeding period are the times of 20 minutes before the first seeded period and after the second seeded period respectively. During the experimental period, the environment was relatively calm, and the relative humidity was higher than 90 %.

Figure 4.4 shows the time series of aerosol size distribution and the four defined intervals that correspond to the different colors. As expected, the aerosol concentration becomes much higher after doing cloud seeding (Figure 4.4 and Figure 4.5). Moreover, due to the almost calm environment (Figure 4.6: wind bar), the hygroscopic particles are surprisingly stagnant suspension around the experimental site in both seeded periods, particularly for the first seeded period.

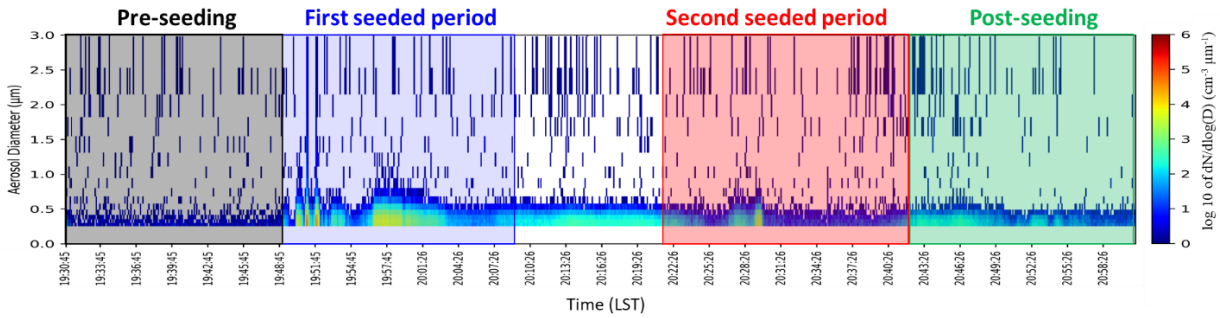

Figure 4.4 The time series (LST) of aerosol size distribution and the four defined periods that correspond to the four different colors (Pre-seeding: black; First seeded: blue; Second seeded: red; Post-seeding: green)..

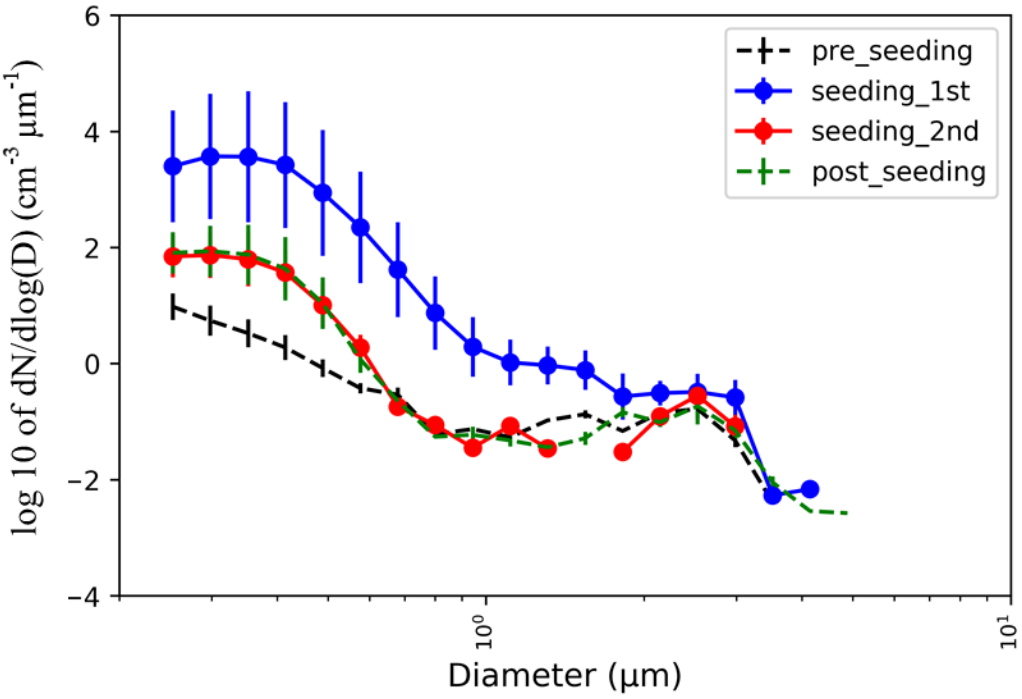

Figure 4.5 The average aerosol size distribution in four different periods that correspond to the four different colors (Pre-seeding: black; First seeded: red; Second seeded: blue; Post-seeding: green). The error bars represent the value of one standard deviation.

However, though the decrease of water vapor mixing ratio (Figure 4.6: black arrow) and the enhancement of liquid water content (LWC) (Figure 4.6: red arrow) is still found in this event, there are not the signals of the increase of temperature as that we saw in Case1. We believe that due to the higher LWC in Case2 (~0.4-0.5 g m^{-3}) than Case1 (~0.3-0.4 g m^{-3}), the hygroscopic particles will probably experience totally different microphysics process. For instance, in the higher LWC environment, after the hygroscopic particles go through the activation process, they will directly turn into droplets and grow up by the collision-coalescence process but not the condensation process. It might be the reason that there are no obvious features of the condensation process (e.g. involving latent heat release and the enhancement of liquid water) in this case. Besides, regarding the raindrops size distribution observed by JWD (Figure 4.7), the number concentration of droplets that ranges from 1 to 1.5 mm increases in the second seeded period.

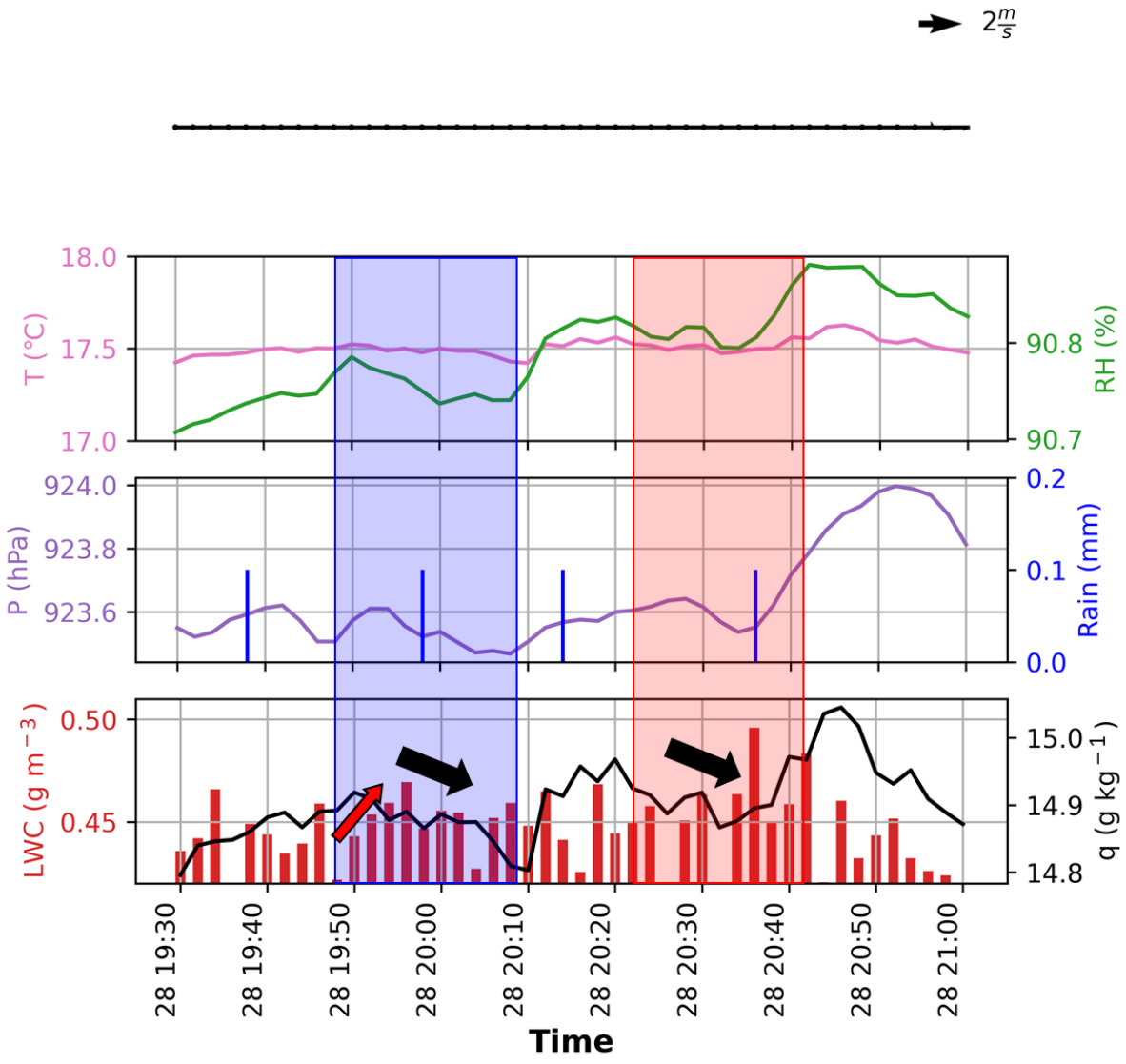

Figure 4.6 The time series (LST) of several parameters provided by AMS (Vaisala) and LWC-300. The shaded of blue and red means the periods of first and second seeded time.

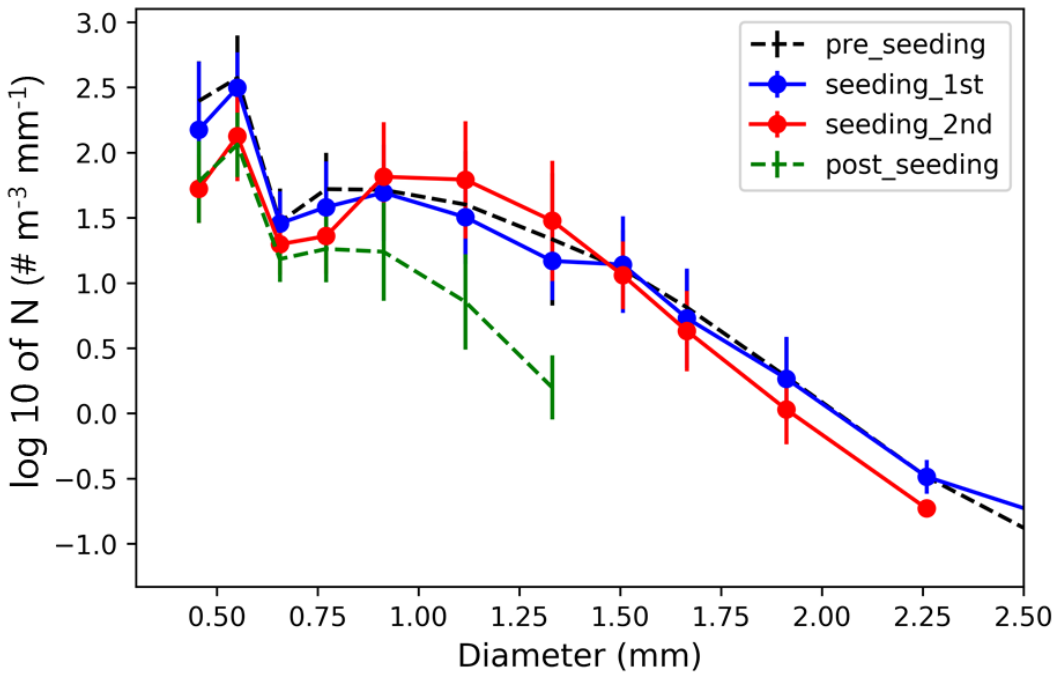

Figure 4.7 The average raindrops size distribution in four different periods that correspond to the four different colors (Pre-seeding: black; First seeded: red; Second seeded: blue; Post-seeding: green). The error bars represent the value of one standard deviation.

Furthermore, this research also compares the JWD data of the Dongyan mountain site to the data of the Xiayunping site, which is about 5 km far from the Dongyan mountain site (Figure 4.8). The Xiayunping site is not only close to the Dongyan mountain site but also has a similar rainfall pattern during the experiment (Figure 4.9). In this case, the Xiayunping site is located upstream so that precipitation happened about 4 minutes earlier than the Dongyan mountain site. After shifting the data of the Xiayunping site to correspond to the rainfall periods of the Dongyan mountain site, the correlation coefficient reaches to 0.89 (Figure 4.10) as compared to 0.76 without shifting (Figure 4.9). Therefore, the Xiayunping site must be a great reference point to investigate the cloud-seeding impacts on raindrops in the Dongyan mountain site. In order to evaluate the effects of cloud seeding on raindrops, the following function (Eq. 7) is

used and described as

$$\text{Fraction} = \frac{N_{i,Dongyan} - N_{i,Xiayunping}}{N_{t,Xiayunping}}, \quad (7)$$

where $N_{i,\ Dongyan}$, $N_{i,\ Xiayunping}$, and $N_{t,\ Xiayunping}$ represent the raindrops number concentration of a particular bin (*i*) in the Dongyan mountain site, the raindrops number concentration of a particular bin (*i*) in the Xiayunping site, and the total (*t*) raindrops number concentration in the Xiayunping site respectively. By Eq.7, the fraction can be calculated per minute as Figure 4.11, and it depicts that the fraction of each bin before doing cloud seeding is mainly negative (Figure 4.11: blue color). However, the fraction of several bins turns positive (Figure 4.11: the red color grids pointed by red arrows) after doing cloud seeding. This result suggests that those hygroscopic particles cause more raindrops to be developed in the Dongyan mountain site.

Figure 4.8 The map of the Dongyan mountain site and the Xiayunping site.

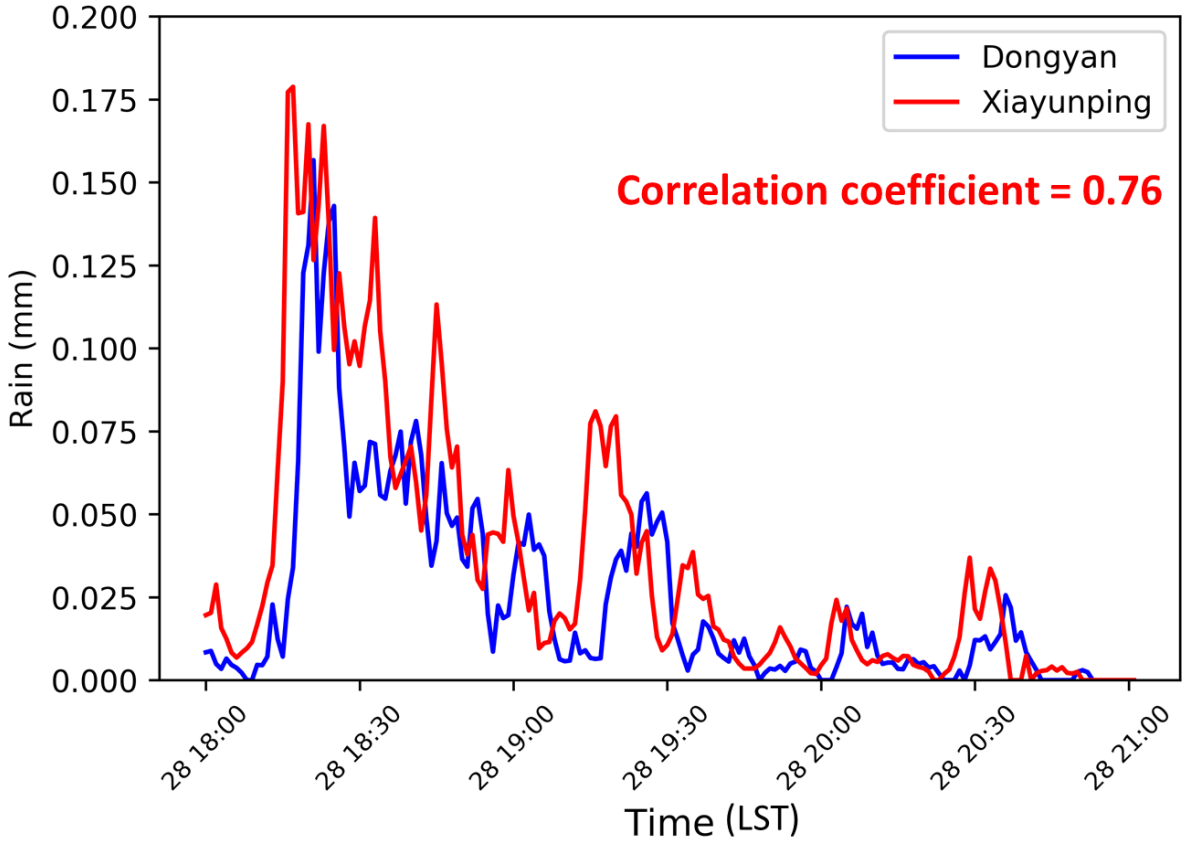

Figure 4.9 The time series (LST) of rainfall in the Dongyan mountain site (blue line) and the Xiayunping site (red line).

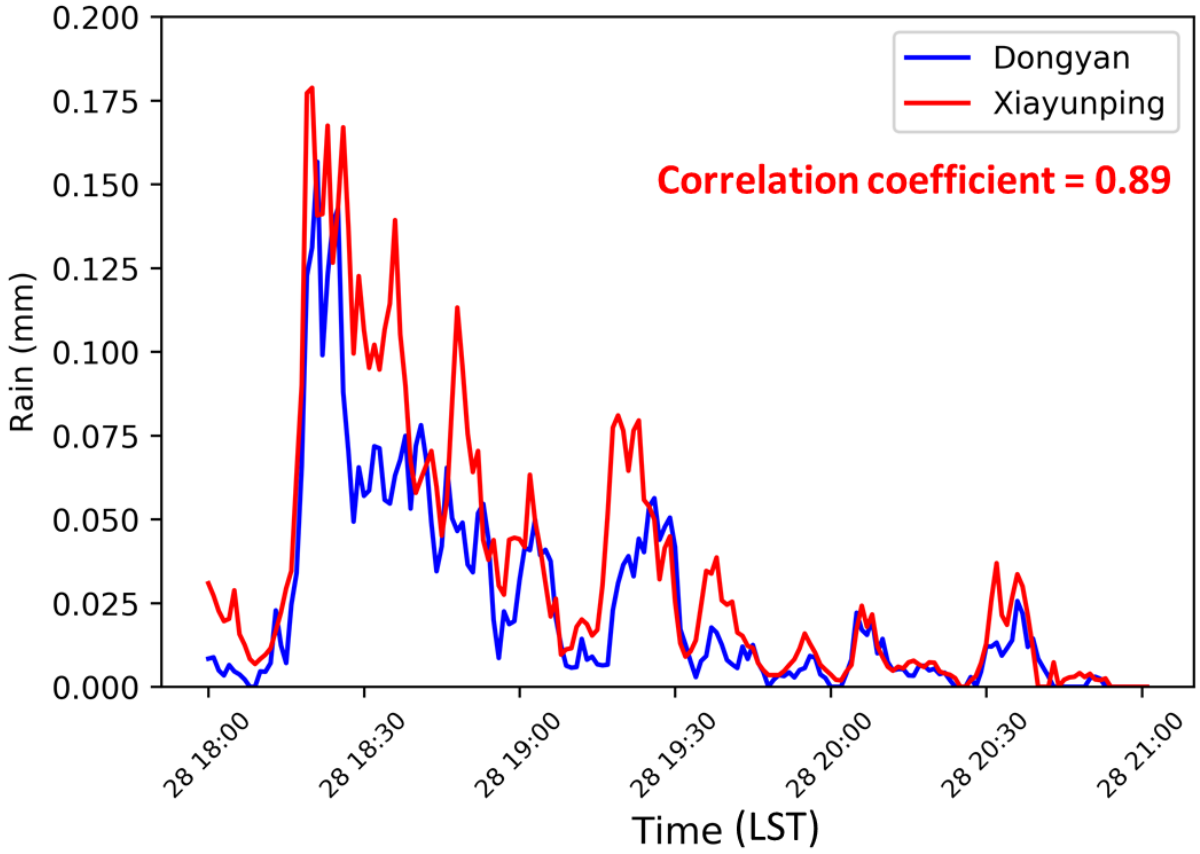

Figure 4.10 The time series (LST) of rainfall in the Dongyan mountain site (blue line) and the Xiayunping site (red line) which data is shifted 4 minutes later.

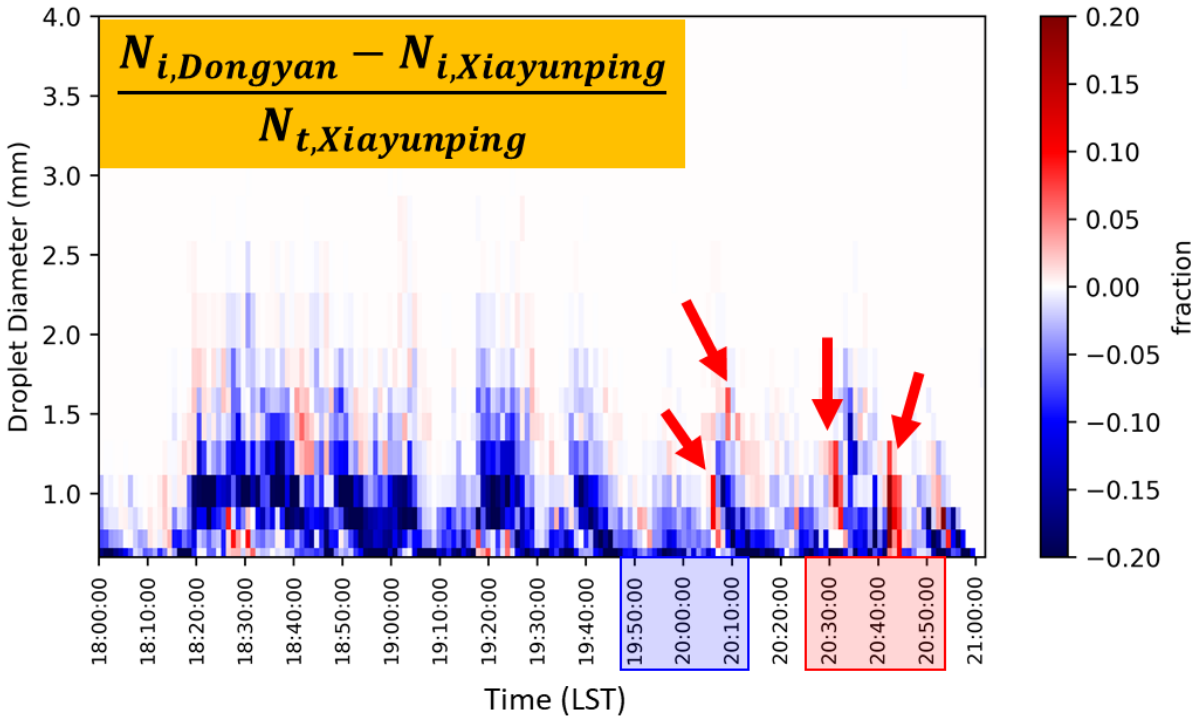

Figure 4.11 The time series (LST) of raindrops variation fraction, which is calculated by Eq.7, in each bin. The blue and red shaded in x-ticks present the first and second seeded period.

4.2 Chamber sampling experiment of seeding agent

4.2.1 The size distribution and number concentration of the seeding agent

Figure 4.12 displays the time series of aerosol spectrum, and it depicts that there are ten sampling periods of the seeding agents. After averaging the size distribution of those periods and removing the concentration of background, which calculates the mean value of one-hour sampling before combusting the seeding agents (Figure 4.13: black dash line), the size distribution of CSRD can be evaluated. The result shows that most of the seeding agents are

smaller than 1 μm.

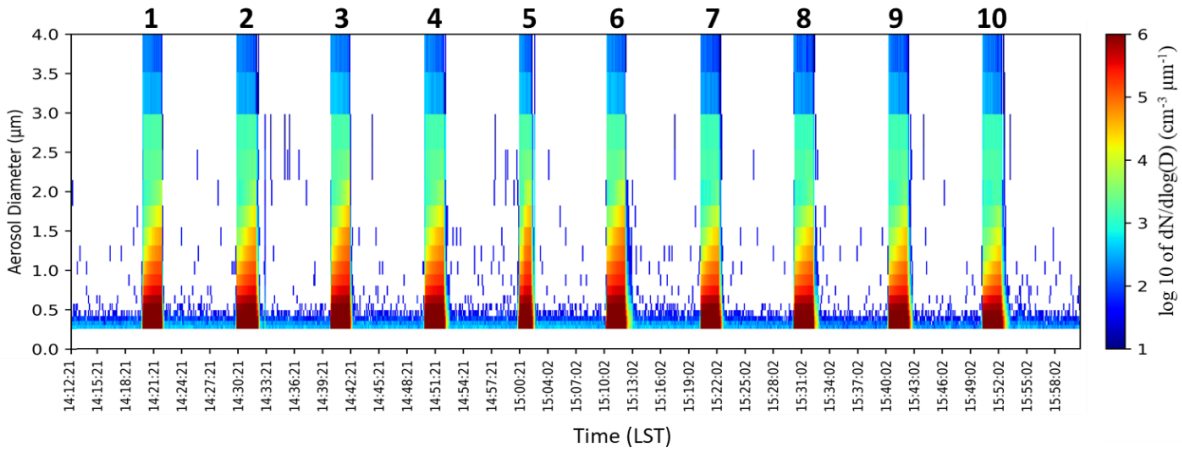

Figure 4.12 The time series (LST) of aerosol size distribution and the ten sampling periods of the seeding agents.

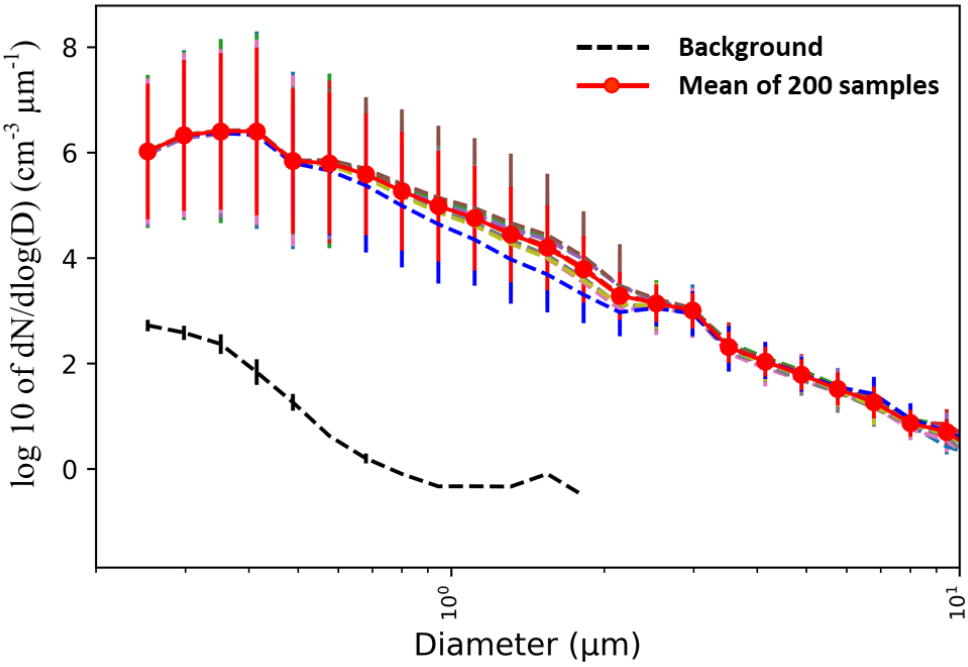

Figure 4.13 The average aerosol size distribution of ten sampling periods of the seeding agents (red line) and the aerosol size distribution of background (black dashed line).

In the chamber sampling experiment, a mass fraction of ~1/2000 CSRD seeding agent was combusted in a 62 liters volume (V) chamber, and was sampled by Aerosol Spectrometer (11-D). Though the size distribution of CSRD can be directly known, the number concentration estimated by Aerosol Spectrometer (N) in the chamber sampling experiment must be far from the concentration of operational experiments (e.g. Dongyan Mountain cloud-seeding experiment and Miaopu validation experiment), because not only the combusted mass of seeding agents but the volume of spreading domain in this experiment are different from the fie. In order to evaluate the number concentration closed to the operational experiments (N^*), the assumptions of about 10 complete CSRD flares are burned and the hygroscopic particles are evenly distributed in a slab of about 100 m × 100 m and 10 m in depth are made. Thus, the number concentration closed to the reality (N^*) can be estimated as a function of the number concentration estimated by Aerosol Spectrometer (N), and the volume of chamber (V) as

$$N^* = N \times 2000 \times 10 \times \frac{V(liter)}{10^8(liter)}, \qquad (8)$$

and the N^* is closed to the value that N multiplies 1/100, known as the diluted factor of 100. The diluted factor of 100 was also used in the numerical study by Cooper (1997) and Tessendorf et al. (2021). After figuring out the information of both number concentration and size distribution of CSRD seeding agent, they can be applied to the model simulation as the trimodal lognormal types (Eq. 4) CCNs size distribution (Figure 4.14: red line). Later, we further apply the observed aerosol concentration and size distribution to the model simulation.

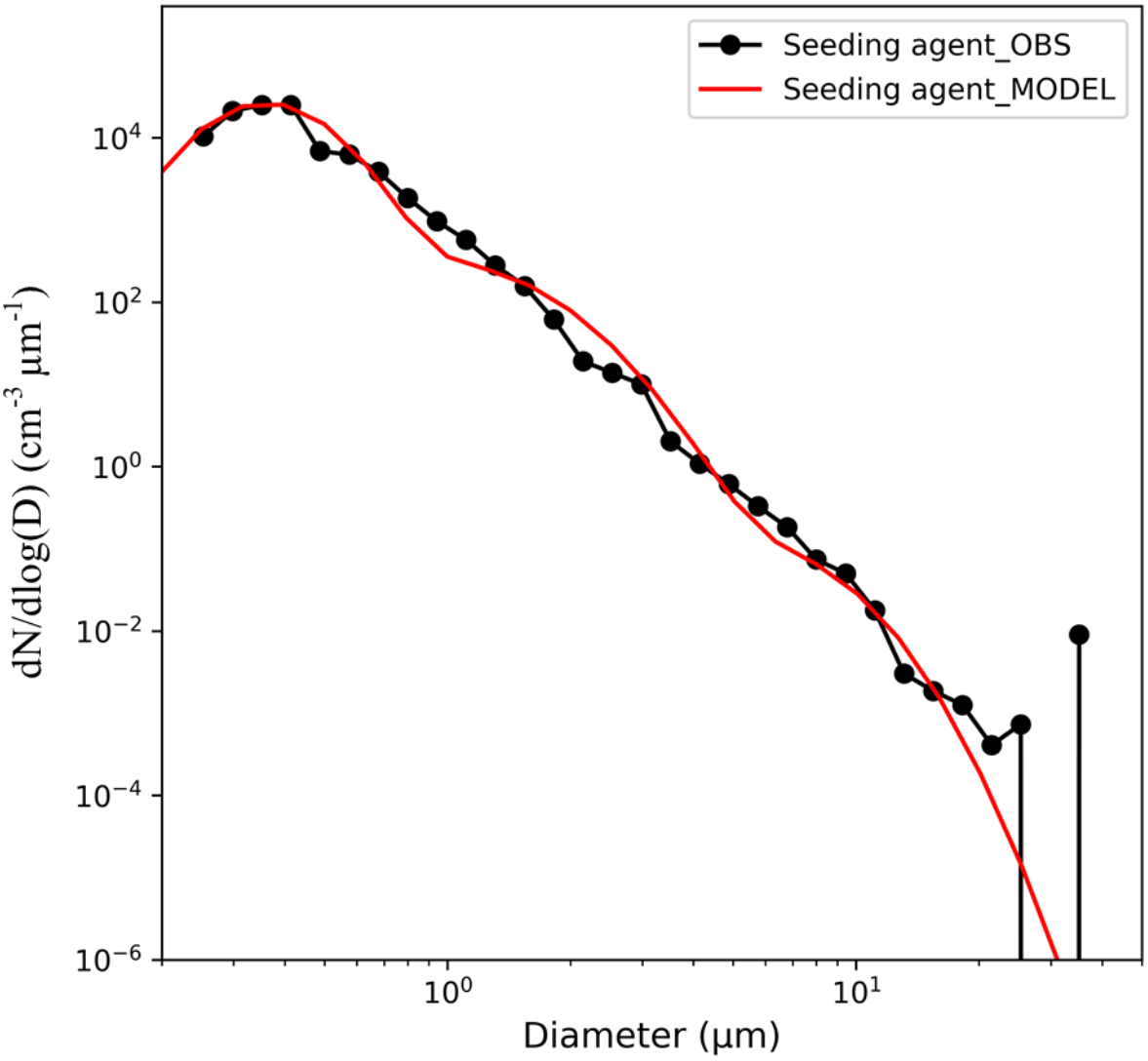

Figure 4.14 The CCNs size distribution (red line), which is based on the observation result (black line), applies in the model simulation.

4.3 Modeling of Miaopu validation experiment in 1 km horizontal resolution domain

4.3.1 Control run (Ctrl)

Before doing the sensitivity test, the comparison between control run and observation is conducted to make sure that the simulation is close to reality. In this research, it takes accumulative rainfall, radar reflectivity, water vapor mixing ratio, temperature, and pressure into consideration. Regarding accumulative rainfall (Figure 4.15), the main features of it are successfully captured by the model, particularly in northern Taiwan where we are interested. Moreover, in order to consider the precipitation pattern with height, the radar reflectivity of RCWF is used. Figure 4.16 and Figure 4.17 depict the radar reflectivity of RCWF and model simulation respectively, and both of them present that most of the reflectivity appears below 5 km, which implies the precipitation is dominated by warm-rain processes. The intensity and location of the simulated and observed reflectivity are also close. Furthermore, the similarity of temperature, pressure, and water vapor mixing ratio between the observational data and a simulated data in the Dongyan mountain site are found (Figure 4.18). Overall, the simulation well captures the atmospheric condition and features of this event. In addition, Figure 4.19 displays the meridional mean (0.1° of latitude cross the Shihmen) of liquid water content (LWC) at 06:30 UTC on 22 October 2020, and depicts the cloud base is at about 500 m height above the mean sea level.

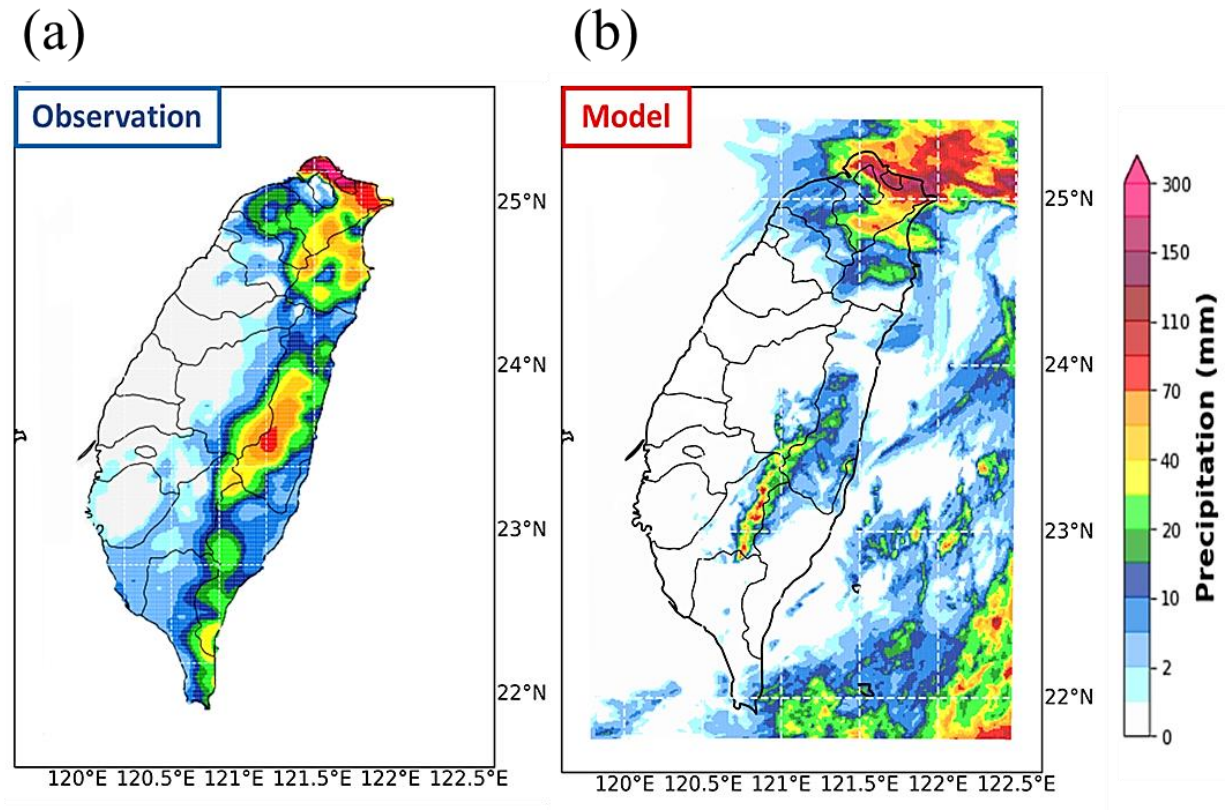

Figure 4.15 The accumulative rainfall of (a) observation and (b) model simulation from 2020/10/21 12:00 UTC to 2020/10/22 12:00 UTC.

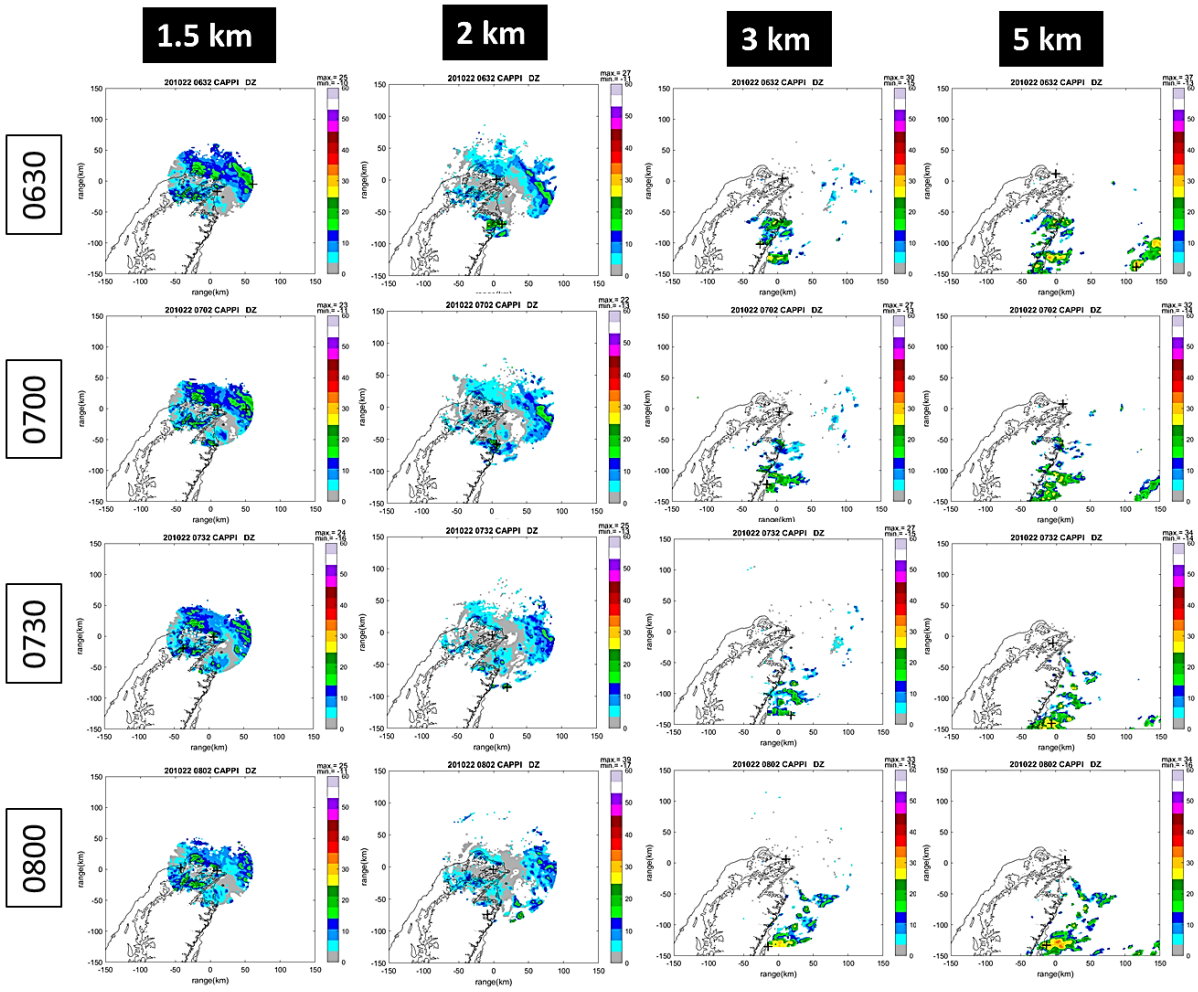

Figure 4.16 The RCWF radar reflectivity of different altitudes (1.5, 2, 3, and 5 km) at different times (0630, 0700, 0730, and 0800 UTC).

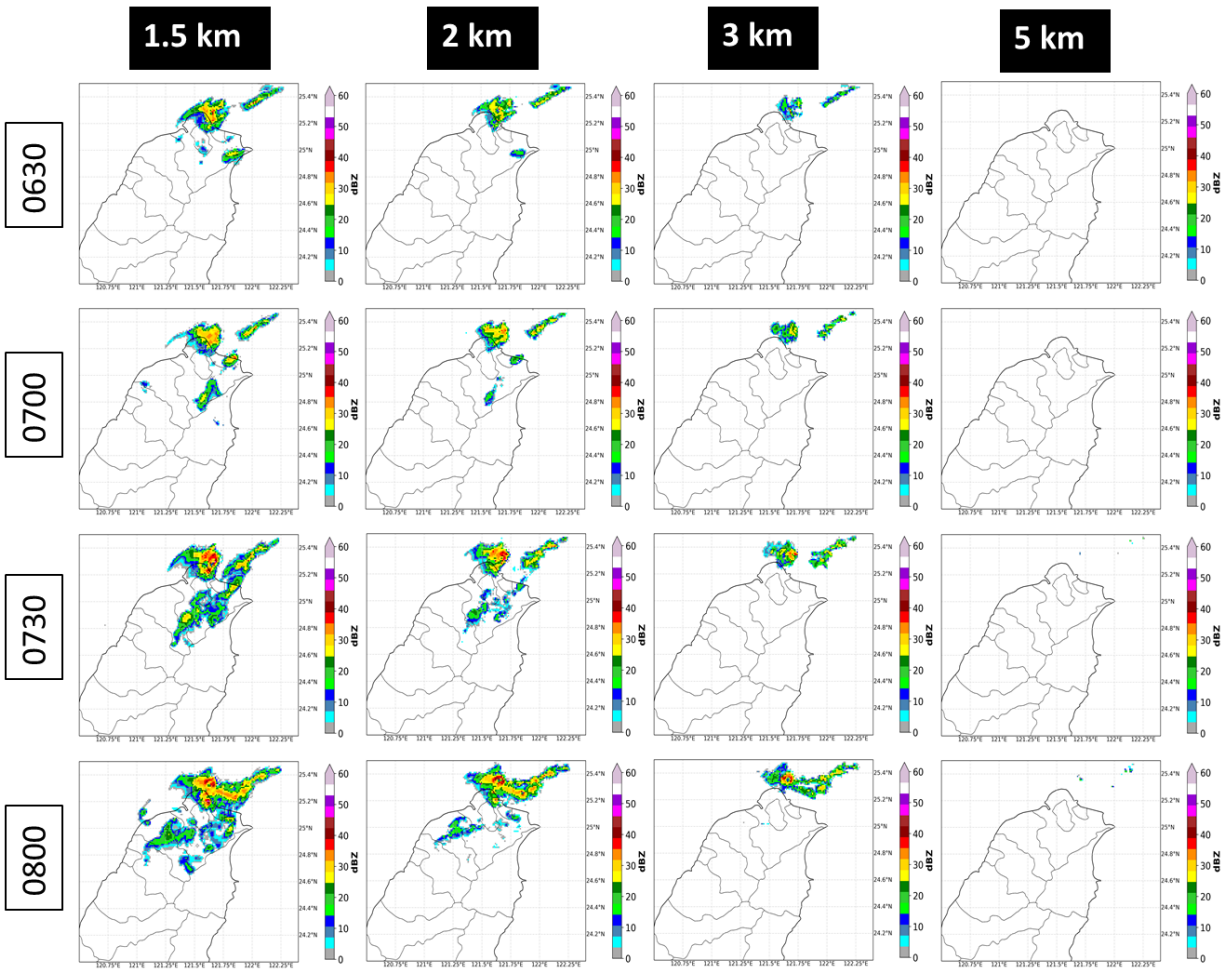

Figure 4.17 The simulative radar reflectivity of different altitudes (1.5, 2, 3, and 5 km) at different times (0630, 0700, 0730, and 0800 UTC).

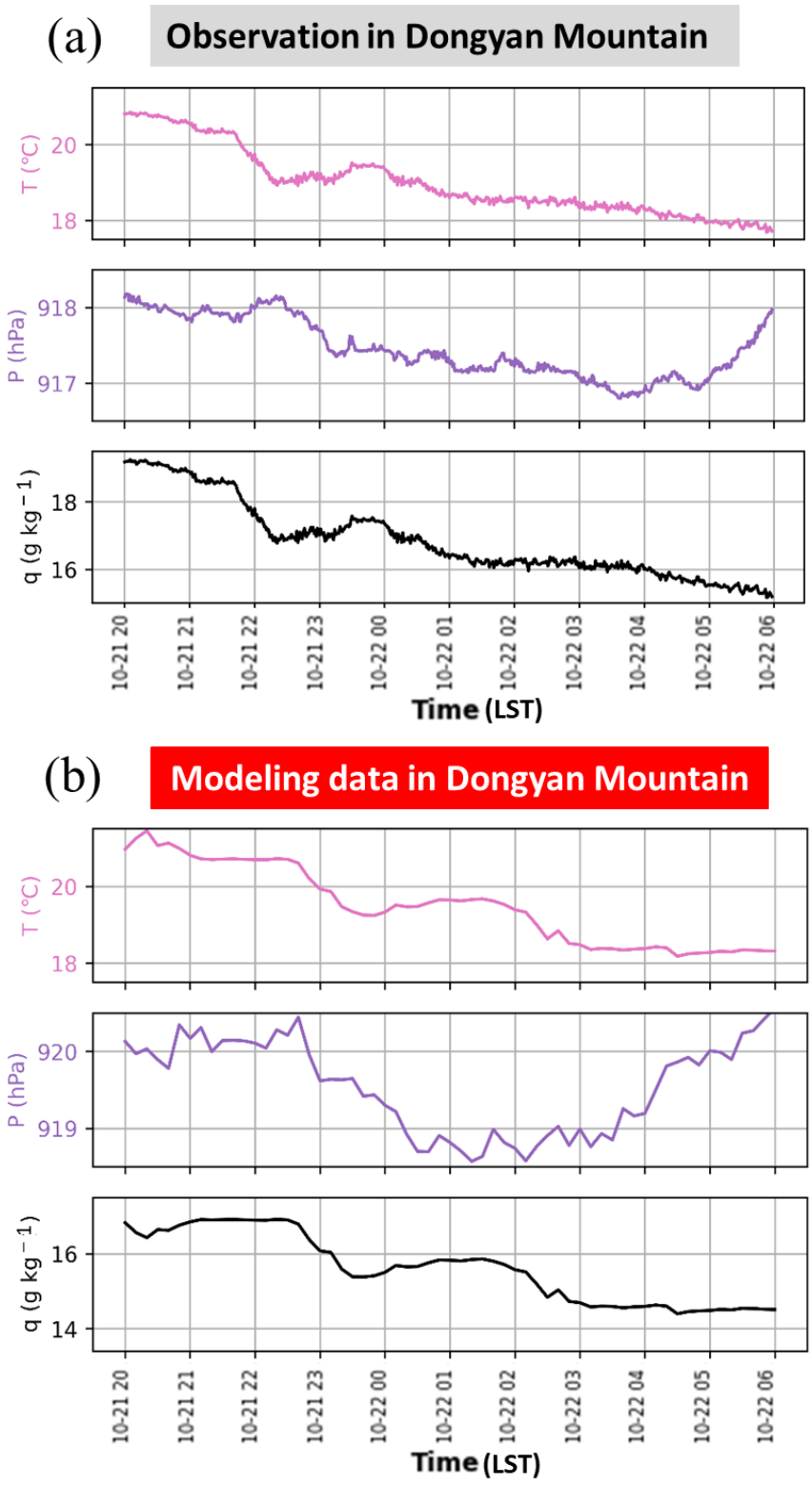

Figure 4.18 The time series (LST) of temperature, pressure, and water vapor mixing ratio of the (a) observation and (b) model simulation in the Dongyan mountain site.

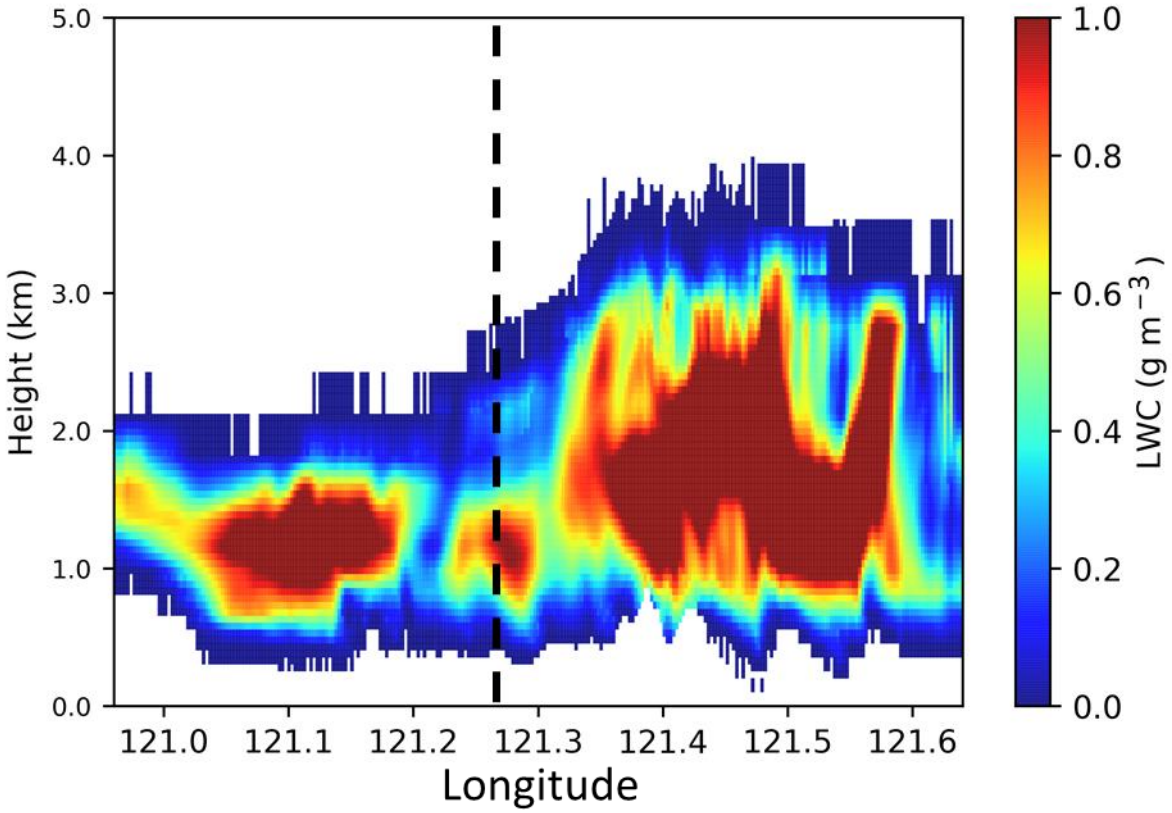

Figure 4.19 The meridional mean (0.1° of latitude crosses the Shihmen region) of liquid water content (LWC) at 06:30 UTC on 22 October 2020. The black dash line means the longitude of the Shihmen region.

4.3.2 Sensitivity of precipitation

In order to examine the cloud-seeding impacts at different seeding heights, four Seed runs (Seed1 to Seed4) that seeding in one horizontal grid (1 km × 1 km) at different seeding levels (~500, 1000, 1300, and 2200 m above mean sea level height) are developed. In Figure 4.20, it shows the difference of accumulative rainfall between Seed runs and Control run, and presents that only seeding above 1000 m but below 2000 m enhances accumulative rainfall (red shaded) in the Shihmen region (red rectangular) in one hour after executing cloud seeding. However, regarding Seed4, though it does not have a positive rainfall signal in the Shihmem region, the enhancement of precipitation appears at the downstream area (Figure 4.20: red arrow). In addition, after evaluating the average of rain rate of Seed runs and Control run in the Shihmen region (Figure 4.21), it indicates that Seed3 enhances a little bit more precipitation than Seed2. Thus, in this study, seeding at 500 m and 1300 m, corresponding to Seed1 and Seed3, are chosen as the least and most rainfall enhancement runs to do the extending sensitivity test and detail analysis in domain five (D05). The results of different seeding heights also mean that seeding at the in-cloud level (Seed2, Seed3, and Seed4) is more efficient than seeding at cloud base (Seed1) in northern Taiwan.

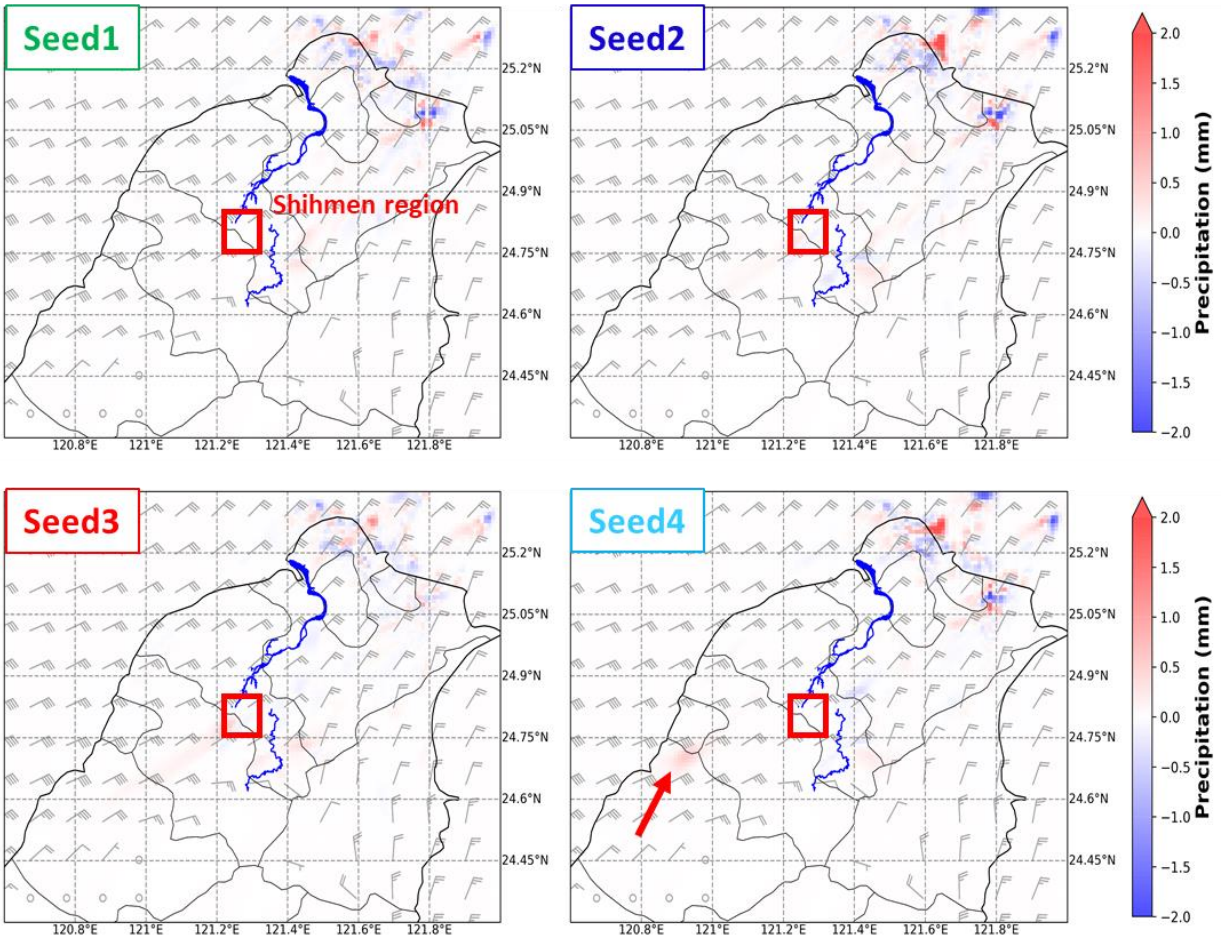

Figure 4.20 The difference (Seed runs minus control run) of accumulative rainfall between Seed runs and Control run for one hour after doing cloud seeding in domain four (D04) show as the shaded and the wind field at 850 hPa also display. The red rectangular means the Shihmen region, and the rivers show on the map are Dahan creek and Danshui river.

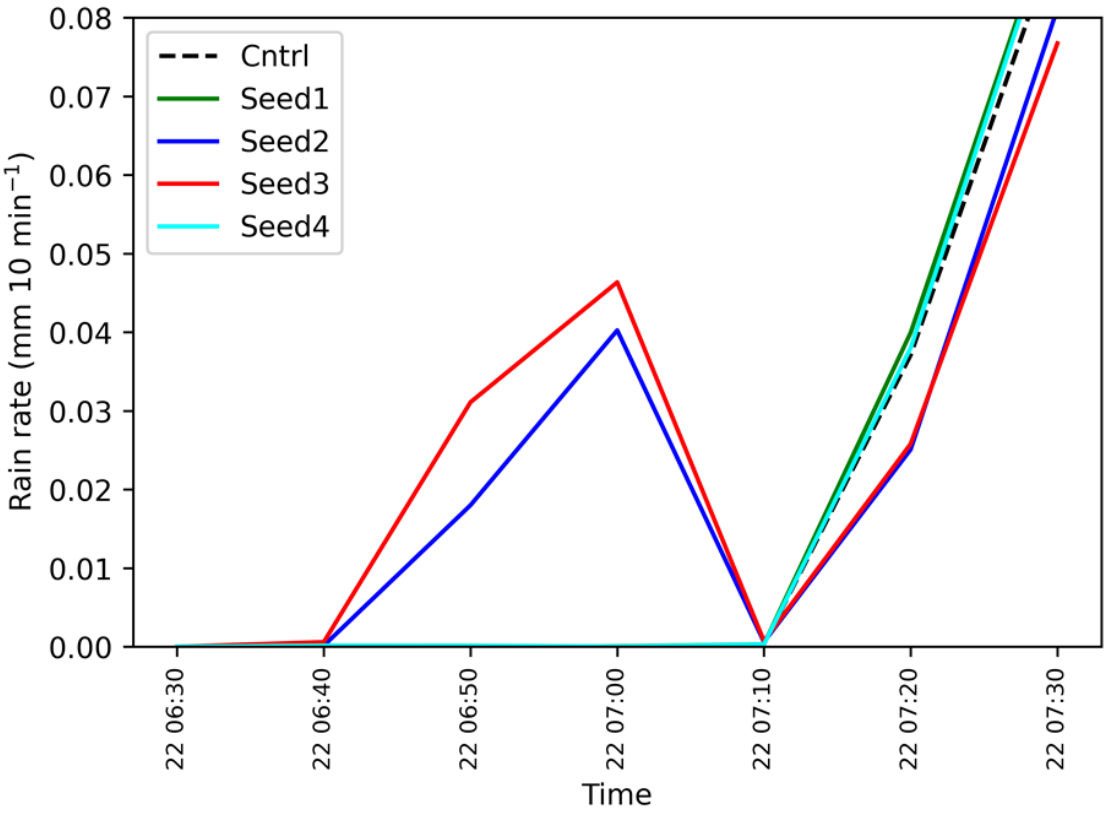

Figure 4.21 The time series (UTC) of averaged rain rate of the rainy grids in Shihmen region for Seed runs and Control run.

4.4 Modeling of Miaopu validation experiment in higher horizontal resolution domain (333 m)

4.4.1 Sensitivity of precipitation

To examine more details of microphysics processes, domain five (D05) is constructed. In domain five (D05), eight runs are conducted to investigate the impacts of cloud seeding in different seeding heights (500 and 1300 m), different seeding areas (1, 10, and 100 km^2), and different seeding concentrations. First of all, regarding the seeding height, seeding at 1300 m enhances more rainfall than seeding at 500 m (Figure 4.22 and Figure 4.23), and it is consistent and similar to the result of domain four (D04). In addition, in the scenarios of seeding at 1300 m, seeding in a bigger domain and higher aerosol concentration are able to increase several folds of rain rate in the Shihmen region (Figure 4.23), particularly for introducing seeding agents into 100 km^2. However, this phenomenon is not obvious in the scenarios that seeding at 500 m. Thus, it revalidates that seeding height plays an extremely important role to impact the cloud-seeding effects. If we do cloud seeding at the appropriate altitude, more precipitation will be developed when we execute cloud seeding in a bigger seeding area or higher aerosol concentration.

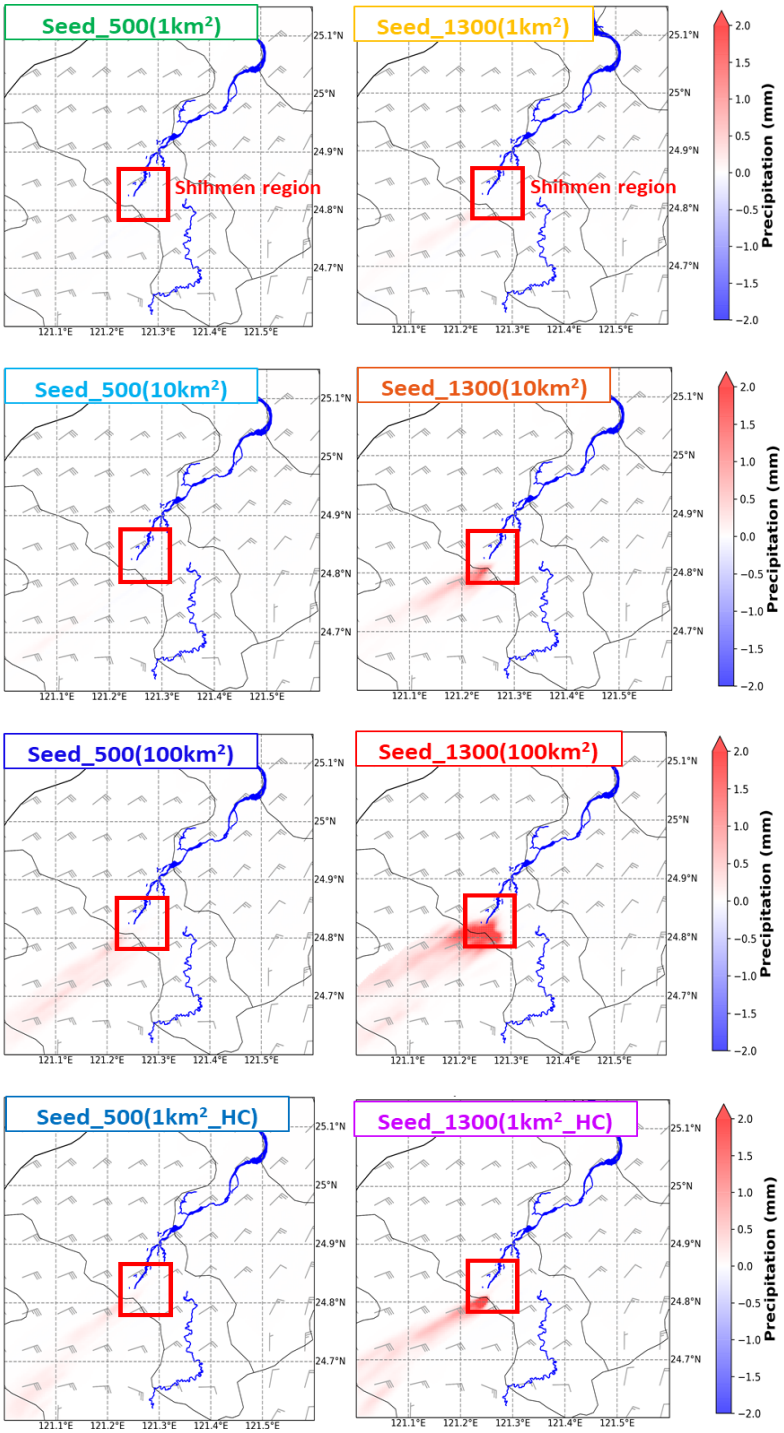

Figure 4.22 The difference (Seed runs minus control run) of accumulative rainfall between Seed runs and Control run for one hour after doing cloud seeding in domain five (D05) show as the shaded and the wind field at 850 hPa also display. The red rectangular means the Shihmen region, and the rivers show on the map are Dahan creek and Danshui river.

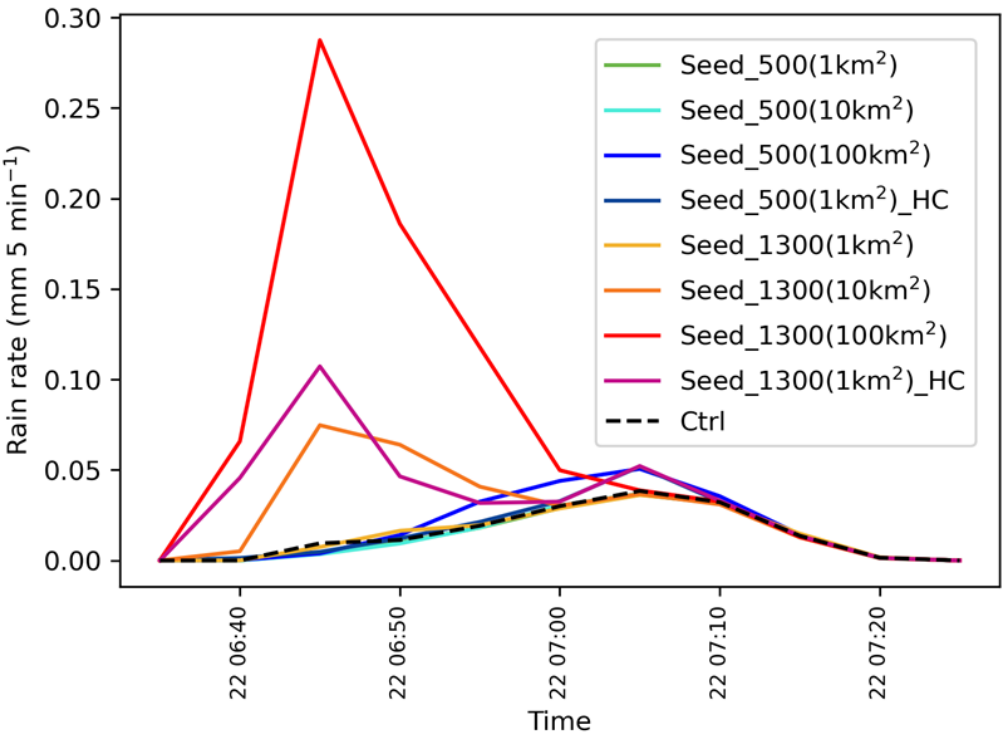

Figure 4.23 The time series (UTC) of averaged rain rate of the rainy grids in the Shihmen region for Seed runs and Control run.

4.4.2 Seeding effects on the microphysics properties

This study investigates the sensitivity of microphysics products to understand the reasons of the cloud-seeding impacts on rainfall. To better describe the parameter features of vertical profile and ensure the fair comparisons between eight scenarios, three steps are implemented. First, we evaluate the difference of microphysical parameters between Seed run and Control run. Second, the value of zero is filtered out. Finally, the average for each vertical level is calculated.

Due to the execution of cloud seeding in the simulation, there is a peak value of seeded

CCN concentration at their seeding height (Figure 4.24). In Figure 4.24, it depicts that there are different transportation patterns between the scenarios that seeding in different heights. The scenarios seeding at 1300 m (Figure 4.24: warm color) show that the distribution of seeded CCNs is thicker and able to transport to higher levels than the scenarios seeding at 500 m (Figure 4.24: cold color). Regarding the mixing ratio of cloud (QCLOUD), Figure 4.25 shows that both scenarios of seeding at 500 m and 1300 m enhance QCLOUD in ten minutes (from 06:30 to 06:40) after doing cloud seeding. However, QCLOUD starts to decrease after 06:40 (ten minutes after doing cloud seeding) in the scenario seeding at 1300 m, but this phenomenon is not obviously found in the scenario seeding at 500 m. For the mixing ratio of rain (QRAIN), Figure 4.26 depicts that seeding at 1300 m increases QRAIN in 30 minutes (from 06:30 to 07:00) after doing cloud seeding, but seeding at 500 m only has a weaker signal of enhancing QRAIN. This phenomenon also explains that cloud droplets are able to turn into raindrops in the scenario seeding at 1300 m and causes QCLOUD starts to decrease after 06:40. In addition, due to the advantage of the double-moment microphysics scheme, we are able to calculate the mean-volume-drop diameter of rain (*Dr*) by the functions as

$$\lambda_r = \left(\frac{4\pi N_r}{\rho_a q_r}\right)^{\frac{1}{3}} \; ; \; D_r = \frac{1}{\lambda_r}(24)^{1/3}, \quad (9)$$

where N_r, Q_r, and ρ_r are number concentration of rain, mixing ratio of rain, and density of air respectively. Figure 4.27 displays that D_r increase more obviously in the scenarios seeding at the in-cloud region (the warm color lines). If more bigger raindrops are developed, chances are more liquid water can reach the ground and enhance the surface rainfall. Last but not least, the model shows the little change of supersaturation ratio between the experiments (Figure 4.28), and it indicates that though the seeding agents are able to compete for water vapor, only a little

water vapor is needed and it cannot cause the extreme impacts on the saturation state of the environment.

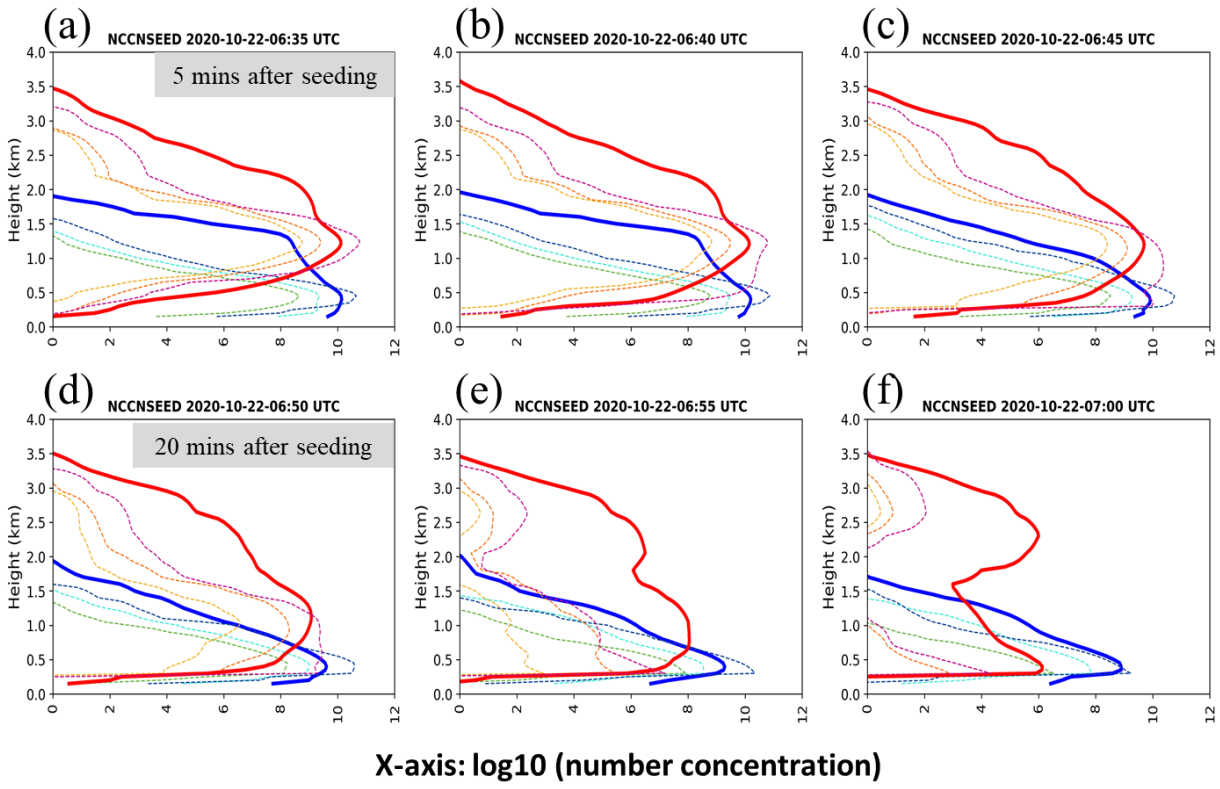

Figure 4.24 The vertical profile of averaged CCN concentration in the Shihmen region after doing cloud seeding (0635 to 0700 UTC). The colors of each scenario are the same as the legend of Figure 4.23 (warm colors represent seeding at 1300 m, and cold colors represent seeding at 500 m). (a) to (c) are the time in 15 mins after doing cloud seeding. (d) to (e) are the time of 20 to 30 mins after doing cloud seeding.

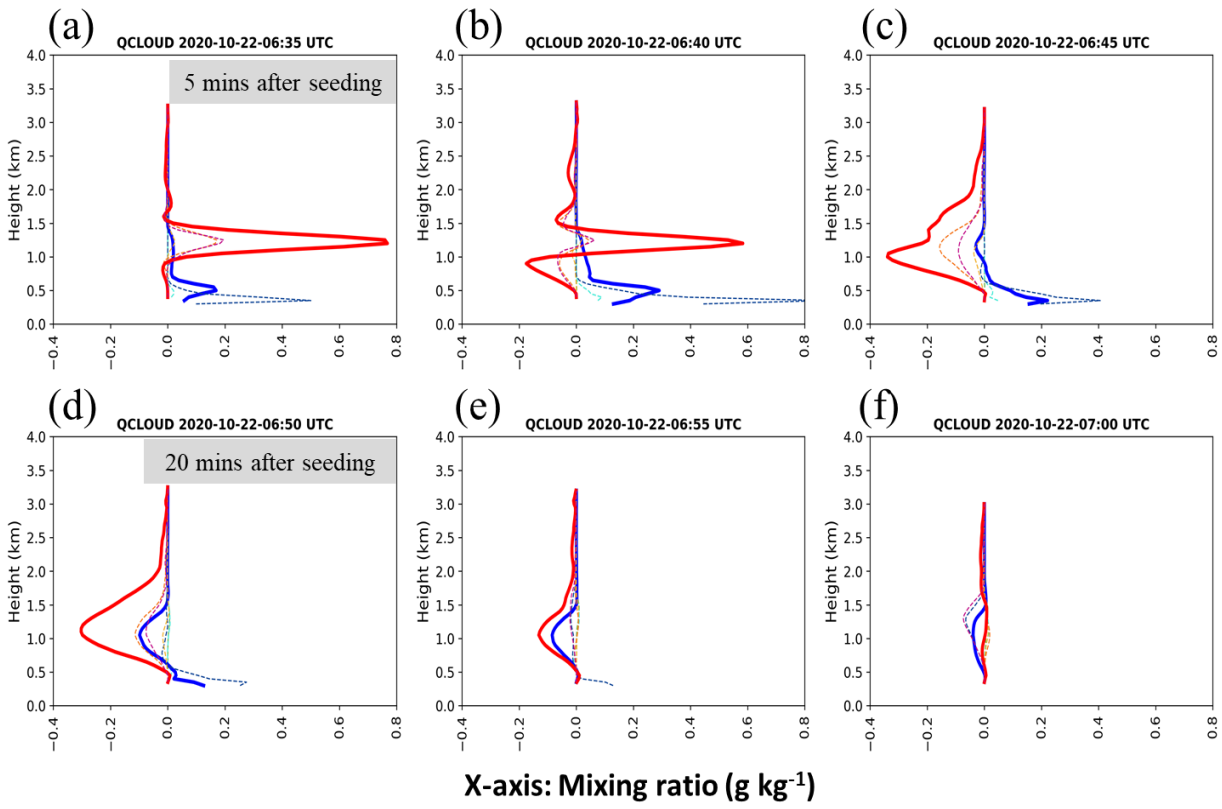

Figure 4.25 The vertical profile of averaged difference between control run and seed runs of QCLOUD (mixing ratio of cloud) in the Shihmen region after doing cloud seeding (from 06:35 to 07:00). The colors of each scenario are the same as the legend of Figure 4.23 (warm colors represent seeding at 1300 m, and cold colors represent seeding at 500 m). (a) to (c) are the time in 15 mins after doing cloud seeding. (d) to (e) are the time 20 to 30 mins after doing cloud seeding.

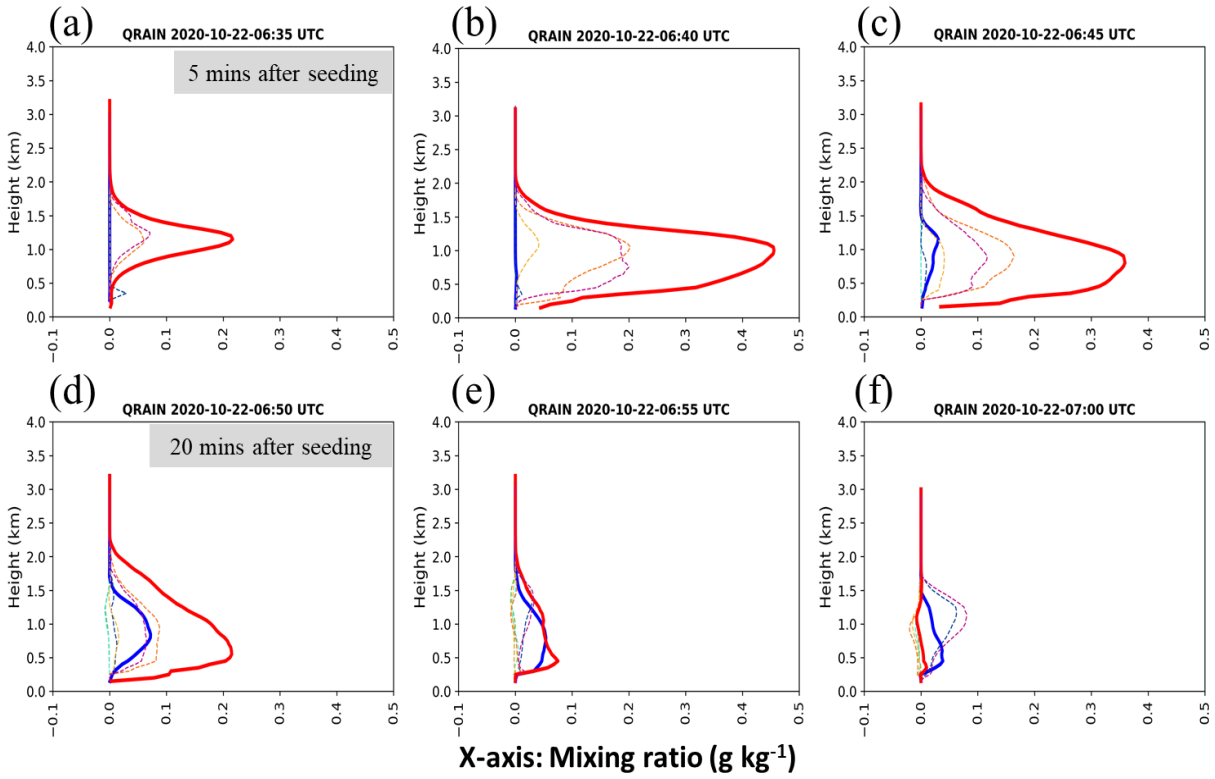

Figure 4.26 The vertical profile of averaged difference between control run and seed runs of QRAIN (mixing ratio of rain) in the Shihmen region after doing cloud seeding (from 06:35 to 07:00). The colors of each scenario are the same as the legend of Figure 4.23 (warm colors represent seeding at 1300 m, and cold colors represent seeding at 500 m). (a) to (c) are the time in 15 mins after doing cloud seeding. (d) to (e) are the time 20 to 30 mins after doing cloud seeding.

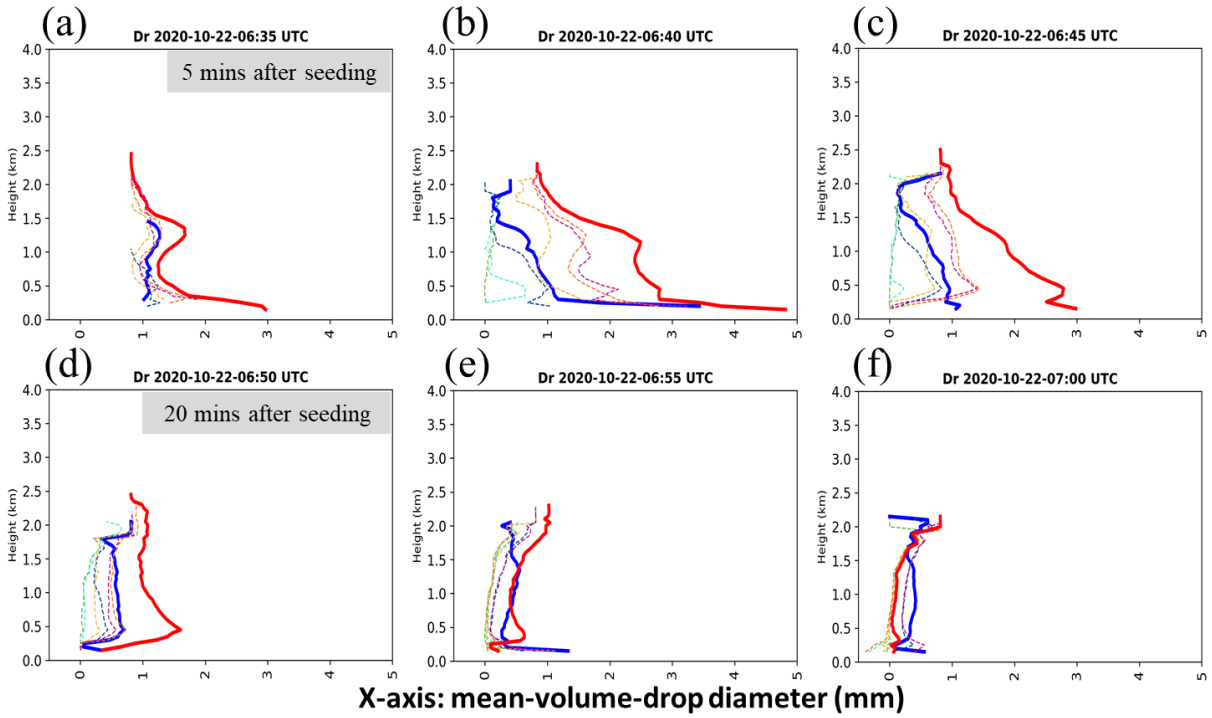

Figure 4.27 The vertical profile of averaged difference between control run and seed runs of Dr (mean-volume-drop diameter of precipitation) in the Shihmen region after doing cloud seeding (from 06:35 to 07:00). The colors of each scenario are the same as the legend of Figure 4.23 (warm colors represent seeding at 1300 m, and cold colors represent seeding at 500 m). (a) to (c) are the time in 15 mins after doing cloud seeding. (d) to (e) are the time 20 to 30 mins after doing cloud seeding.

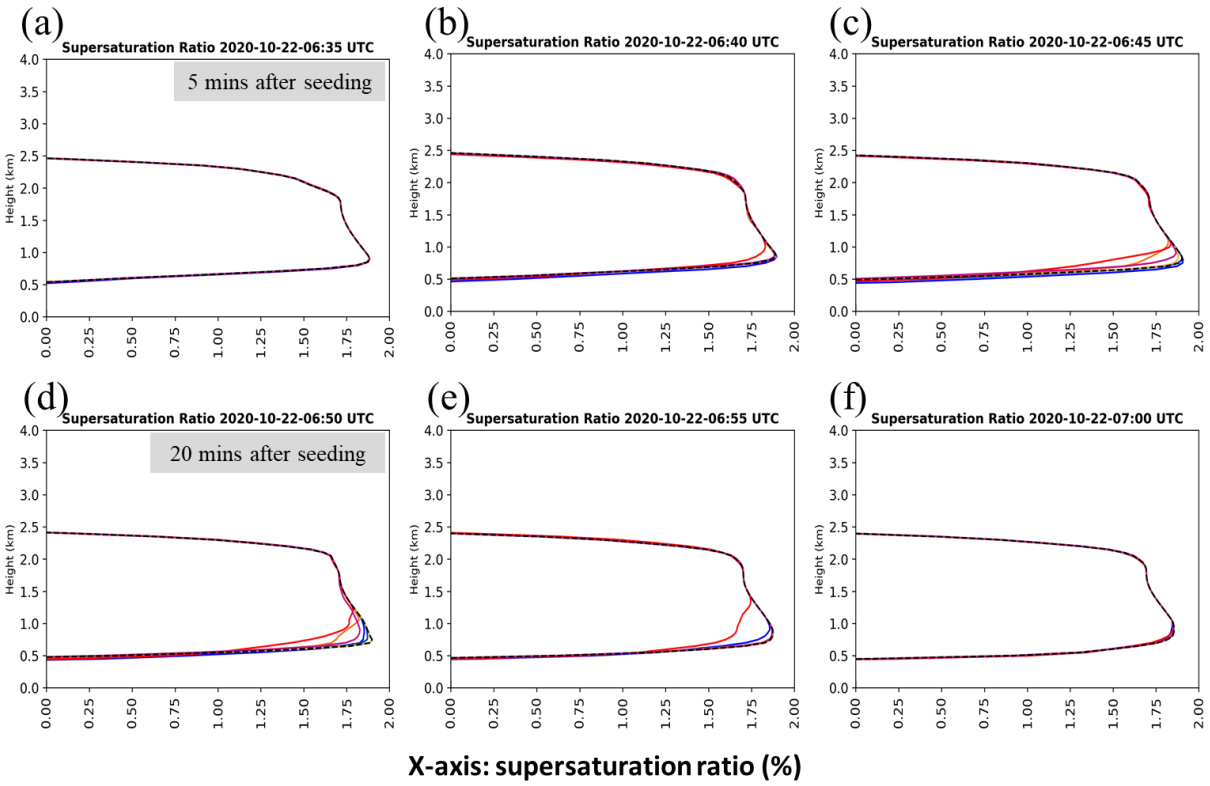

Figure 4.28 The vertical profile of averaged supersaturation ratio in the Shihmen region after doing cloud seeding (from 06:35 to 07:00). The colors of each scenario are the same as the legend of Figure 4.23 (warm colors represent seeding at 1300 m, and cold colors represent seeding at 500 m). (a) to (c) are the time in 15 mins after doing cloud seeding. (d) to (e) are the time 20 to 30 mins after doing cloud seeding.

Regarding the microphysical processes, five products are taken into consideration, including cloud activation (Pcact), cloud condensation (Pcond), evaporation of rain (Prevp), auto-conversion of rain (Praut), and accretion of rain (Pracw). Figure 4.29 displays the schematic of the warm rain process in WDM6-NCU after executing cloud seeding. To investigate the major microphysics processes, we do the integration with heights below 5 km for the averaged difference between control run and seed runs of each parameter. Figure 4.30,

sampled 10 minutes after doing cloud seeding, indicates that the seeding effect mainly goes through three products, including Pcact, Praut, and Pracw. For Pcact, Figure 4.31 depicts that the activation process is intense at the height introduced the seeding agents, which mainly happens in 10 minutes after doing cloud seeding. Moreover, because the supersaturation ratio at 1300 m is higher than the supersaturation ratio at 500 m (Figure 4.28), seeding at 1300 m has a stronger Pcact than seeding at 500 m. Regarding Praut, only the scenarios seeding into 100 km^2 at 500 m and 1300 m have the obvious but opposite signals. In Figure 4.32, it displays that the auto-conversion process obviously strengthens in Seed_500(100km^2) but weakens in Seed_1300(100km^2) in 15 minutes after doing cloud seeding. However, regarding Pracw, the scenarios seeding at 1300 m (Figure 4.33: warm color) have a more intense accretion process than the scenarios seeding at 500 m (Figure 4.33: cold color). Thus, in our model simulation, introducing the seeding agents with CSRD size distribution can enhance the activation process (Pcact), and seeding at 1300 m is able to activate more seeded CCNs into clouds. In addition, because of the strengthening of accretion process (Pracw), more precipitation can be developed in the scenarios seeding at 1300 m. However, for the scenarios seeding at 500 m, it is capable to enhance a little bit rainfall which is mainly caused by the enhancement of auto-conversion process (Praut) when we introduce seeding agent into the area of 100 km^2, whereas sometimes seeding into such a big domain is not practical and effective. Therefore, doing cloud seeding at 1300 m (in-cloud area) seems to be the better choice to increase the rainfall.

More details of the cloud-seeding impacts on the cloud microphysical properties are obtained by the figure of seeded CCN size distribution with time in Seed_1300(100 km^2) (Figure 4.34). Figure 4.34 depicts that the fraction of hygroscopic particles with the size larger than 0.4 μm decreases over time. This phenomenon indicates those particles bigger than 0.4 μm are the main factor contributing to cloud-seeding effects.

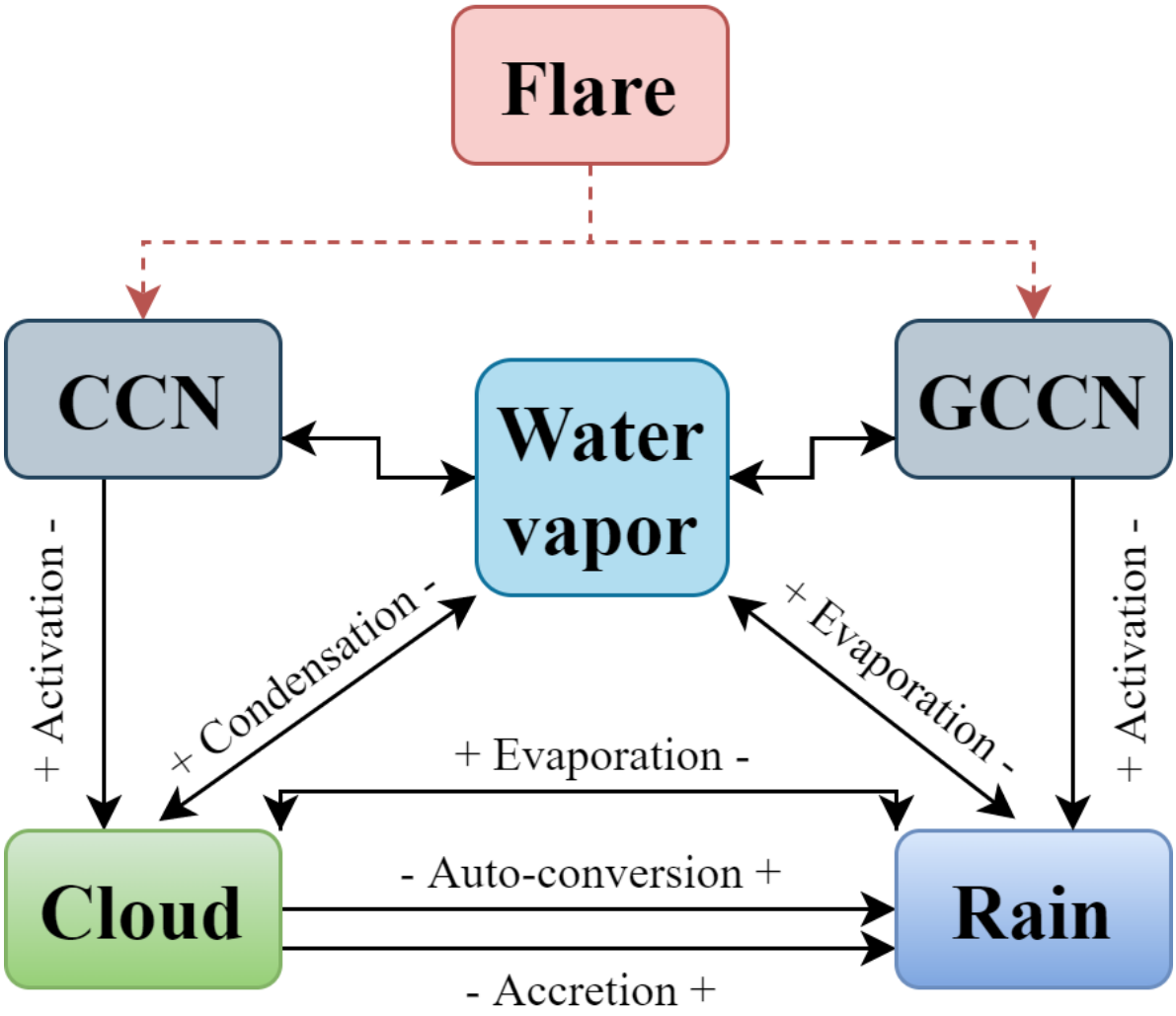

Figure 4.29 The schematic of the warm rain process in WDM6-NCU after executing cloud seeding. The arrows represent the conversion pathways that experience different microphysics processes as the texts.

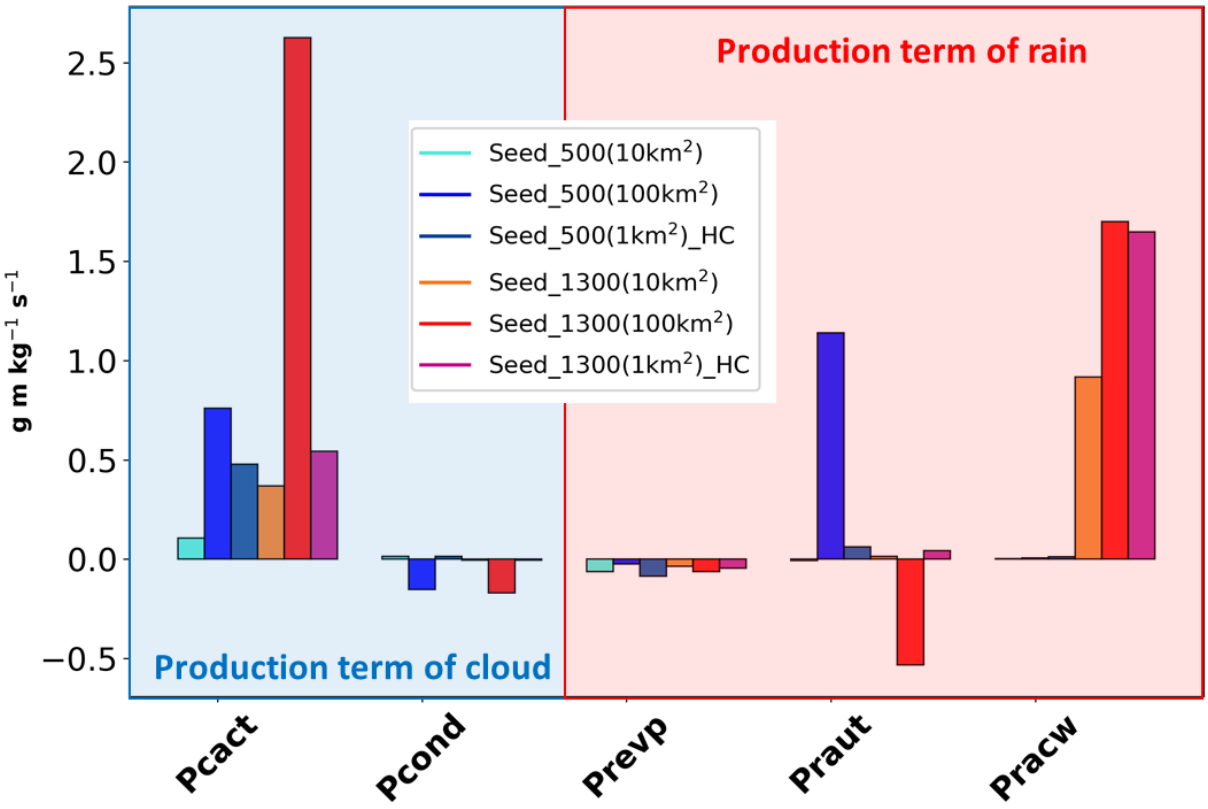

Figure 4.30 The integration with height below 5 km for the averaged difference between control run and seed runs of each parameter. Blue and red shaded areas represent the production term of cloud and rain respectively.

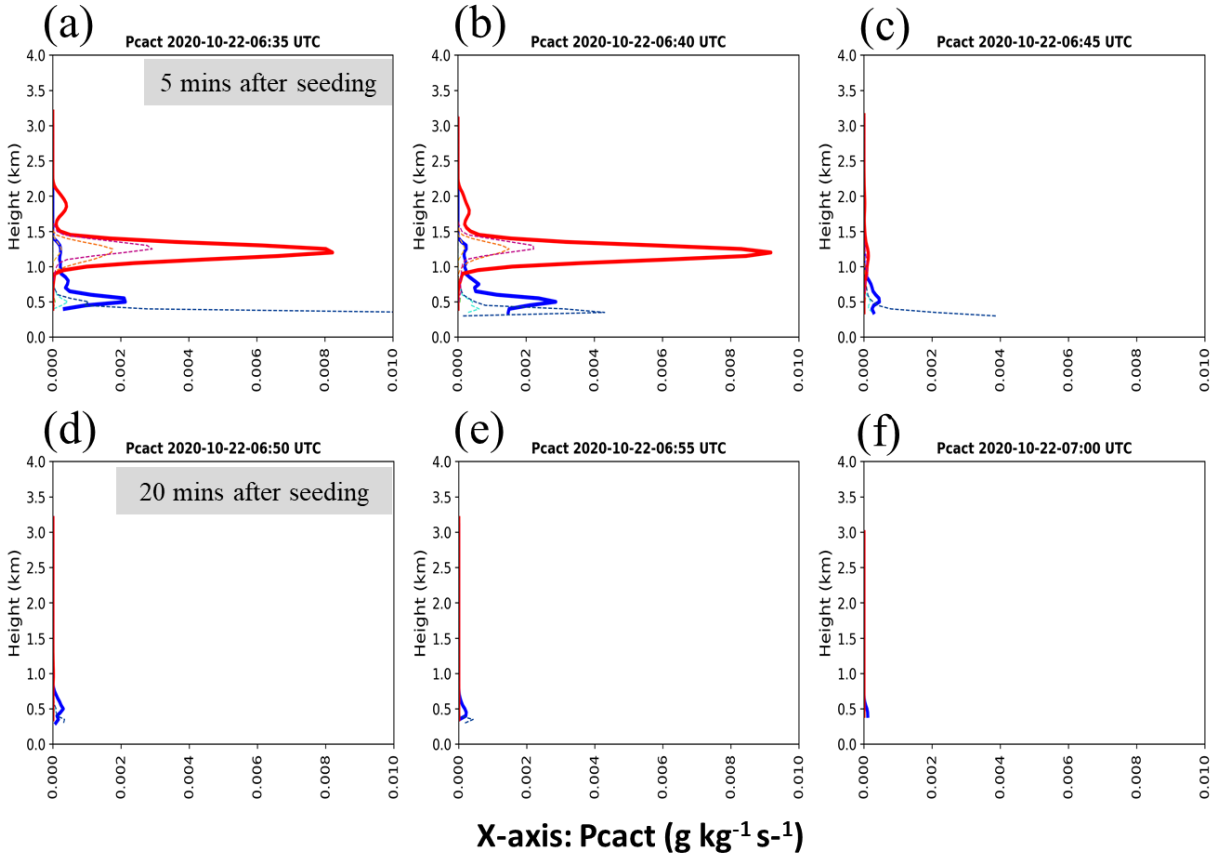

Figure 4.31 The vertical profile of averaged difference between control run and seed runs of Pcact (cloud activation process) in the Shihmen region after doing cloud seeding (from 06:35 to 07:00). The colors of each scenario are the same as the legend of Figure 4.23 (warm colors represent seeding at 1300 m, and cold colors represent seeding at 500 m). (a) to (c) are the time in 15 mins after doing cloud seeding. (d) to (e) are the time 20 to 30 mins after doing cloud seeding.

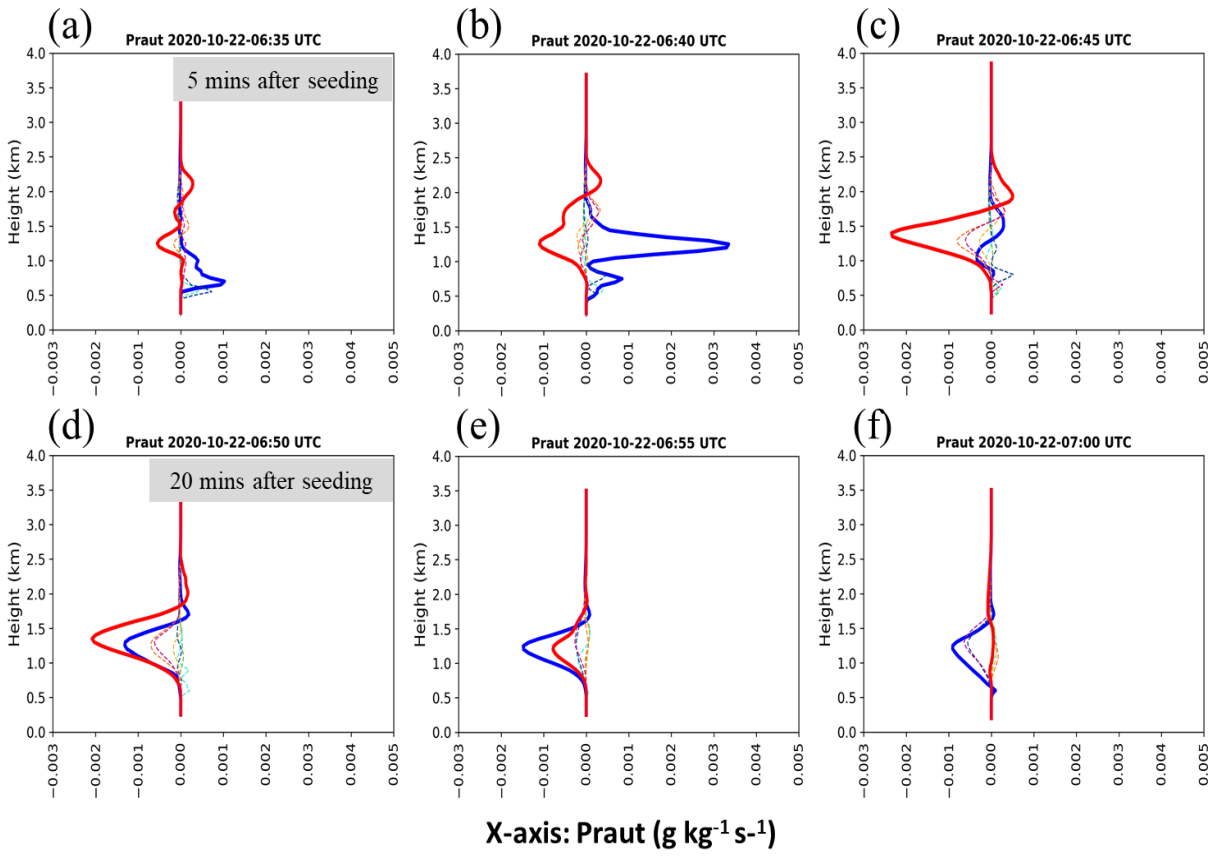

Figure 4.32 The vertical profile of averaged difference between control run and seed runs of Praut (auto-conversion process of rain) in the Shihmen region after doing cloud seeding (from 06:35 to 07:00). The colors of each scenario are the same as the legend of Figure 4.23 (warm colors represent seeding at 1300 m, and cold colors represent seeding at 500 m). (a) to (c) are the time in 15 mins after doing cloud seeding. (d) to (e) are the time 20 to 30 mins after doing cloud seeding.

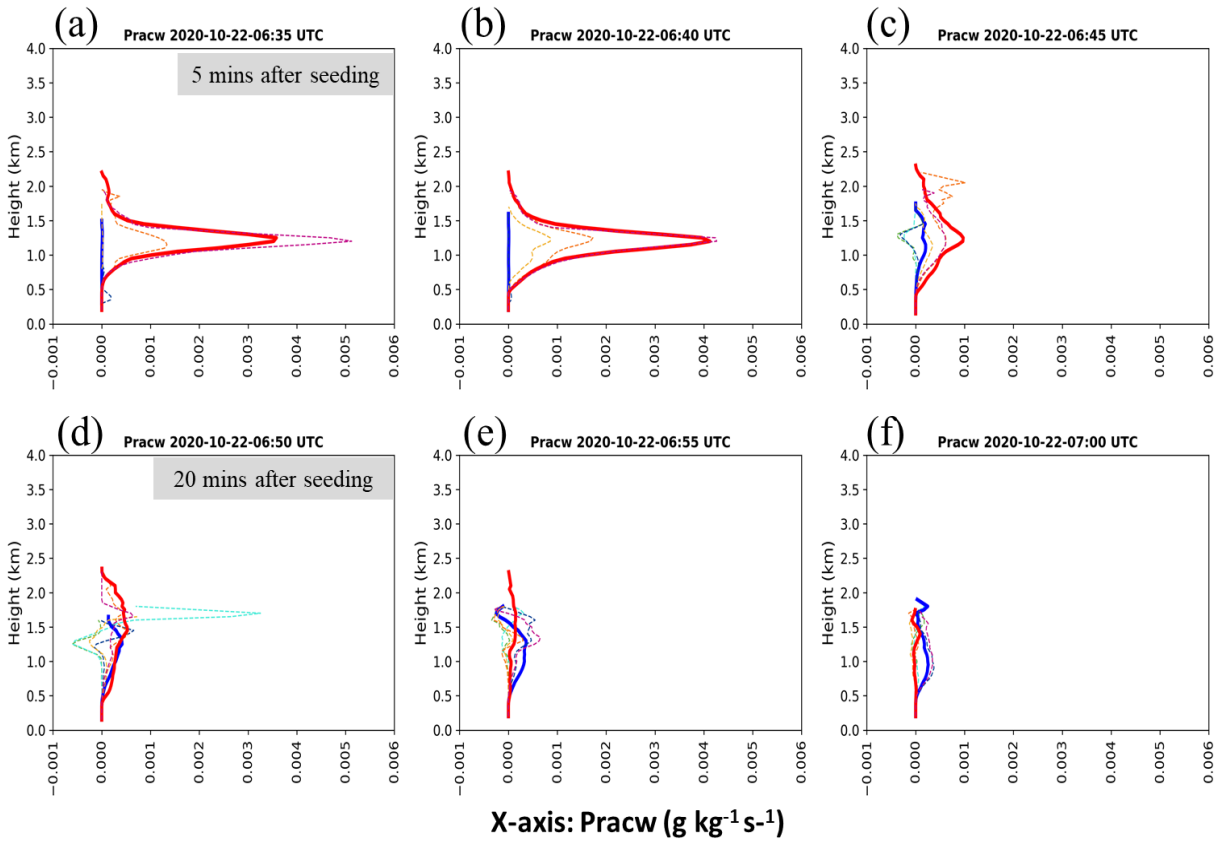

Figure 4.33 The vertical profile of averaged difference between control run and seed runs of Pracw (accretion process of rain) in the Shihmen region after doing cloud seeding (from 06:35 to 07:00). The colors of each scenario are the same as the legend of Figure 4.23 (warm colors represent seeding at 1300 m, and cold colors represent seeding at 500 m). (a) to (c) are the time in 15 mins after doing cloud seeding. (d) to (e) are the time 20 to 30 mins after doing cloud seeding.

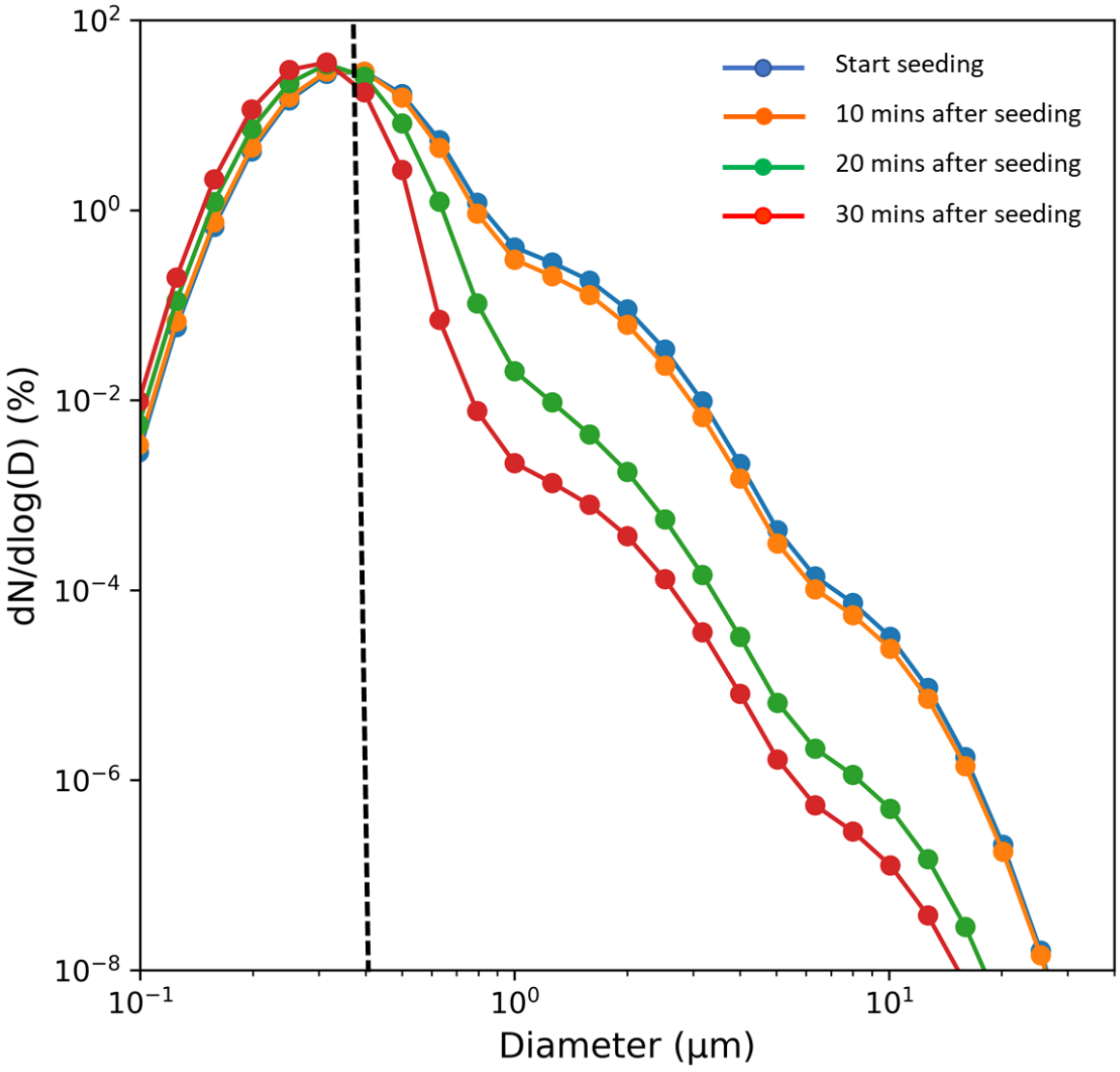

Figure 4.34 The size distribution of seeded CCNs in different time after doing cloud seeding. The black dash line is the line separating the size of particles larger than 0.4 μm and smaller than 0.4 μm.

4.5 Discussion and advice for TCSRP

In this study, two key points are gained. First, introducing the seeding agents at in-cloud levels can enhance more precipitation than seeding at cloud base due to the increase of the accretion process. Second, spreading the hygroscopic particles into the bigger areas in the in-cloud region is more effective to enhance more rainfall. However, for the operation of cloud seeding, two questions are extremely important, including that: 1) what kinds of environmental conditions are appropriate to execute hygroscopic cloud seeding in the stratiform system? 2) what is the suggestion of the seeding area for the operational works?

Regarding the first question, the environmental condition of 1300 m above mean sea level (the in-cloud region) in the simulation, which is able to increase the most rainfall after doing cloud seeding, can be seen as the reference. In this case, the cloud base is at about 500 m, and the supersaturation ratio is in the range of 1.5 % to 2 % near the altitude of 1300 m in the Shihmen region (Figure 4.28). However, after executing the cloud seeding, the supersaturation ratio can be consumed up to 0.5 % (Figure 4.28 e). Moreover, the LWC is about 0.6 g m^{-3} to 1 g m^{-3} near the altitude of 1300 m in the Shihmen region. Therefore, in the stratiform system, we suggest introducing hygroscopic particles into the in-cloud region where the supersaturation ratio should be more than 0.5 % and LWC is higher than 0.6 g m^{-3}. For the second question, in order to find out the reasonable seeding area with the effective increment of precipitation, two more runs, which do cloud seeding into the seeding area of 36 km^2 and 64 km^2 at the altitude of 1300 m, are created. Figure 4.35 displays the average of enhancement rain rate in the Shihmen region in one hour in the scenarios with different seeding areas, and the results show that when the seeding area is smaller than 64 km^2 the rain rate obviously enhances with the

bigger seeding area. However, for the seeding area larger than 64 km^2, seeding in the bigger area just causes a little increment of rain rate. Thus, we recommend that spreading the seeding agents into the area of about 40-60 km^2 can provide the advantages of not only having the most efficient enhancement of rain rate but also conducting cloud seeding in the more reasonable seeding area.

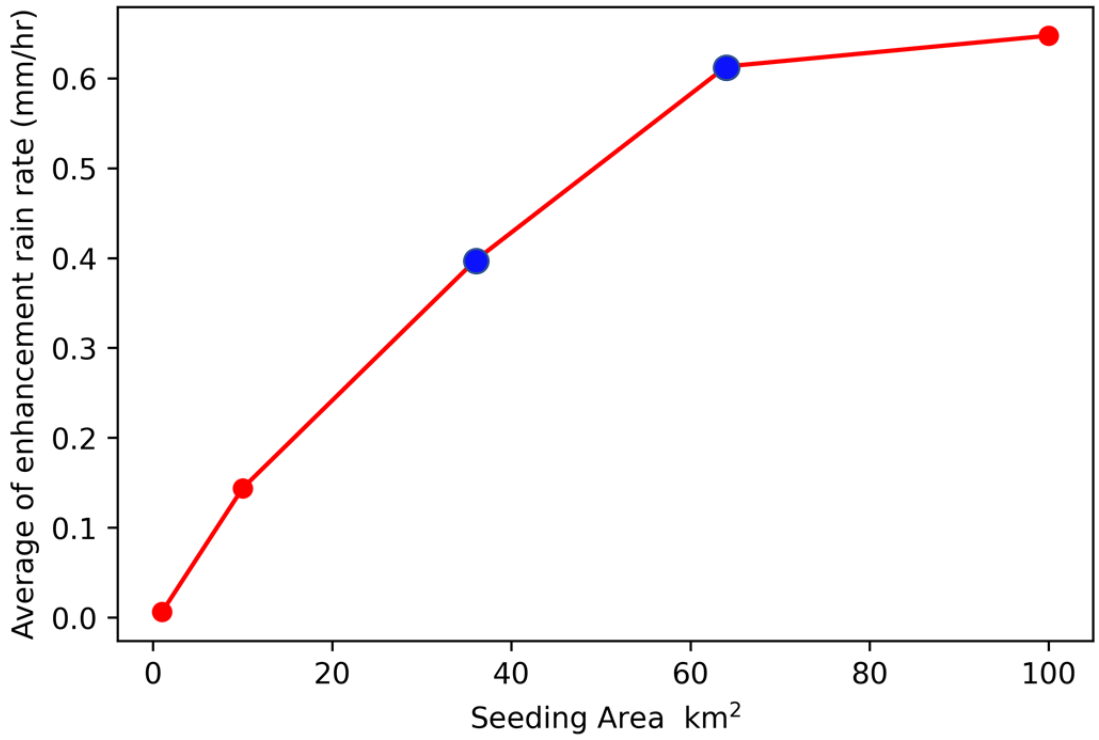

Figure 4.35 The average of enhancement rain rate in the Shihmen region in one hour in the scenarios with different seeding areas, including 1, 10, 36, 64, and 100 km^2. The blue dots are the more two runs to investigate the reasonable seeding area with the most effective increment of precipitation.

Chapter 5. Conclusion and future work

5.1 Conclusion

The goals of this study are to explore the direct observational evidence of cloud seeding and investigate the cloud-seeding effects by the model simulation. To find the direct observational evidence, the Dongyan mountain cloud-seeding experiments were conducted. This study discusses two events of the Dongyan mountain cloud-seeding experiment on 21 October 2020 (Case1) and 28 April 2021 (Case2), and both of them have the appropriate environmental condition for cloud-seeding experiments. In the case on 21 October 2020, the aerosol concentration obviously increases after combusting the CSRD flares, particularly for the first seeded period. Moreover, during the first seeded period, clear signals of increasing in LWC and reducing in water vapor are found, which seems to imply the existence of the competition effect. Besides, the latent heat released by condensation process that seems to be found by the increment of temperature and LWC in the first seeded period. For another case on 28 April 2021, there are similar features of aerosol concentration and water vapor mixing ratio during the seeded periods, but the signal of condensation process seems to be not obvious. We believe that due to the higher LWC in Case2 (~0.4-0.5 g m^{-3}) than Case1 (~0.3-0.4 g m^{-3}), the hygroscopic particles will probably experience totally different microphysics process. Furthermore, after comparing the JWD data to the upstream observational site, the Xiayunping site, it seems to imply more raindrops are developed in Dongyan mountain by conducting cloud seeding.

To adopt the realistic CCN size distribution into the model simulation, the chamber sampling experiment is designed, and it successfully evaluates the aerosol size distribution of CSRD flare. After fitting the size distribution of CSRD flare with trimodal lognormal function, the sensitivity experiment of hygroscopic cloud seeding can start to be executed by the model simulation. In this research, the WRF model with WDM6-NCU microphysics scheme, which is able to describe the seeded CCN size distribution by 43 bins and precisely evaluate the activation of seeded CCNs, is developed and used to simulate the case on 21-22 October 2020. Regarding the fourth nested domain (D04), one Control run and four Seed runs (Seed1 to Seed4) that seeding in one horizontal grid (1 km × 1 km) at different seeding levels (~500, 1000, 1300, and 2200 m above the mean sea level) are made. The results show that seeding above 1000 m but below 2000 m enhances accumulative rainfall in the Shihmen region for one hour after doing cloud seeding, and seeding at 500 m (cloud base) and 1300 m (in-cloud region), corresponding to Seed1 and Seed3, are chosen as the least and most rainfall enhancement runs to do the extending sensitivity test and detail analysis in domain five (D05).

In domain five (D05), eight runs are developed to examine the impacts of cloud seeding in different seeding heights (500 and 1300 m), different seeding areas (1, 10, and 100 km^2), and different seeding concentrations. Regarding the sensitivity of precipitation, the model simulation shows that more precipitation is developed in the scenarios seeding at the in-cloud region, and introducing hygroscopic particles into a bigger domain or with higher concentration are able to increase several folds of precipitation in the in-cloud seeding simulations. Moreover, the scenarios seeding at different heights have different microphysics properties. First of all, seeding at 1300 m are able to transport seeded CCNs to higher levels and cause thicker CCNs vertical distribution than the scenarios seeding at 500 m. Second, both seeding at 500 m and 1300 m can enhance QCLOUD in ten minutes after doing cloud seeding, but QCLOUD

decreases earlier in the scenarios seeding at 1300 m because more cloud droplets can turn into raindrops. Third, seeding at 1300 m has a stronger enhancement on QRAIN than seeding at 500 m in 30 minutes after doing cloud seeding. For the mean-volume diameter of raindrop (D_r), it increases more obviously in the scenarios seeding at the 1300 m and makes more liquid water can reach the ground to enhance the surface rainfall. Besides, the signals are always more intense in the runs with bigger seeding domains or higher seeded CCNs concentrations. Furthermore, the result presents that only a few water vapor is competed by hygroscopic particles and it cannot cause extreme impacts on the saturation state of the environment. Regarding the seeding effects on microphysics process, three main products are chosen to discuss, including cloud activation (Pcact), auto-conversion of rain (Praut), and accretion of rain (Pracw). The results show that the seeding agents with CSRD size distribution can enhance the activation process (Pcact), and seeding at 1300 m is able to activate more seeded CCN into clouds. In addition, because of the strengthening of accretion process (Pracw), more precipitation can be developed in the scenarios seeding at 1300 m (in-cloud region). Though the scenarios seeding at 500 m and into the area of 100 km^2 has the ability to enhance a little bit rainfall which is mainly caused by the enhancement of auto-conversion process (Praut), it is not efficient. Last but not least, the CCNs size distribution after doing cloud seeding illustrates that those hygroscopic particles bigger than 0.4 μm are the main factor contributing to the series of cloud-seeding effects.

Overall, in this study, some direct observational evidences of in-cloud seeding effects are found, and the impacts of in-cloud seeding are also validated by model simulation. Furthermore, based on the modeling results, the constructive advice on hygroscopic cloud-seeding strategy for Taiwan area to enhance precipitation is made. In the stratiform system, we suggest introducing hygroscopic particles into the in-cloud region where the supersaturation ratio

should be more than 0.5 % and LWC is higher than 0.6 g m^{-3}. Furthermore, spreading the seeding agents into the area of about 40-60 km^2 can provide the advantages of not only having the most efficient enhancement of rain rate but also conducting cloud seeding in the more reasonable seeding area.

5.2 Future work

Regarding observation, though many signals can be found in the two Dongyan mountain cloud-seeding experiments, more similar cases are needed to validate those results. Having more cases also provides the advantages to do the statistical analysis, e.g. Silverman (2000) and Tessendorf et al. (2021), etc. In addition, we expect to have further instruments, e.g. Cloud droplet probe and cloud radar, for observing cloud microphysics characteristics and analyzing more details about the changing of cloud droplet size distribution after conducting the cloud seeding. For model simulation, this study selects a case with great model performance and a typical weather condition, the stratiform systems are caused by strong northeastern wind, in northern Taiwan to do the series of cloud-seeding sensitivity tests. However, we would also like to take other cases with different weather conditions into consideration, e.g. the frontal system or convective system, to realize the appropriate cloud-seeding strategies in different meteorology conditions in Taiwan.

Reference

Bo-Tao, Z. H. O. U., & Jin, Q. I. A. N. (2021). Changes of weather and climate extremes in the IPCC AR6. *Advances in Climate Change Research,*, **17**(6), 713. https://doi.org/10.12006/j.issn.1673-1719.2021.167

Bruintjes, R. (2003). Similarities between the effects of hygroscopic seeding and anthropogenic pollution on clouds. 8th WMO Scientific Conference on Weather Modification, Casablanca, Morocco.

Caro, D., Wobrock, W., andFlossmann, A. I. (2002). A numerical study on the impact of hygroscopic seeding on the development of cloud particle spectra. *Journal of Applied Meteorology*, **41**(3), 333-350.

Chen, G. T.-J., C.-M. Liu, B. J.-D. Jou, and J.-P. Chen. (1995). An assessment study and planning on precipitation enhancement program in Taiwan (in Chinese). *Technical Report 84-2M-10, Central Weather Bureau, Ministry of Transportation and Communications, R.O.C. (Taiwan).*

Dudhia, J. (1989). Numerical study of convection observed during the winter monsoon experiment using a mesoscale two-dimensional model. *Journal of Atmospheric Sciences*, **46**(20), 3077-3107.

Flossmann, A. I., Manton, M., Abshaev, A., Bruintjes, R., Murakami, M., Prabhakaran, T., and Yao, Z. (2019). Review of advances in precipitation enhancement research. *Bulletin of the American Meteorological Society*, **100**(8), 1465-1480.

Grell, G. A., andDévényi, D. (2002). A generalized approach to parameterizing convection

combining ensemble and data assimilation techniques. *Geophysical Research Letters*, **29**(14), 38-31-38-34.

Guo, J., Deng, M., Lee, S. S., Wang, F., Li, Z., Zhai, P., Liu, H., Lv, W., Yao, W., and Li, X. (2016). Delaying precipitation and lightning by air pollution over the Pearl River Delta. Part I: Observational analyses. *Journal of Geophysical Research: Atmospheres*, **121**(11), 6472-6488. https://doi.org/10.1002/2015jd023257

Guo, X., Fu, D., Li, X., Hu, Z., Lei, H., Xiao, H., andHong, Y. (2015). Advances in cloud physics and weather modification in China. *Advances in atmospheric sciences*, **32**(2), 230-249.

Hong, S.-Y., Noh, Y., and Dudhia, J. (2006). A new vertical diffusion package with an explicit treatment of entrainment processes. *Monthly Weather Review*, **134**(9), 2318-2341.

Jensen, J. B., and Lee, S. (2008). Giant Sea-Salt Aerosols and Warm Rain Formation in Marine Stratocumulus. *Journal of the Atmospheric Sciences*, **65**(12), 3678-3694. https://doi.org/10.1175/2008jas2617.1

Jung, E., Albrecht, B. A., Jonsson, H. H., Chen, Y. C., Seinfeld, J. H., Sorooshian, A., Metcalf, A. R., Song, S., Fang, M., andRussell, L. M. (2015). Precipitation effects of giant cloud condensation nuclei artificially introduced into stratocumulus clouds. *Atmospheric Chemistry and Physics*, **15**(10), 5645-5658. https://doi.org/10.5194/acp-15-5645-2015

Kerr, R. A. (1982). Cloud seeding: One success in 35 years. *Science*, **217**(4559), 519-521.

Lee, S. S., Guo, J., and Li, Z. (2016). Delaying precipitation by air pollution over the Pearl River Delta: 2. Model simulations. *Journal of Geophysical Research: Atmospheres*, **121**(19), 11,739-711,760.

Lelieveld, J. (1993). Multi-phase processes in the atmospheric sulfur cycle. In *Interactions of C, N, P and S biogeochemical cycles and global change* (pp. 305-331). Springer.

Lim, K.-S. S., andHong, S.-Y. (2010). Development of an effective double-moment cloud microphysics scheme with prognostic cloud condensation nuclei (CCN) for weather and climate models. *Monthly Weather Review*, **138**(5), 1587-1612.

Mather, G., Terblanche, D., Steffens, F., andFletcher, L. (1997). Results of the South African cloud-seeding experiments using hygroscopic flares. *Journal of Applied Meteorology*, **36**(11), 1433-1447.

Mlawer, E. J., Taubman, S. J., Brown, P. D., Iacono, M. J., and Clough, S. A. (1997). Radiative transfer for inhomogeneous atmospheres: RRTM, a validated correlated-k model for the longwave. *Journal of Geophysical Research: Atmospheres*, **102**(D14), 16663-16682.

Monin, A. S., andObukhov, A. M. (1954). Basic laws of turbulent mixing in the surface layer of the atmosphere. *Contrib. Geophys. Inst. Acad. Sci. USSR*, **151**(163), e187.

Rosenfeld, D., Lohmann, U., Raga, G. B., O'Dowd, C. D., Kulmala, and M., F., S., Reissell, A., and Andreae, M. O. (2008). Flood or drought: how do aerosols affect precipitation? *Science*, **321**, 1309–1313.

Rosenfeld, D., Sherwood, S., Wood, R., andDonner, L. (2014). Climate effects of aerosol-cloud interactions. *Science*, **343**(6169), 379-380.

Segal, Y., Khain, A., Pinsky, M., andRosenfeld, D. (2004). Effects of hygroscopic seeding on raindrop formation as seen from simulations using a 2000-bin spectral cloud parcel model. *Atmospheric Research*, **71**(1-2), 3-34.

Silverman, B. A. (2003). A critical assessment of hygroscopic seeding of convective clouds for

rainfall enhancement. *Bulletin of the American Meteorological Society*, **84**(9), 1219-1230.

Silverman, B. A., & Sukarnjanaset, W. (2000). Thailand warm-cloud hygroscopic particle seeding experiment. *Journal of Applied Meteorology and Climatology*, **39**(7), 1160-1175.

Tessendorf, S. A., Chen, S., Weeks, C., Bruintjes, R., Rasmussen, R. M., andXue, L. (2021). The Influence of Hygroscopic Flare Seeding on Drop Size Distribution Over Southeast Queensland. *Journal of Geophysical Research: Atmospheres*, **126**(6). https://doi.org/10.1029/2020jd033771

Tonttila, J., Afzalifar, A., Kokkola, H., Raatikainen, T., Korhonen, H., andRomakkaniemi, S. (2021). Precipitation enhancement in stratocumulus clouds through airborne seeding: sensitivity analysis by UCLALES-SALSA. *Atmospheric Chemistry and Physics*, **21**(2), 1035-1048. https://doi.org/10.5194/acp-21-1035-2021

Weigel, A. P., Chow, F. K., andRotach, M. W. (2007). On the nature of turbulent kinetic energy in a steep and narrow Alpine valley. *Boundary-layer meteorology*, **123**(1), 177-199.

Xue, L., Chu, X., Rasmussen, R., Breed, D., Boe, B., andGeerts, B. (2014). The Dispersion of Silver Iodide Particles from Ground-Based Generators over Complex Terrain. Part II: WRF Large-Eddy Simulations versus Observations. *Journal of Applied Meteorology and Climatology*, **53**(6), 1342-1361. https://doi.org/10.1175/jamc-d-13-0241.1

Yin, Y., Levin, Z., Reisin, T., & Tzivion, S. . (2000). Seeding convective clouds with hygroscopic flares: Numerical simulations using a cloud model with detailed microphysics. . *Journal of Applied Meteorology*, **39**(9), 1460-1472.